Numerical Transducer Modeling

Cutanda Henriquez, Vicente; Jacobsen, Finn

Publication date:
2002

Document Version
Publisher's PDF, also known as Version of record

Numerical Transducer Modeling

Ph.D. dissertation by:

Vicente Cutanda Henríquez (EF 752)

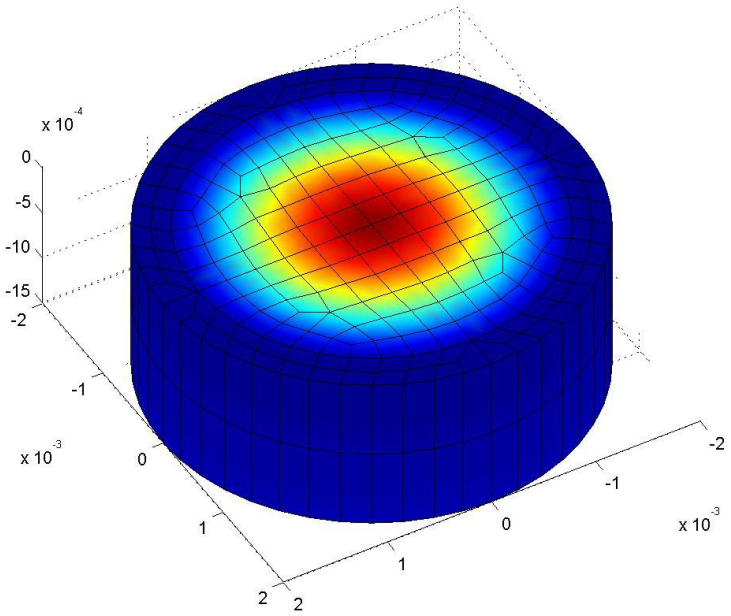

In cooperation with:

Danish Academy of Technical Sciences (ATV)

Ørsted*DTU - Section of Acoustic Technology
Technical University of Denmark

Brüel & Kjær Sound & Vibration Measurement A/S

Brüel & Kjær

DTU

Numerical Transducer Modeling

by

Vicente Cutanda Henríquez

Ørsted•DTU - Section of Acoustic Technology

Technical University of Denmark

Brüel & Kjær Sound & Vibration Measurement A/S

Cover: Sound pressure on the internal surface of a microphone at 60 kHz, calculated using the Boundary Element Method with viscous and thermal losses.

Preface

This thesis is submitted in partial fulfillment of the requirements for the Danish Ph.D. degree, as part of a Danish Industrial Ph.D. project administered by the Danish Academy of Technical Sciences (ATV) and financially supported by the Danish Agency for Trade and Industry. The work has been carried out under the supervision of Associate Professor Finn Jacobsen at the Section of Acoustic Technology at Ørsted*DTU, Technical University of Denmark and M.Sc. Johan Gramtorp at Brüel & Kjær Sound & Vibration, from 1st September 1998 to 30th November 2001.

I would like to thank my supervisors for their constant support and guidance. I would also like to thank:

- Peter Møller Juhl for the fruitful discussions about the BEM, proofreading of the manuscript and especially for the guidance provided during my stay at Odense University in 2000.
- Mabrouk Ben Tahar, for the help and assistance during my stay at Université de Technologie de Compiègne (France) in 1999.
- Erling Sandermann Olsen at Brüel & Kjær for all the discussions and countless meetings.
- Jean-Dominique Polack for his physical and mathematical insight into the problem of viscous and thermal losses in fluids.
- Morten Skaarup Jensen, for the valuable discussions.
- Manuel Sobreira Seoane, for his interest and cooperation from Spain and during his visit to DTU.

OpenBEM is a set of formulations of the Boundary Element Method originated by the thesis work of Peter Møller Juhl on axisymmetrical BEM and has been programmed by Peter Møller Juhl, Morten Skaarup Jensen and the author. It has been employed and contributed to during the project.

Summary

This thesis describes the development of a numerical model of the propagation of sound waves in fluids with viscous and thermal losses, with application to the simulation of acoustic transducers, in particular condenser microphones for measurement. The theoretical basis is presented, numerical tools and implementation techniques are described and performance tests are carried out.

The equations that govern the motion of fluids with losses and the corresponding boundary conditions are reduced to a form that is tractable for the Boundary Element Method (BEM) by adopting some hypotheses that are allowable in this case: linear variations, absence of flow, harmonic time variation, thermodynamical equilibrium and physical dimensions much larger than the molecular mean free path.

A formulation of the BEM is also developed with an improvement designed to cope with the numerical difficulty associated with very close surfaces, as found in condenser microphones, where the membrane has a backplate very close behind. This improvement could be useful for many other problems where the BEM is applied.

The numerical implementation that includes both viscous and thermal effects is then worked out. Some numerical manipulations are developed to satisfy the more complicated boundary conditions, and a model of a condenser microphone with a coupled membrane is developed. The model is tested against measurements of ¼ inch condenser microphones and analytical calculations. A detailed discussion of the results is given.

Resumé

Denne afhandling beskriver udviklingen af en numerisk model for lydfelter i et medium med termiske og viskose tab, med særlig henblik på modellering af akustiske transducere, herunder specielt kondensatormikrofoner. Den teoretiske baggrund præsenteres, de numeriske værktøjer og implementeringsteknikker beskrives, og modellerne afprøves.

Det vises hvorledes de grundlæggende ligninger for et medium med tab kan reduces til en form der kan løses med boundary element metoden (BEM) når der kan antages lineære forhold, ingen strømning i mediet, harmonisk tidsvariation, termodynamisk ligevægt, og fysiske dimensioner som er meget større end den molekylære middelvejlængde.

Der udvikles endvidere en BEM-formulering som kan håndtere overflader tæt ved hinanden, således som det forekommer i kondensatormikrofoner, hvor membran og bagelektrode er meget tæt på hinanden. Den forbedrede BEM-formulering vil kunne bruges ved modellering af mange andre problemer.

Herefter præsenteres den udviklede numeriske model af en kondensatormikrofon med termiske og viskose tab og en tilkoblet membran. Forskellige numeriske manipulationer til at løse problemets randbetingelser beskrives. Randbetingelserne er væsentlig mere komplicerede end i det tabsfri tilfælde. Modellen afprøves ved sammenligning med en analytisk model og med eksperimentelle resultater bestemt med ¼-tomme mikrofoner.

TABLE OF CONTENTS

Table of symbols

$\perp$	normal direction
$//$	tangential direction
β	rate of increase of pressure with temperature at constant volume
γ	ratio of specific heats C_p/C_v
Δ	laplacian
$\Delta_{//}$	tangential laplacian
$\frac{\delta}{\delta n}$	normal derivative
$\frac{\delta}{\delta \xi}, \frac{\delta}{\delta \zeta}$	local tangential derivatives
ε	normal displacement of the membrane
ζ	local tangential coordinate within an element
η	bulk viscosity or second viscosity
λ	thermal conductivity
μ	coefficient of viscosity
$\mu(Q)$	double-layer potential, pressure jump
ξ	local tangential coordinate within an element
ρ	density, variation around the static value
ρ'	density, total value
ρ_0	density, equilibrium value
ρ_s	surface density of the membrane

$\sigma(Q)$	single-layer potential, jump of the normal derivative of the pressure
τ_a , τ_h	constants depending on the physical properties of the fluid
τ_{ij}	viscous stress tensor
ϕ_a , ϕ_h	constants depending on the physical properties of the fluid
ω	angular frequency
$\boldsymbol{A}$	coefficient matrix for the pressure
$\boldsymbol{A}_a$	acoustic coefficient matrix $\boldsymbol{A}$
$\boldsymbol{A}_h$	thermal coefficient matrix $\boldsymbol{A}$
A_n	expansion coefficients of the membrane
$\boldsymbol{A}_v$	viscous coefficient matrix $\boldsymbol{A}$
$\boldsymbol{B}$	coefficient matrix for normal derivative of the pressure
$\boldsymbol{B}_a$	acoustic coefficient matrix $\boldsymbol{B}$
$\boldsymbol{B}_h$	thermal coefficient matrix $\boldsymbol{B}$
$\boldsymbol{B}_v$	viscous coefficient matrix $\boldsymbol{B}$
$\boldsymbol{C}$	diagonal matrix of C constants
c	speed of sound
$C(P)$	geometrical constant
C_p	specific heat at constant pressure
$curl$	curl
C_v	specific heat at constant volume
d_h	thermal boundary layer thickness
div	divergence
$div_{//}$	tangential divergence
d_v	viscous boundary layer thickness

f	frequency
$G(R)$	Green's function
$\overrightarrow{grad}$	gradient
$\overrightarrow{grad}_{//}$	tangential gradient
i	imaginary unit
J	Jacobian matrix
J_0	Bessel function of the first kind, order 0
J_1	Bessel function of the first kind, order 1
k	wavenumber, ideal fluid
k_a	acoustic wavenumber
k_h	thermal wavenumber
k_n	zeros of J_0 (divided by R)
k_v	viscous wavenumber
l_h	thermal characteristic length
l_v', l_v	viscous characteristic lengths
n	normal vector
N_i	shape functions
P	observation point
p	sound pressure variation around the static value
p'	sound pressure, total value
p_0	sound pressure, equilibrium value
p_a	acoustic component of the pressure
p_h	thermal component of the pressure
p^I	incident pressure

p_{inc}	incident pressure
Q	surface integration point
Q	volume velocity
R	membrane radius
r	radial position
s	entropy variation around the static value
S	boundary surface
s'	entropy, total value
s_0	entropy, equilibrium value
T	membrane tension
T	temperature variation around the static value
t	time
T'	temperature, total value
T_0	temperature, equilibrium value
T_a	acoustic component of the temperature
T_b	thermal component of the temperature
V	volume
$\vec{v}$	particle velocity variation around the static value
$\vec{v}_0$	particle velocity, equilibrium value
$\vec{v}'$	particle velocity, total value
$\vec{v}_a$	acoustic velocity
$v_{a,\perp}$	normal acoustic velocity
$v_{boundary,\perp}$	normal boundary velocity
$v_{boundary,//}$	tangential boundary velocity

$\vec{v}_h$	thermal velocity
$v_{h,\perp}$	normal thermal velocity
$\vec{v}_l$	irrotational velocity
$\vec{v}_v$	viscous velocity
$\vec{v}_{v,//}$	tangential viscous velocity
$v_{v\xi}$	local tangential viscous velocity in the ξ direction
$v_{v\zeta}$	local tangential viscous velocity in the ζ direction
$v_{v,\perp}$	normal viscous velocity
v_{vn}	local normal viscous velocity

Figures and tables

Figures

Tables

1. INTRODUCTION

The present project is an Industrial Ph.D. project (Erhvervsforskeruddannelsen). Such projects involve a Ph.D. study in a university and, at the same time, industrial research in a company. The two aspects are considered equally important. The project must therefore have, on the one hand, sufficient scientific interest to merit a university Ph.D. On the other hand it must also possess a clear industrial value for the company that contributes to it. This double nature of the project gives the student a valuable insight into the two worlds, which very often have different views and motivations regarding science and technology.

This report deals with the scientific and engineering aspects of the project. There is also a Business Report, required by ATV, which supplements it with a study of the strategic impact and the management view of the research in the company.

The industrial motivation of this work is the need for a better method of predicting the behavior of measurement condenser microphones, produced by Brüel & Kjær. The design of these devices is made with a series of prototypes and using the experience of the designers to find the best way to achieve the desired specifications of the new model. The existing lumped parameter models, with a long tradition in the literature, help in this process. However, the phenomena in the microphone around and above the first resonance of the membrane are not well understood. Viscous and thermal damping in the thin layer of air between membrane and back electrode play an important role in the microphone performance. In chapter 2 a brief description of the condenser microphone is given.

For this reason it was considered that the use of numerical methods could contribute very much to the improvement of the design process. Besides, new technologies for producing condenser microphones are being implemented in Brüel & Kjær, like MEMS microphones (Micro Electro-Mechanical Systems), etched in silicon, or thick film microphones. These new products are in need of numerical predictions, even more than the classical designs.

From the scientific point of view, the project also presents some interesting features. The study of viscous and thermal losses of sound waves in fluids is a classical topic in Acoustics that, however, is still subject to theoretical development. The phenomenon is governed by a set of equations often called the *Navier-Stokes-Fourier model.* [30,33,6] These equations can describe phenomena like viscous flow and non-linear effects and are an extension of the ideal fluid equations. The *Navier-Stokes-Fourier model* must be reduced to a tractable form so as to obtain a solution for a particular problem. We will develop the theory related with our case by imposing the adequate hypotheses in chapter 2.

The use of numerical methods in the design of products and in the simulation of their behavior as an alternative to actual measurements are tendencies, or very often general practice, in many fields of engineering. In the case of manufacturing of acoustic transducers, however, these methods are a novelty. For this reason this project has also the side effect of introducing the use of numerical simulation in an environment where it is scarcely employed. The participation in parallel projects that use numerical simulation has been a constant in this Ph.D., both at the company and at the University. There is a lot to learn about the practical use of numerical methods. As Seybert puts it, "we are trying to answer questions such as what the best predictive method for a given application is, how sensitive a given method to modeling error is, how we know when we have a good model, and, for that matter, what is meant by 'good'?".[37]

The Boundary Element Method (BEM) has been used to model the microphone's interior; a brief presentation is included in chapter 2. The formulation of the BEM used in the project is direct collocation, which is known to have difficulties in the modeling of objects with very close surfaces.[29,27,40] This problem is addressed in chapter 3 and in a journal paper, included in Appendix D. A technique that overcomes this limitation is proposed and implemented in BEM. The BEM formulation thus modified is used in the subsequent developments.

Chapter 4 contains the details of the proposed implementation of viscous and thermal losses in a numerical model of a condenser microphone. The advantages and shortcomings of the model are addressed and discussed. The model is validated in chapter 5; results and

comparisons are shown, described and commented on. Further discussion of the whole project is made in chapter 6, including possible extensions of the work. It is hoped that this project serves as an inspiration for other researchers in the field; it certainly points to some possible lines of research. Some general conclusions are summarized in chapter 7.

The report contains also four appendices. Appendix A has a summary of the analytical model used for validation. Appendix B briefly describes and discusses an alternative approach to this problem, taken from the literature. Appendix C concerns the actual implementation of the numerical model in Matlab. Finally, Appendix D is a paper published in the Journal of the Acoustical Society of America, related with the developments in chapter 3.

2. BASIC THEORY

In this chapter the background theory for the thesis is briefly reviewed. A wide range of fields is covered by this project, involving physics, mathematics, computers and transducers. Sufficient understanding of every aspect is necessary to produce a complete model of a microphone.

2.1. The condenser microphone

It is not intended in this section to give a complete description of all aspects related with microphone construction, operation and calibration. The reader can find suitable descriptions in the literature.[8,39,4] There are nevertheless some topics that are relevant for further discussion in connection with this Ph.D. work.

Microphones for different applications are based on a number of different transduction principles and are built under specific requirements. The most widely used device for precision acoustic measurement is the condenser microphone. The desired properties of this device are:[8]

- Wide frequency range and flat frequency response.
- Wide linear dynamic range, low noise and distortion.
- Low influence from the environment: static pressure, temperature, humidity, vibration, electromagnetic fields.
- Good mechanical robustness and chemical resistance.
- High stability: small short and long term changes.
- Simplicity of design, suitable for calibration.

2.1.1. Description of the condenser microphone

Despite constant improvement in manufacturing, materials and production technology, the operation principle of the condenser microphone has remained unchanged for decades. A diaphragm under tension is exposed to the sound field. Its vibration is sensed by measuring the capacitance of the condenser formed by the membrane and a plate situated very close behind, inside the microphone body. The setup is sketched in Figure 2-1.

The internal pressure is equalized by means of a vent hole small enough to allow good measurements down to very low frequencies. The transduction from sound pressure to electrical signals is achieved by applying a constant electrical charge to the diaphragm-backplate condenser and measuring the voltage variations. This charge is either built-in or created through external polarization.

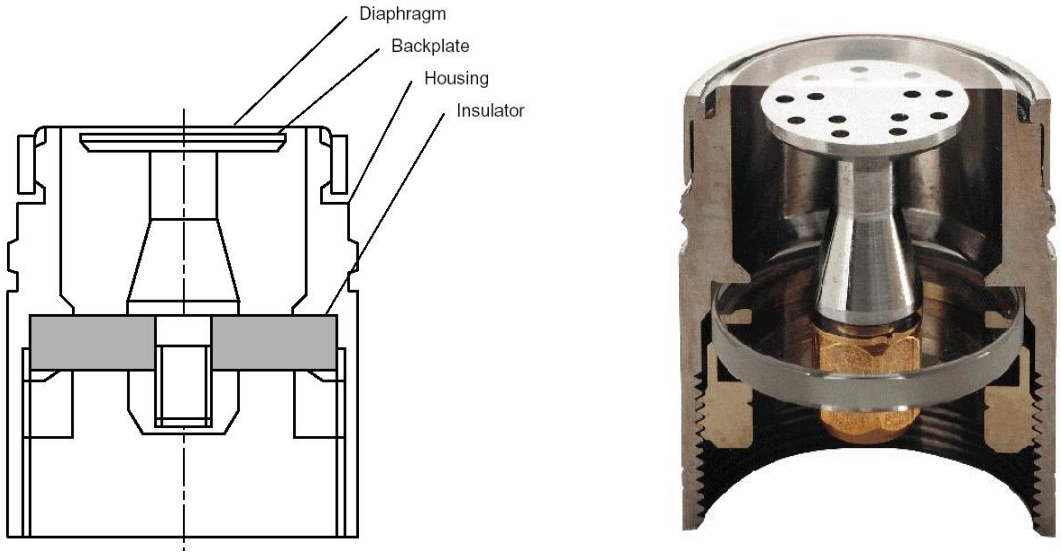

Figure 2-1. Classic design of a condenser microphone. (Brüel & Kjær)

There are a number of different technologies used in building condenser microphones. The classical microphone assembled as shown in Figure 2-1 is still widely used, but micro-mechanical microphones and thick-film microphones are already being produced for specific

applications. However, the working principle is basically the same, and therefore the developments in this thesis are valid also in other cases, barring some changes in the geometry and properties of the materials.

2.1.2. Equivalent circuit model of a condenser microphone

The aim of this thesis is to provide a model of the behavior of condenser microphones, and therefore it is convenient to briefly explain the existing models, what are their weaknesses and what should be expected from a more complete simulation.

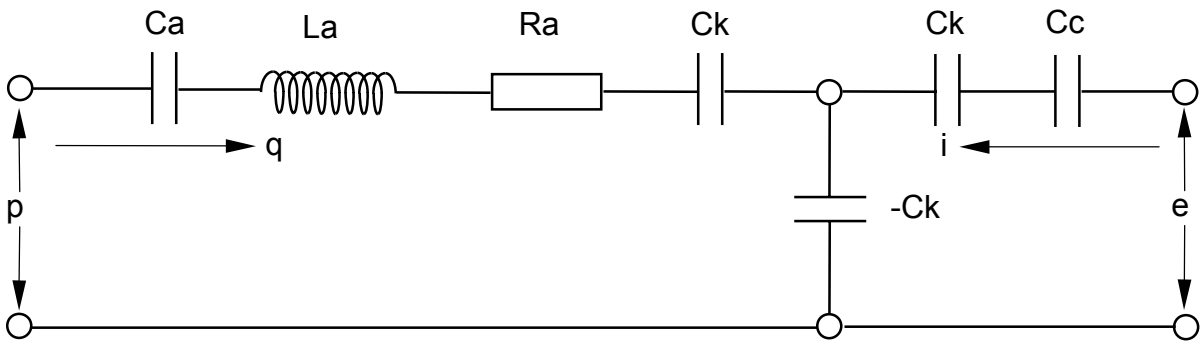

Ca = Acoustical compliance of diaphragm when the electrical terminals are unloaded.

La = Acoustical mass of diaphragm.

Ra = Acoustical damping resistance of diaphragm.

Cc = Electrical capacitance of the microphone when the diaphragm is rigidly fixed.

Ck = Compliance due to the electroacoustical coupling in the transducer.

q = Volume velocity.

i = Electrical current.

p = pressure across acoustical terminals, outside of the diaphragm.

e = voltage across electrical terminals.

Figure 2-2. Equivalent circuit of a condenser microphone.

The usual representation of a condenser microphone in a way that includes all the relevant effects is its equivalent circuit. Every component has a meaning related with some electrical or acoustical property that plays a role in the transduction process. Figure 2-2, taken from [17],

shows an example of such a circuit. The left side is the acoustical part, and the right side is the electrical part.

However, the circuit does not imply a complete understanding of the phenomena inside the transducer. It quantifies the different effects in order to obtain a practical tool that facilitates the use of the device. It has nevertheless proved to be very useful for the design and calibration of condenser microphones. Construction parameters like dimensions, membrane density and tension, backplate design, etc influence the performance and this is reflected in the components of the circuit.

Some acoustical effects inside a condenser microphone that are crucial for its correct performance are however quite complex. The load of the air layer between diaphragm and backplate, represented by *Ra* in Figure 2-2, involves viscous and thermal dissipation mechanisms. The designers use this damping effect to control the resonances of the membrane and shape the frequency response, playing with the geometry of the air layer and boring holes in the backplate. This is a trial and error process that involves the construction of prototypes.

The model developed in this work should give a better understanding of the acoustical behavior inside condenser microphones and make the design process easier.

2.1.3. Calibration using an electrostatic actuator

There are several calibration methods available for condenser microphones. In this work we are interested in particular in the use of an electrostatic actuator. This device is a metallic grid placed close to the diaphragm and subjected to large AC and DC voltages that create electrostatic forces directly on the diaphragm.[8] The measurement is done using the set-up described in Figure 2-3. Figure 2-4 shows two examples of actual actuators.

The interesting property of the frequency response thus obtained is the fact that it does not depend on the sound field. There is a uniform force on the diaphragm originated by the

actuator; therefore there is very little acoustical coupling between the diaphragm and the outside medium.

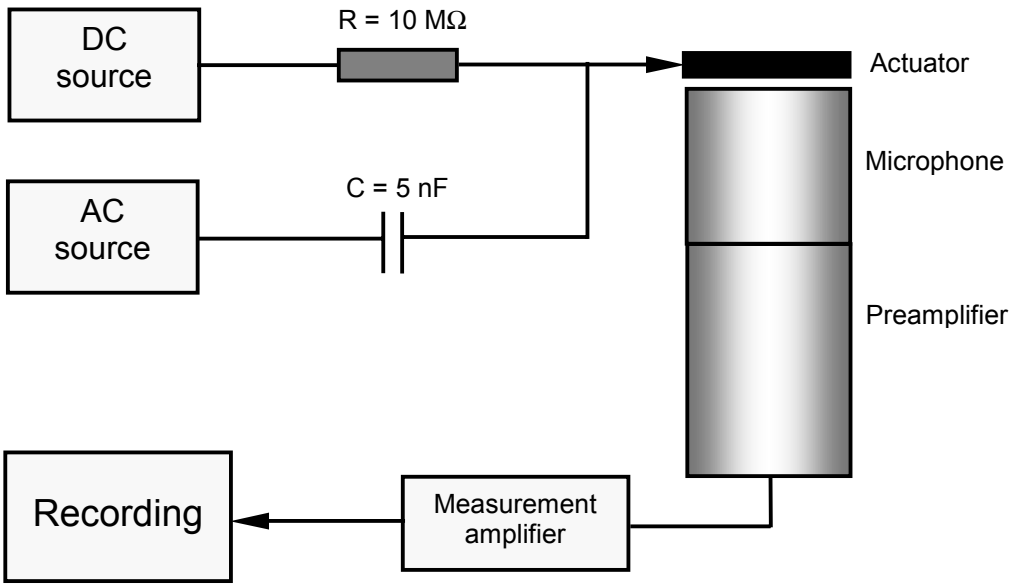

Figure 2-3. Set-up for measurement using an electrostatic actuator.

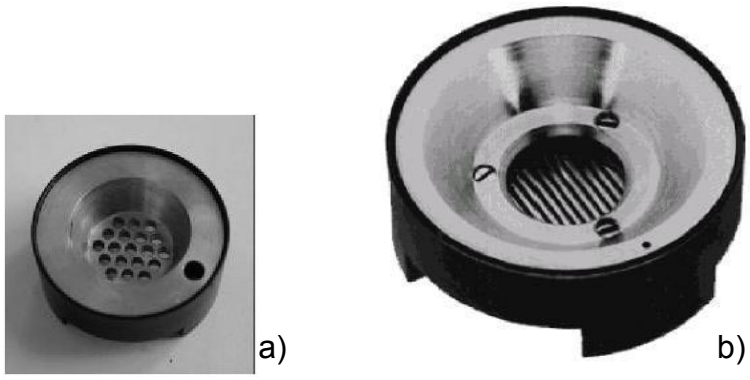

Figure 2-4. Examples of electrostatic actuators. a) for half-inch microphones, b) for one-inch microphones.

In order to validate the numerical model of a microphone it is convenient to use the most simplified example that includes the effects to simulate. The analytical model to be used for this validation is defined under uniform pressure excitation, and can be compared with the response of a real condenser microphone excited with an actuator. For this reason we will use electrostatic actuator measurements for validation.

2.2. Propagation of sound in fluids with thermal and viscous losses

Physical acoustics deals with acoustic waves propagating in an elastic fluid. In most cases of practical interest the process can be considered ideal, that is, without any loss of energy contained in the sound wave. However, when the wave propagates over long distances, in small enclosures, through narrow ducts or over sharp boundaries, the losses become noticeable and should not be neglected.

The subject of this thesis, the condenser microphone, has a thin layer of air under its diaphragm where losses take place. The very performance of the device is actually based on such losses; an understanding is therefore necessary of the mechanisms that produce them.

In this section we introduce a theoretical description of viscous and thermal losses in fluids, with special focus on the case under study. A practical understanding of the phenomena is intended, and the reader should consult the references for a more rigorous and complete development.[30,33,6]

2.2.1. Hypotheses

The equations that describe acoustic wave motion in fluids with losses are too complex to be solved without any simplification. We must therefore define a set of hypotheses that are suitable for the problem under study. These hypotheses are:

- In linear acoustics the variations are small and therefore the fluid has a linear behavior. This means that higher order terms in the equations can be excluded.

- Ambient conditions and physical properties of the fluid do not change with time. The fluid is in equilibrium.

- The fluid is still: there is no flow. The static value of the particle velocity is zero.

- The variation is harmonic, of the form $x(t) = x_0 e^{-i\omega t}$.

- The dimensions of the setup and the wavelength are larger than the molecular mean free path, which is about 10^{-7} m for air in normal conditions. A typical condenser microphone has a distance from diaphragm to backplate of about $2 \cdot 10^{-5}$ m.

2.2.2. Equations for a fluid with losses

A set of five equations is needed to determine the five variables:

- Pressure: $p' = p_0 + p$
- Velocity: $\vec{v}' = \vec{v}_0 + \vec{v}$
- Density: $\rho' = \rho_0 + \rho$
- Temperature: $T' = T_0 + T$
- Entropy: $s' = s_0 + s$

where x' indicates total value, x_0 equilibrium value and x is the variation around the static value. In order to determine the behavior of these five variables, the basic physical and thermodynamical properties of a fluid with viscous and thermal losses must be used. The five equations needed are the conservation of mass, the conservation of energy, the conservation of momentum (Navier-Stokes equation), the second law of thermodynamics and the equation of state. If we consider that the particle velocity is a vector field, it has three components to be determined; therefore there are seven unknowns and seven equations, since the Navier-Stokes equation is a vectorial relation.

Conservation of mass

$$\frac{\partial \rho'}{\partial t} + div(\rho' \vec{v}') = 0 \quad \xrightarrow{\text{First order}} \quad \frac{\partial \rho}{\partial t} + \rho_o div(\vec{v}) = 0 \tag{2.1}$$

This relationship shows that the variation of mass in a volume of fluid must be counterbalanced by the flow of mass through its bounding surface. It is valid whether the fluid has losses or not.

Conservation of energy

In a perfect fluid acoustic wave motion is an adiabatic process, and therefore the entropy does not vary. In a real fluid temperature variations associated with acoustic pressure variations induce flux of heat, therefore loss of energy in the sound wave and increase of entropy. The process is shown schematically in Figure 2-5. The flux of heat is proportional to the temperature gradient: $\vec{q} = \lambda \overrightarrow{grad}\, T'$. The proportionality constant λ is called *thermal conductivity*.

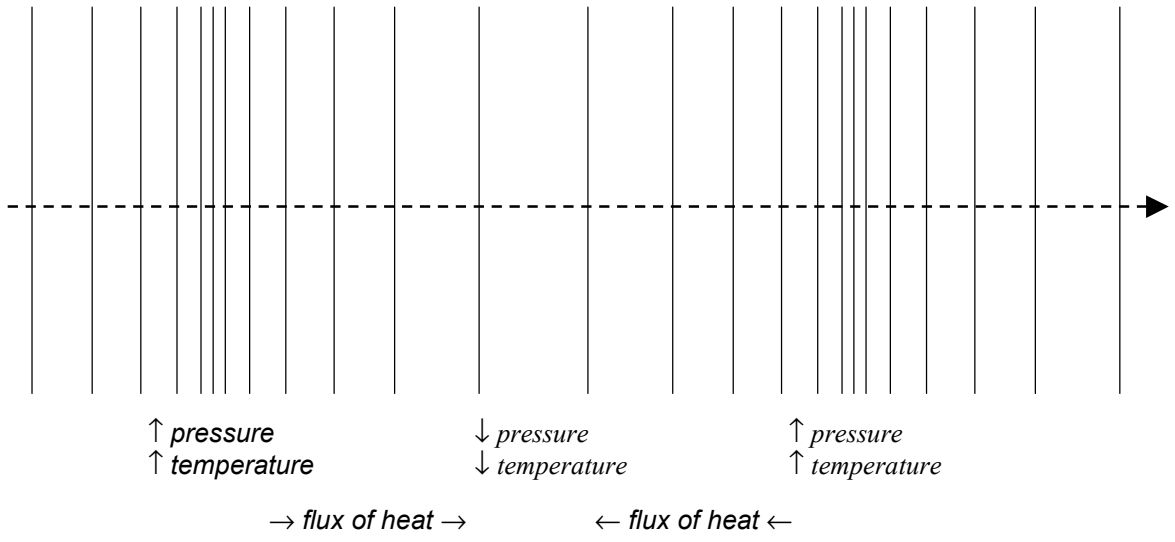

Figure 2-5. Thermal conduction in a plane sound wave.

The movement of fluid particles induces also momentum diffusion because faster particles tend to drag slower ones and slow down themselves in the process. Figure 2-6 helps to understand this idea showing how the variations in of the velocities of the particles throughout the fluid create stress and loss of energy. These are the viscous losses in the fluid,

where the induced shear stress is proportional to the velocity variations. The proportionality constant μ is called the *coefficient of viscosity*.

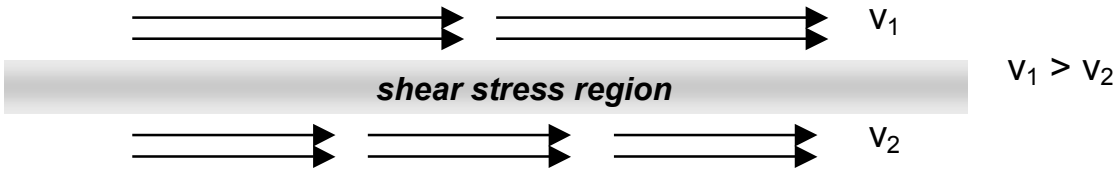

Figure 2-6. Viscous losses in a fluid. A shear stress and losses can be originated by differences of the particle velocities at neighboring regions in the fluid.

The energy balance in the fluid is expressed by the conservation of energy equation:

$$\rho' T' \frac{ds'}{dt} = div(\lambda \overrightarrow{grad}\, T') + \tau_{ij} \frac{\partial v_i'}{\partial x_i} \quad \xrightarrow{\text{First order}} \quad \rho_o T_o \frac{\partial s}{\partial t} = \lambda \Delta T \qquad (2.2)$$

The quantity τ_{ij} is the viscous stress tensor:

$$\tau_{ij} = \mu\left(\frac{\partial v_i}{\partial x_j} + \frac{\partial v_j}{\partial x_i} - \frac{2}{3}\delta_{ij}\, div\,\vec{v}\right) + \eta\,\delta_{ij}\, div\,\vec{v}$$
$$\delta_{ij} = 1 \quad if\ i = j \qquad (2.3)$$
$$\delta_{ij} = 0 \quad if\ i \neq j$$

The quantity η is the bulk viscosity or second viscosity and describes the molecular motion losses in the fluid under compression. The bulk viscosity is negligible in monoatomic gases.

Therefore, the increase of heat in the fluid volume (the left-hand side in (2.2)) is equal to the thermal losses (the first term in right-hand side of (2.2)) plus the viscous losses (the second term in right-hand side of (2.2)). The viscous losses term turns out to be of second order and disappears after linearization. However, the effect of viscosity will be taken into account in the equation for conservation of momentum.

Conservation of momentum (Navier-Stokes)

This equation describes the motion in a viscous fluid. The full expression of the stress tensor must be used, including viscous stress. After some manipulations the Navier-Stokes equation is obtained:

$$\rho \frac{d\vec{v}'}{dt} = -\overrightarrow{grad}\, p' + \left(\eta + \frac{4}{3}\mu\right)\overrightarrow{grad}\left(div\,\vec{v}'\right) - \mu\,\overrightarrow{curl}\left(\overrightarrow{curl}\,\vec{v}'\right) \tag{2.4}$$

To first order approximation, it is:

$$\rho_o \frac{\partial \vec{v}}{\partial t} = -\overrightarrow{grad}\, p + \left(\eta + \frac{4}{3}\mu\right)\overrightarrow{grad}\left(div\,\vec{v}\right) - \mu\,\overrightarrow{curl}\left(\overrightarrow{curl}\,\vec{v}\right) \tag{2.5}$$

It can be seen that the Navier-Stokes equation (2.4) reduces to Euler's equation $\rho \frac{d\vec{v}'}{dt} = -\overrightarrow{grad}\, p'$ for perfect fluids. Also note that it is a vector equation and therefore equivalent to three scalar ones.

Thermodynamic equations

The thermodynamic equations relate pressure, density, temperature and entropy:

$$\begin{aligned} ds' &= \frac{C_p}{T'}\left(dT' - \frac{\gamma-1}{\beta\gamma}dp'\right) \quad \xrightarrow{\text{First order}} \quad s = \frac{C_p}{T_o}\left(T - \frac{\gamma-1}{\beta\gamma}p\right) \\ d\rho' &= \frac{\gamma}{c^2}\left(dp' - \beta\, dT'\right) \quad \xrightarrow{\text{First order}} \quad \rho = \frac{\gamma}{c^2}\left(p - \beta T\right) \end{aligned} \tag{2.6}$$

where γ is the ratio of specific heats C_p/C_v, C_p is the specific heat at constant pressure, C_v is the specific heat at constant volume, c is the speed of sound (adiabatic) and β is the rate of

increase of pressure with temperature at constant volume. The first equation is the second law of thermodynamics and the second is the equation of state.

2.2.3. Decoupling of viscous, thermal and acoustic modes

The hypotheses introduced in 2.2.1 lead to a more simplified and convenient way of expressing the fundamental equations that describe wave motion in visco-thermal fluids. We will show in this sub-section how these simplified equations can be manipulated to produce three uncoupled modes that describe separately viscous, thermal and acoustic effects. The coupling will only take place on the boundary surfaces.

Decomposition of the velocity – viscous mode

The particle velocity can be split into a sum of two components:

$$\vec{v} = \vec{v}_l + \vec{v}_v \qquad \text{where} \quad \begin{matrix} \overrightarrow{curl}\,\vec{v}_l = 0 \\ div\,\vec{v}_v = 0 \end{matrix} \tag{2.7}$$

since any vector field can be considered as a superposition of a potential field and a solenoidal field. The component $\vec{v}_l$ is called irrotational or laminar velocity.

The Navier-Stokes equation (2.5) can therefore be split in two equations as well:

$$\rho_o \frac{\partial \vec{v}_l}{\partial t} + \overrightarrow{grad}\, p - \left(\eta + \frac{4}{3}\mu\right)\overrightarrow{grad}\left(div\,\vec{v}_l\right) = 0 \tag{2.8}$$

$$\rho_o \frac{\partial \vec{v}_v}{\partial t} + \mu\,\overrightarrow{curl}\left(\overrightarrow{curl}\,\vec{v}_v\right) = 0 \tag{2.9}$$

Equation (2.8) will be used to obtain a decoupled form of the thermal and acoustic modes, as we will see later. Equation (2.9) describes the behavior of the so-called rotational, viscous or

transverse velocity $\vec{v}_v$ that is uncoupled with the rest except at the boundaries. This velocity, under the current hypotheses, is not associated with any pressure, temperature or entropy changes. If we consider a basic relationship for the laplacian operator:

$$\Delta\vec{v}_v = \overrightarrow{grad}\left(div\vec{v}_v\right) - \overrightarrow{curl}\left(\overrightarrow{curl}\vec{v}_v\right) = -\overrightarrow{curl}\left(\overrightarrow{curl}\vec{v}_v\right) \tag{2.10}$$

With (2.10) and introducing harmonic variation in (2.9) we obtain:

$$\left(\Delta + k_v^2\right)\vec{v}_v = 0 \quad and \quad div\,\vec{v}_v = 0 \tag{2.11}$$

$$k_v^2 = \frac{i\rho_o\omega}{\mu} = \frac{i\omega}{c\,l_v'} \qquad l_v' = \frac{\mu}{\rho_o c} \tag{2.12}$$

where k_v is the viscous wavenumber and l_v' is the viscous characteristic length. Another viscous characteristic length that includes the bulk viscosity is defined as $l_v = (\eta + 4/3\mu)/\rho_o c$, it will be needed later. Equation (2.11) is of the Helmholtz form and, considering the values of k_v in acoustics, describes a very fast attenuation of the viscous mode. This mode is only important close to the boundaries, where it is excited by the no-slip boundary condition, discussed later. The thickness of this *viscous boundary layer* is:[30]

$$d_v = \sqrt{\frac{2\mu}{\rho_o\omega}} = \sqrt{\frac{2l_v'c}{\omega}} \approx 2.1\cdot 10^{-3}\,\frac{1}{\sqrt{f}} \quad m \tag{2.13}$$

This effect is depicted in Figure 2-7, showing that both tangential and normal components of the velocity must be observed at the boundary, if viscous losses are considered.

Note that the sign of k_v in (2.12) would change if we had used the other sign convention for the harmonic variation, $e^{j\omega t}$ instead of $e^{-j\omega t}$ assumed in this development. Other signs in the following would also be changed.

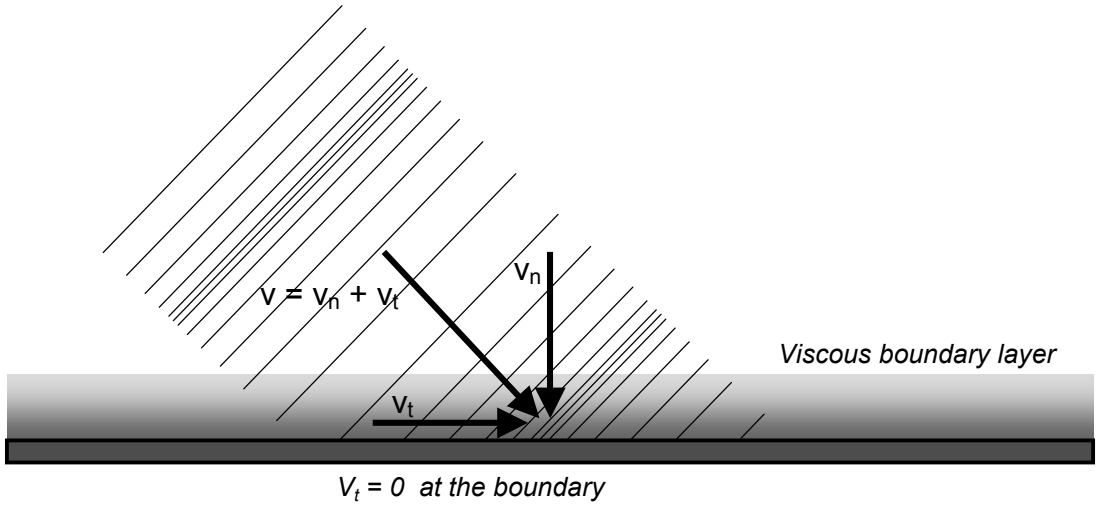

Figure 2-7. Viscous losses near a boundary. In an ideal fluid, a wave that hits the boundary obliquely has a tangential velocity component parallel to the surface. If viscosity is considered, the tangential component is cancelled and a viscous boundary layer created.

Thermal and acoustic modes

Any of the variables pressure (p), temperature (T) or irrotational velocity ($\vec{v}_l$) can be decomposed into two modes, a propagating acoustic wave and a diffusion field that contains the thermal losses. The first is called acoustic or propagational, while the second is called thermal or entropic.[30,33] We will adopt in this text the names acoustic and thermal respectively.

These two modes are uncoupled, given the hypotheses, except at the boundaries. In the same way as the viscous mode described before, the thermal mode dies out rapidly when going away from the boundaries, where it is excited by the usually higher thermal conductivity of the boundary surface that forces negligible temperature variation. The main feature of this mode is the entropy change, and this is obvious if we consider that the linearized equation for the conservation of energy (2.2) neglects the higher-order viscous term leaving only the thermal effects. Only the acoustic mode remains in open space, where the usual perfect fluid (adiabatic) approximation is justified. The thickness of the *thermal boundary layer* is similar to the viscous one:[30]

$$d_h = \sqrt{\frac{2\lambda}{\rho_o \omega C_P}} = \sqrt{\frac{2 l_h c}{\omega}} \approx 2.5 \cdot 10^{-3} \frac{1}{\sqrt{f}} \quad m \tag{2.14}$$

Figure 2-8 shows a schematic representation of the phenomena at the thermal boundary layer created by the flux of heat in the neighborhood of the boundary surface.

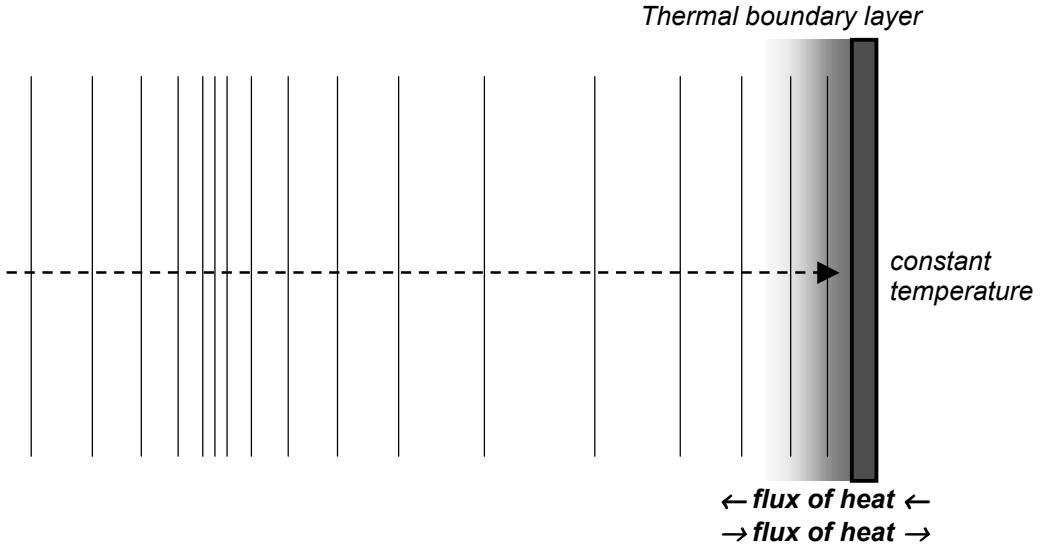

Figure 2-8. Thermal losses near a boundary: the surface creates a flux of heat, and losses occur within a thermal boundary layer.

The entropic characteristic length $l_h = \lambda/(\rho_o\ C_P\ c)$ is of the same order as the viscous characteristic length l_v' (and l_v) in gases. In air they are about 10^{-7} m, and, for the theoretical development to be valid, the wavelength must be larger than that. This condition is satisfied at all acoustic frequencies of interest. Additionally, the physical dimensions of the acoustic domain should be in any case larger than the characteristic lengths, as stated in the initial hypotheses in 2.2.1.

The decoupled expressions that describe acoustic and thermal modes are obtained combining equations (2.1), (2.2), (2.6) and (2.8). In the following we will refer to the development by M. Bruneau *et al.*, which produces a theoretical framework more suitable for numerical

implementation.[6] Other approaches take new assumptions and simplifications in order to facilitate a better understanding of the physical phenomena involved and adapt the results to the most common situations in acoustics.[30,33]

The main improvement introduced by Bruneau *et al.* is a new version of the classical *Kirchoff's dispersion relation* that considers the time-domain and includes bulk viscosity. Its solutions are the so-called dispersion relations (k as a function of ω) that define the two modes and can be brought back to the time domain as differential equations. An equation of the form:

$$\alpha_1 \Delta\Delta\psi + \alpha_2 \Delta\psi + \alpha_3 \psi = 0 \tag{2.15}$$

where the α_i contain physical parameters and time derivatives, is deduced. The ψ represents either pressure, temperature or irrotational velocity $\vec{v}_l$. This expression is equivalent to the mentioned Kirchoff's dispersion equation, if relaxation is considered. In order to decouple acoustic and thermal modes and find suitable harmonic differential equations that describe them, some terms must be neglected. This is justified under the hypotheses stated above in this sub-section, that is, both wavelength and physical dimensions are larger than the characteristic lengths (l_h, l_v and l_v'). The harmonic equations are:

$$(\Delta + k_a^2)\ \psi_a = 0 \tag{2.16}$$

$$(\Delta + k_h^2)\ \psi_h = 0 \tag{2.17}$$

$$\textit{where} \quad \psi = \psi_a + \psi_h$$

The acoustic wavenumber k_a contains terms depending on thermal and viscous effects, but it nevertheless describes a propagating wave and reduces to the adiabatic wavenumber $k = \omega/c$ away from boundaries. The entropic or thermal wavenumber k_h is of similar order as the viscous one k_v introduced in the previous sub-section, that is, complex and large. This corresponds to the physical phenomena associated with thermal and viscous modes, described in the literature as heat diffusion and momentum diffusion respectively, opposed to the true propagational behavior of the acoustic mode.[30,33]

The wavenumbers have expressions in series, which are reduced to their first terms by some authors for the sake of clarity. The expressions from [6] are reproduced here:

$$k_a^2 = \frac{k^2}{1 - ik[l_v + (\gamma - 1)l_h] - k^2 l_h(\gamma - 1)(l_h - l_v)} \tag{2.18}$$

$$k_h^2 = \frac{ik}{l_h[1 + ik(\gamma - 1)(l_h - l_v)]} \tag{2.19}$$

$$k_v^2 = \frac{ik}{l_v'} \tag{2.20}$$

where l_h, l_v and l_v' have been defined earlier in this section. In this work thermal and acoustic equations will be used with the acoustic pressure in this form:

$$(\Delta + k_a^2)\, p_a = 0 \tag{2.21}$$

$$(\Delta + k_h^2)\, p_h = 0 \tag{2.22}$$

$$where \quad p = p_a + p_h$$

where the thermal pressure p_h and the acoustic pressure p_a will be calculated. The analysis is harmonic.

2.2.4. Boundary conditions

In perfect fluids, a single boundary condition on the pressure or normal velocity suffices to obtain the sound field in the domain analytically or, if that is not feasible, numerically. In the present development more variables are involved, therefore more boundary conditions must be imposed. An acoustic wave with no losses would not be able to satisfy all of them without the existence of viscous and thermal modes. The boundary conditions for an acoustic wave with losses relate all three modes, which are coupled through them. The now more complex acoustic boundary conditions (pressure and velocity) must be supplemented with a thermal boundary condition.

Thermal boundary conditions

In order to fulfill conservation of energy, the normal heat flux and temperature must be continuous at the boundary. Considering that the thermal conductivity of the boundary material is usually much larger than the fluid's, it is possible to simplify these conditions and just state that the temperature variation at the boundary is zero. In the notation adopted here:

$$T = 0 \qquad \textit{at the boundary} \tag{2.23}$$

The temperature variation (T) can be expressed as the sum of acoustic and thermal components, ($T = T_a + T_h$), as explained in the previous sub-section. Besides, the basic equations can be manipulated to find a relation between pressure and temperature. If harmonic variation is assumed and the hypotheses used to simplify the expressions, this boundary condition will link acoustic and thermal pressures:

$$T = T_a + T_h = \tau_a p_a + \tau_h p_h = 0 \tag{2.24}$$

$$\textit{where}: \qquad \tau_a = \frac{\gamma - 1}{\beta\gamma} \frac{1}{1 + i\dfrac{c}{\omega} l_h k_a^2} \qquad \tau_h = \frac{\gamma - 1}{\beta\gamma} \frac{1}{1 + i\dfrac{c}{\omega} l_h k_h^2} \tag{2.25}$$

The parameters τ_a and τ_h depend on the physical properties of the fluid and the frequency. Otherwise they can be considered constant under the assumptions made. Since the total pressure is the sum of the acoustic and thermal components ($p = p_a + p_h$), it is possible to obtain p_a and p_h at the boundary if a pressure boundary condition is given.

Velocity boundary conditions

A fluid with viscosity cannot slide over a boundary surface, that is, its tangential velocity must equal that of the boundary (no-slip condition). In addition, like in perfect fluids, the normal velocity must also be continuous at the boundary. Therefore, the velocity boundary condition can be expressed in a vectorial form:

$$\vec{v}_{boundary} = \vec{v}_a + \vec{v}_h + \vec{v}_v \qquad \text{at the boundary} \tag{2.26}$$

As mentioned before, the viscous velocity $\vec{v}_v$ does not have any associated acoustic pressure; it is only linked to the other components by this boundary condition. On the other hand, considering the irrotational velocity $\vec{v}_l$ is the sum of acoustic and thermal velocities ($\vec{v}_l = \vec{v}_a + \vec{v}_h$), it is possible once again to manipulate the basic equations to obtain the expression:

$$\vec{v}_l = \vec{v}_a + \vec{v}_h = \phi_a \overrightarrow{grad}\, p_a + \phi_h \overrightarrow{grad}\, p_h \tag{2.27}$$

$$where: \qquad \phi_a = \frac{-i}{\rho_o \omega} \frac{1}{1 + i\frac{c}{\omega} l_v k_a^2} \qquad \phi_h = \frac{-i}{\rho_o \omega} \frac{1}{1 + i\frac{c}{\omega} l_v k_h^2} \tag{2.28}$$

Replacing (2.27) in (2.26), the boundary condition becomes:

$$\vec{v}_{boundary} = \phi_a \overrightarrow{grad}\, p_a + \phi_h \overrightarrow{grad}\, p_h + \vec{v}_v \qquad at\ the\ boundary \tag{2.29}$$

where ϕ_a and ϕ_h can be considered constant for a given frequency. This vectorial condition is usually split into normal and tangential components, the latter being a two-dimensional vector expression:

$$v_{boundary,\perp} = \phi_a \frac{\partial p_a}{\partial n} + \phi_h \frac{\partial p_h}{\partial n} + v_{v,\perp} \tag{2.30}$$

$$\vec{v}_{boundary,//} = \phi_a \overrightarrow{grad}_{//}\, p_a + \phi_h \overrightarrow{grad}_{//}\, p_h + \vec{v}_{v,//} \tag{2.31}$$

The subscripts ⊥ and // indicate normal and tangential directions respectively. In many cases, such as a microphone's diaphragm, the boundary moves mainly in the normal direction, therefore eq. (2.31) can be made equal to zero.

2.3. The Boundary Element Method

The Boundary Element Method (BEM) has been chosen as the foundation on which the numerical model with viscous and thermal losses is built. In particular, the formulation utilized is *direct collocation*. This formulation is described here as a basis for further developments.[12,19]

The BEM is based on the Helmholtz Integral Equation (HIE). This equation, in its direct version, relates the pressure and its normal derivative on the domain boundaries, to the pressure at any point in the domain and the pressure of an incoming wave. For this reason, the numerical implementation of the BEM only involves the meshing of the domain boundaries, as opposed to the Finite Element Method (FEM), which is based on the wave equation and demands the discretization of the whole domain.

The HIE is derived from the Helmholtz differential equation:

$$\left(\nabla^2 + k^2\right) p = 0 \tag{2.32}$$

where p is the sound pressure and $k=\omega/c=2\pi f/c$ is the wavenumber. The latter is a function of the frequency f and the speed of sound c. The Helmholtz differential equation is the time-harmonic version of the wave equation that governs acoustic wave motion in fluids.

In principle, the fluid is assumed to be ideal, that is, without losses. In this thesis the expressions that describe the propagation of sound in fluids with losses will be reduced to equations of the Helmholtz form, like (2.32). An adequate treatment of the more complicated boundary conditions will allow the use of the BEM in visco-thermal fluids.

To obtain the expression of the HIE from (2.32), it is needed to define the Green's function *G(R)*, with $R=|r-r_0|$, where r_0 is the position of a point source. *G(R)* is then defined as the solution of the inhomogeneous equation:

$$\left(\nabla^2 + k^2\right) G(R) = -4\pi\,\delta(R) \tag{2.33}$$

The point source located at r_0 has unit strength. There are different solutions of (2.33) for cases like half-space, two-dimensional formulations, and others. We are only concerned here with the three-dimensional free-space solution of *G(R)*, which is:

$$G(R) = \frac{e^{-ikR}}{R} \tag{2.34}$$

After some manipulations of equations (2.32), (2.33) and (2.34), the HIE can be obtained in this form:[36]

$$C(P)\,p(P) = \int_S \left(\frac{\partial G(Q)}{\partial n}\, p(Q) - \frac{\partial p(Q)}{\partial n}\, G(Q) \right) dS + 4\pi\, p^I(P)\,, \tag{2.35}$$

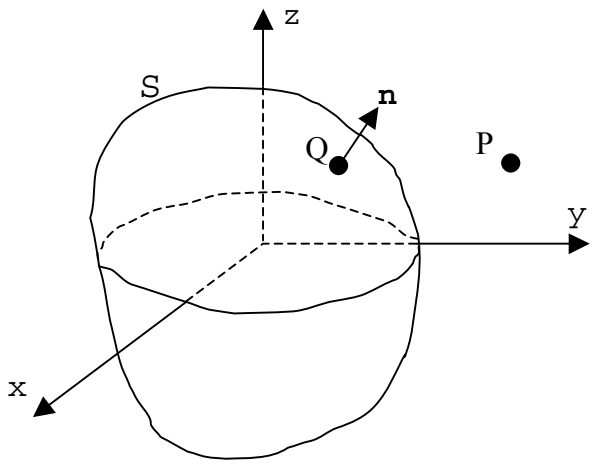

Figure 2-9. Generic integration domain and boundary surface for the HIE.

where S is the surface of the body, Q a point on its surface, P any exterior or interior point and p^I is the incident sound pressure. The factor $C(P)$ is the geometrical constant and represents the exterior solid angle at P. It is calculated using:

$$C(P) = 4\pi + \int_S \frac{\partial}{\partial n}\left(\frac{1}{R}\right) dS \tag{2.36}$$

The expression (2.36) is valid for exterior problems; for interior problems 4π should be subtracted. The normal vector n is directed into the computational domain. This is shown schematically in Figure 2-9 for a case where the integral is defined in the exterior domain. In such cases the so-called Sommerfield condition is satisfied, thus allowing removing the part of the integral defined on the limiting boundary at the infinity. The direct HIE can also be defined in an interior domain, as will be the case in this thesis, if the normal vector is made to point inwards.

In the formulation for ideal fluids, the normal derivative of the pressure in equation (2.35) can be expressed as a function of the normal velocity. We will not take that step since this is not allowed in the formulation with viscous and thermal losses.

If the proper boundary conditions are imposed, equation (2.35) can be solved numerically by discretizing the boundary surface and the acoustic variables defined on it. The procedure is similar to the Finite Element Method: a set of simple shape functions defined in small portions of the surface (the boundary elements) is used to describe both geometry and acoustic variables all over the boundary. There are different kinds of shape functions defined on a variety of element types. The element and shape functions used in our particular case are described in section 4.3. Every element has a number of nodes where the variables are defined and determine their behavior within its surface.

The collocation technique evaluates the pressure at point P in equation (2.35) on the nodes of the surface elements, noted Q. If either the pressure or its normal derivative on the surface are defined as boundary conditions, the result is a system of N equations, where N is the number of nodes on the surface. The system is expressed as:

$$\mathbf{C}\ p_i = \mathbf{A}\ p_i - \mathbf{B}\ \frac{\partial p_i}{\partial n} + 4\pi\ p_i^I \tag{2.37}$$

where the pressures p_i and their normal derivatives are defined on every node *i*. The matrix $\boldsymbol{C}$ is a diagonal matrix containing the *C* constants defined in (2.36) on the nodes. The term on the left-hand side of equation (2.37) is usually subtracted from the first term on the right-hand side, thus obtaining:

$$0 = \mathbf{A}\ p_i - \mathbf{B}\ \frac{\partial p_i}{\partial n} + 4\pi\ p_i^I \tag{2.38}$$

where the new matrix $\boldsymbol{A}$ is the result of subtracting the matrix $\boldsymbol{C}$ from $\boldsymbol{A}$ in (2.37). In the implementation in this thesis, there is no excitation in the form of an incident sound pressure; therefore the last term on the right-hand side of (2.38) is removed. Matrices $\boldsymbol{A}$ and $\boldsymbol{B}$ are in general complex and frequency dependent, and this is a difference with FEM. This is due to the presence of the Green's function, which depends on the wavenumber.

In this way the system can be solved and the values of the pressure and its normal derivative on the surface nodes obtained. With this result it is also possible to obtain the pressure on any point *P* in the domain by calculating new coefficients of the matrices $\boldsymbol{A}'$ and $\boldsymbol{B}'$ and using the discretized version of the Helmholtz Integral Equation:

$$4\pi\ p(P) = \mathbf{A'}\ p_i - \mathbf{B'}\ \frac{\partial p_i}{\partial n} + 4\pi\ p^I(P) \tag{2.39}$$

The HIE can also be solved using the *indirect variational* formulation of the BEM. In this formulation, the HIE is expressed using the so-called single-layer and double-layer potentials instead of the pressure and its normal derivative. The single-layer potential $\sigma(Q)$ is the difference in the normal derivatives of the pressure at both sides of the boundary, while the double-layer potential $\mu(Q)$ is the difference of the pressure at the two sides of the boundary:

$$\sigma(Q) = \frac{\partial p(Q^+)}{\partial n} - \frac{\partial p(Q^-)}{\partial n}$$
$$\mu(Q) = p(Q^+) - p(Q^-) \tag{2.40}$$

The indirect HIE can be solved more efficiently using the variational BEM. This approach consists on the minimization of a functional all over the boundary surface and results in a symmetrical system of equations. The calculation of the system's coefficients is, on the other hand, not as simple computationally as it is using the direct collocation BEM.

It is believed that the boundary conditions needed for the problem of viscous and thermal losses can be handled more efficiently with the direct collocation formulation of the BEM. This formulation has, nevertheless, a difficulty when dealing with close surfaces that will be treated in the next chapter.

However, numerical modeling of visco-thermal fluids could also be grounded on the indirect variational Boundary Element Method or in the Finite Element Method. Two visco-thermal models in the literature use these two approaches.[1,22] They are discussed later in this thesis.

3. MODELING OF CLOSE SURFACES USING BEM

Numerical modeling of condenser microphones poses a problem that has nothing to do with the viscous and thermal losses in the fluid. It is a purely numerical difficulty derived from the particular geometry of these acoustic transducers.

Condenser microphones, as we saw in section 2.1, have a transduction principle based on the capacitance changes of a capacitor formed by a metallic membrane and a backing electrode situated very close behind. The distance between the membrane and the backplate is typically around 20 μm. This means that the ratio smallest/largest dimension of the setup, the so-called *aspect ratio*, is of the order of $2 \cdot 10^{-3}$ for ¼ inch microphones and of 10^{-3} for ½ inch microphones.

The direct collocation BEM formulation is known to have difficulties when surfaces are very close to each other. The modeling of thin bodies is a well known topic in the BEM literature.[29,11,40,27] However, the reciprocal problem, the narrow gap, is only rarely touched upon in the references. The condenser microphone falls into this latter class of problems.

In this chapter the topic is reviewed and a solution is proposed. A paper has been published in the Journal of the Acoustical Society of America that analyzes the subject and presents an implementation of the proposed solution using the axisymmetrical BEM formulation.[13] It is included in Appendix D. This paper is a complete account of the work done, therefore only a synopsis is written in section 3.1. In section 3.2 the implementation of the same solution in three-dimensional BEM is described and some performance tests are presented. Section 3.3 analyzes the use of the formulation for the case of field points that are very close to a boundary surface. Finally section 3.4 is a discussion on the topics treated in the chapter.

3.1. The problem of close surfaces and its implementation in axisymmetrical BEM

The difficulty associated with the modeling of close surfaces using the standard direct collocation BEM formulation is derived from the particular nature of the numerical integration over a boundary element when the collocation point is placed on a very close surface. This effect is shown in Figure 3-1, where the integration is done on the surface S_+ and the collocation point is placed on the very close surface S_-. The calculation of the coefficient matrices in BEM requires, as we saw in 2.3, placing (or *collocating*) the point P on every node of the surface mesh and integrate the equation over all the elements; therefore this situation will arise whenever two domain boundaries are very close.

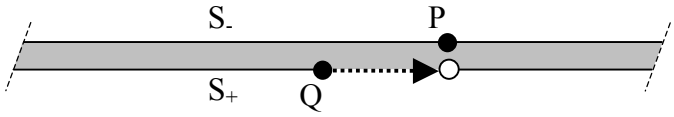

Figure 3-1. The problem of close domain surfaces.

This kind of integral is called *near-singular* because it has a behavior that resembles a singularity, but in fact the integrand is finite within the integration domain. The integral tends, in the limit of zero distance, to a singular integral, and the strength of this near-singularity is proportional to $1/d^2$ for matrix $\boldsymbol{A}$ and to $1/d$ for matrix $\boldsymbol{B}$ in equation (2.38), where d is the distance.

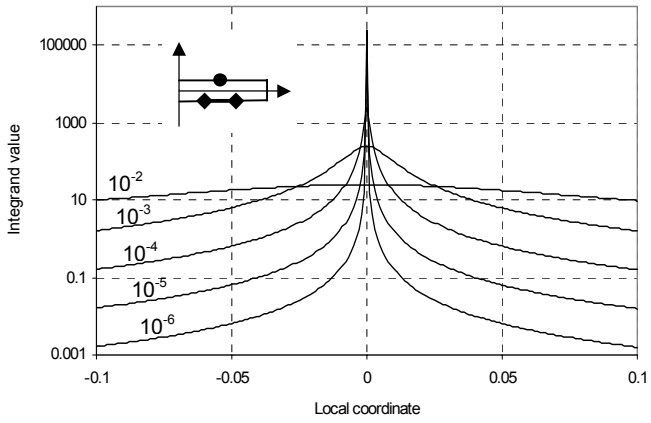

Figure 3-2. Near-singular behavior of an integrand in the thin disc calculation. Abscissas are local coordinates along the element [-1,1], ordinates are values of the integrand on a logarithmic scale. The curves are integrands with a collocation point at 10^{-2}, 10^{-3}, 10^{-4}, 10^{-5}, and 10^{-6} units' distance from the local coordinate 0. The disc radius is one unit. Five linear elements per disc side are used.

Figure 3-2 shows an example of a near-singular integrand for a progressively closer collocation point. The integrand has a perturbation around the projection of the collocation point that is larger the shorter the distance.

The treatment of such near-singular integrals is problematic. If the problem is just ignored, as most standard direct collocation implementations do, there will be a value of the distance between surfaces that will make the numerical integration fail and miss the effect of the collocation point. This is often called in the literature the *thin shape breakdown*.

The thin body and the narrow gap are the two reciprocal cases that present this behavior. In the former the calculation domain is exterior to the close surfaces, while in the latter the domain of interest is the space between the close surfaces. The usual ways to treat the thin body case in the literature are multidomain formulations and formulations using the normal derivative of the pressure.[11,9,29,40,27] These formulations become problematic or impractical when applied to the narrow gap case.

The approach taken in this work is not an analytical removal of the near-singular integral or a re-formulation of the whole problem. It is an improvement of the numerical integration that extends the range of aspect ratios, that is, of distances between close surfaces, where the near-singular integrals can be successfully calculated.

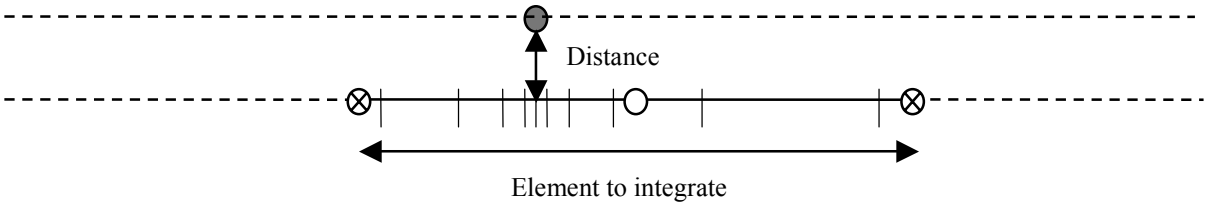

Figure 3-3. Exponential interval division on a one-dimensional quadratic element. Relative distance and local coordinate of the projection of the collocation point are used to calculate the number and sizes of the subintervals.

After some study of the available choices, it was decided to employ an exponential division of the integration domain around the near-singularity. Figure 3-3 shows schematically this

technique for a one-dimensional boundary element. The extra computing cost is not excessive because the technique is only applied when it is needed and the number of divisions is a function of the distance to the collocation point. The processing time was only increased by 10-20% for the axisymmetrical BEM implementation, as shown in Table 3-1.

a)

Gap width	10^{-2}	10^{-3}	10^{-4}	10^{-5}	10^{-6}
Time (s)	82.7	83.0	83.2	82.7	82.6
Result	Good	Fail	Fail	Fail	Fail

b)

Gap width	10^{-2}	10^{-3}	10^{-4}	10^{-5}	10^{-6}
Time (s)	91.4	93.2	93.9	94.4	96.7
Result	Good	Good	Good	Good	Fail

Table 3-1. Processing time results on a DEC Alpha 433 MHz for the axisymmetrical narrow gap test case with 60 elements. a) Gauss-Legendre numerical integration of order 20 and b) the interval division technique are compared.

The benefit of the technique is also clear in Table 3-1. The range of aspect ratios that can be dealt with is extended by three orders of magnitude. This places most practical engineering problems within reach of the improved method, including the condenser microphone that is the subject of this thesis. It can also be applied to other acoustic transducers, like sound intensity probes.[18]

The technique has been tested using an axisymmetrical version of the BEM.[20,19] This formulation is applied to setups that consist of one or more axisymmetrical bodies with the same axis. A cylindrical coordinate system is employed. The boundary conditions and the results of the calculation can be non-axisymmetrical since the acoustic variables are expressed as cosine expansions. In this way only the generator must be discretized, making the process simpler and less costly computationally.

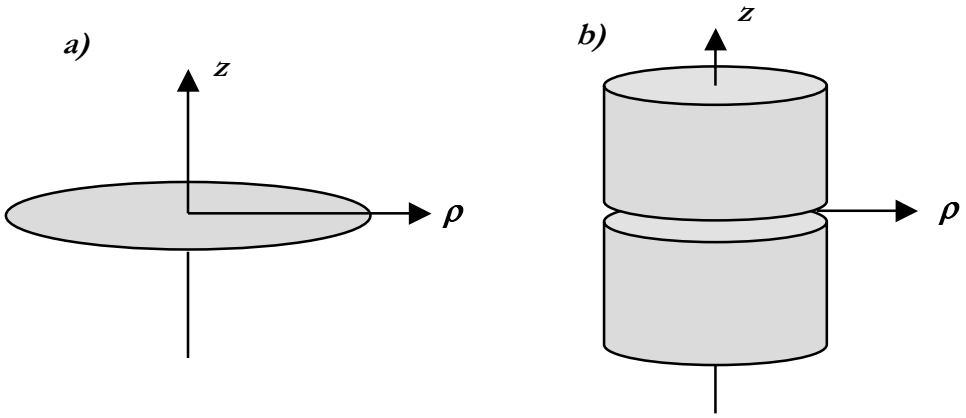

Figure 3-4. Axisymmetrical test cases. a) thin disc, b) narrow gap.

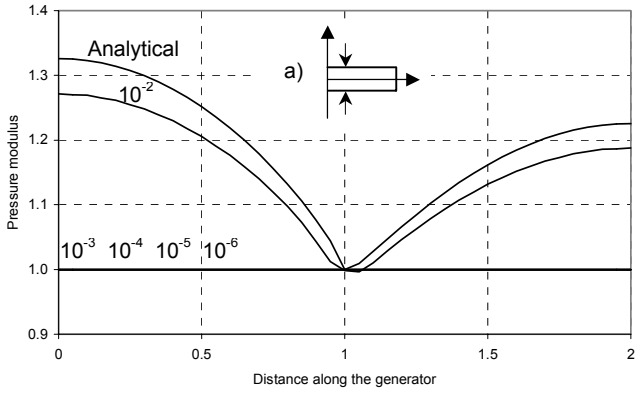

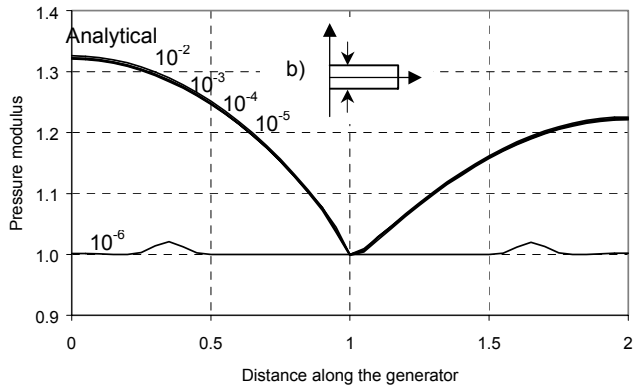

Figure 3-5. Calculated sound pressure modulus on the generator of a disc of variable thickness using 20 elements in total, for different thicknesses. The analytical solution for an infinitely thin disc is also plotted. An axial plane wave of kR=1 and unit amplitude is scattered by the disc. Calculations using a) Gauss-Legendre numerical integration of order 20, b) with interval division.

The test cases are a thin disc and a narrow gap formed by two close cylinders, with the radii normalized to R=1; they are shown in Figure 3-4. Calculations have been run for several frequencies and thicknesses/widths. In this summary we only present the results for the thin disc in Figure 3-5; they are sufficient to demonstrate the performance of the implementations.

The thin disc results are compared with an analytical solution for an infinitely thin disc.[5,16,42] Figure 3-5 shows clearly the benefit of the interval division technique: only discs with a thickness of 10^{-6} fail to give good results, while the standard Gauss-Legendre numerical integration can hardly cope with the 10^{-2} case. The results for the narrow gap case are similar, as shown in Appendix D. The calculations have also demonstrated that this behavior is not very much influenced by the frequency or the mesh density: only the aspect ratio determines the difficulty of the calculation. A convergence study has been performed that proves this statement.

The BEM performance is also influenced by an ill-conditioning of the coefficient matrix when close surfaces are present. This ill-conditioning is a consequence of the nature of the problem and cannot be avoided if the standard direct collocation BEM has to be used. When the BEM is not modified, the above mentioned *thin shape breakdown* has also the effect of reducing the ill-conditioning drastically. This only indicates that the integral is not performed properly and the coefficients of the matrices are not correct, therefore the result is well conditioned, but wrong.

The breakdown observed in the calculation fitted with the interval division integration technique has a different nature. The ill-conditioning of the coefficient matrices increases as the thickness/width decreases, up to a point where the limited precision of the computer makes it unable to solve the system of equations. Figure 3-6 shows the condition number, a measure of the matrix ill-conditioning, for several thicknesses of the disc case and for several mesh densities. One can observe the effect of the *thin shape breakdown* in the calculation with standard integration, a general drop of the condition number. The calculation with interval division integration experiments a logarithmic increase of the condition number the thinner the disc, indicating a correct treatment of the integrands. It is also worth noting that the

condition number in Figure 3-6 b) seems to depend on the aspect ratio only, not the mesh density.

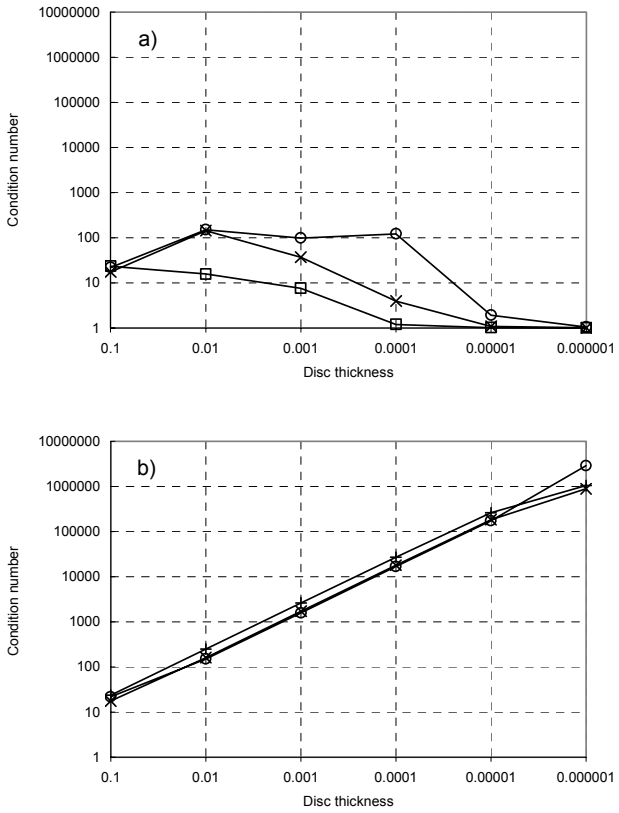

Figure 3-6. Condition number of the coefficient matrix for the thin disc test case, as a function of the thickness. Three mesh densities are plotted: 2 (+), 10 (X) and 60 (O) elements per side. Calculations using a) Gauss-Legendre numerical integration of order 20, b) with interval division. Calculation made with $kR=1$.

3.2. Implementation using three-dimensional BEM

At some stage of the project, it was decided to develop the visco-thermal implementation using the three-dimensional version of the BEM, for reasons discussed later in this thesis. A new implementation of the interval division technique developed for the axisymmetrical BEM was built for the three-dimensional BEM.

In three dimensions, the boundary elements are two-dimensional surface elements. The interval division, or perhaps better called *surface division*, is performed in the present

implementation as presented in Figure 3-7. The element is square and the positions and weights of the integration points are shown.

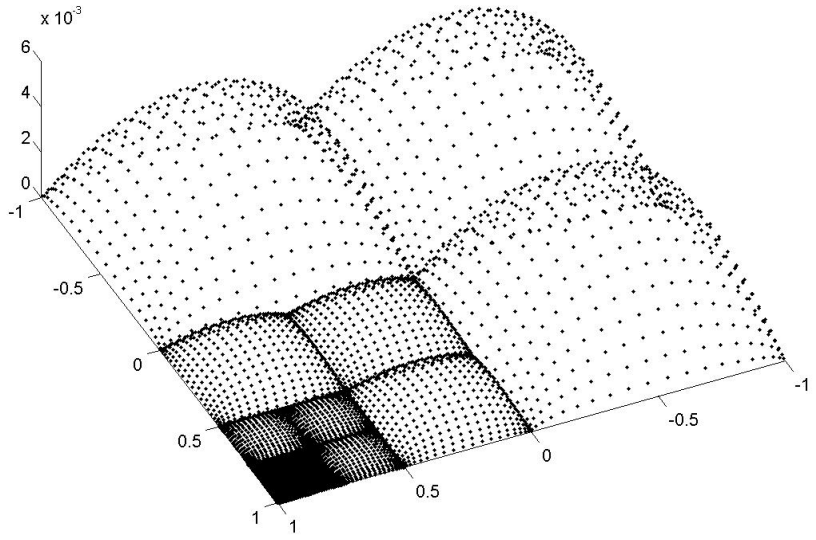

Figure 3-7. Near-singular integration on a square element, showing the positions of the integration points, 20×20 points per division. The x and y axes are the local coordinates and the z coordinate indicates the weights associated with the integration points. The projection of the collocation point is at (1,1).

The surface division has as yet only been programmed for collocation points approaching to the nodal positions, therefore it is required that the meshes of the close surfaces have matching nodes. The elements used are square elements with 4 or 8 nodes. An extension to a general case where the near-singularity is placed anywhere in the element could be possible in further developments.

The problem originated by the near-singularity of the integrals described in section 3.1 is basically the same in three dimensions. Figure 3-8 shows the behavior of a two dimensional near-singular integrand. The situation is equivalent to the case depicted in Figure 3-2 for one-dimensional boundary elements.

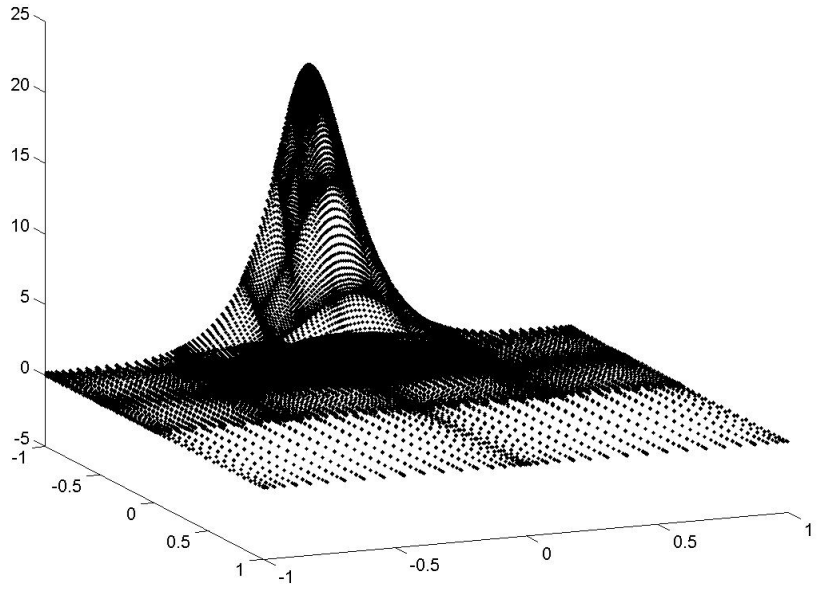

Figure 3-8. Near-singular integrand on a square element with the projection of the collocation point at (0,-1). The values at the integration points before the evaluation of the integral are shown.

This improved version of the three-dimensional BEM has been tested using the rigid thin disc test case. The thin disc mesh is shown in Figure 3-9, where square elements have been employed. As we saw in the previous section, this test case has an analytical solution to compare with.

The results of the calculations for a plane wave coming from the $z+$ direction are plotted in Figure 3-10. The agreement is good, but in this case the range of thicknesses that can be treated successfully using surface division is three orders of magnitude larger than it was with the axisymmetrical BEM: an aspect ratio of 10^{-8} can be dealt with.

The explanation for this increased performance is probably the relative simplicity of the integrands in the three-dimensional BEM, if we compare with the axisymmetrical BEM. In the latter, some mathematical manipulations are needed to solve analytically the part of the integrand that depends on the rotational position.

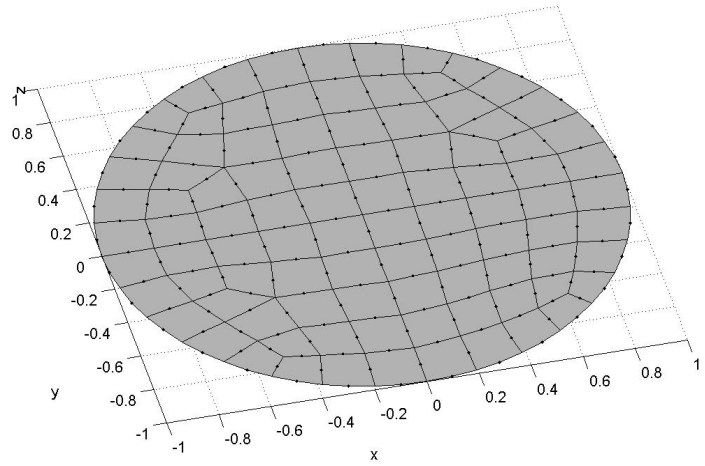

Figure 3-9. Three-dimensional surface mesh of a thin disc. Test case for the near-singular integration technique.

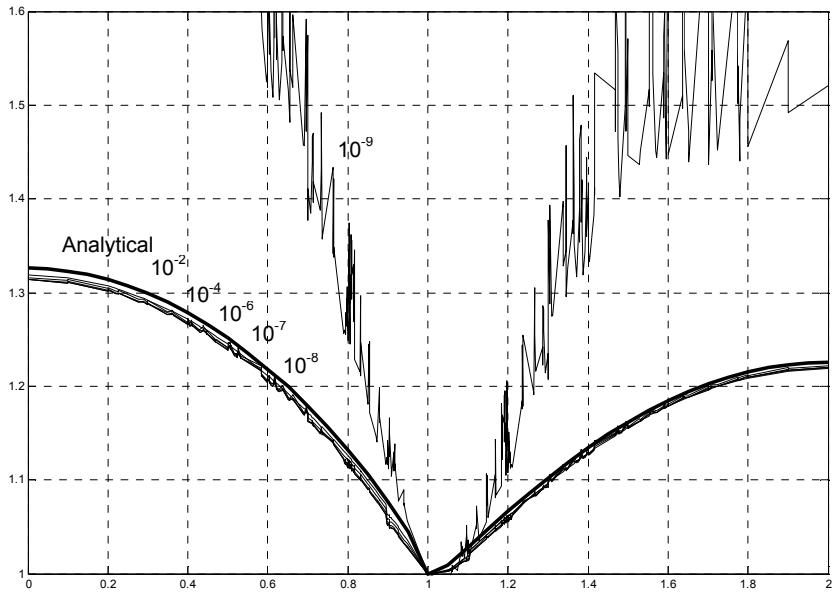

Figure 3-10. Calculated sound pressure modulus on the surface of a three-dimensional disc of variable thickness as a function of the radius, for different thicknesses. The analytical solution for an infinitely thin disc is also plotted with a thicker line. An axial plane wave of kR=1 and unit amplitude is scattered by the disc. The near-singular integral improvement is used.

As we saw, the breakdown of the BEM formulations fitted with the new integration technique is a consequence of the increasing ill-conditioning of the system of equations. Eventually, the limited precision of the computer is not enough to cope with it and fails. In the three-dimensional BEM, the calculations are less demanding, thus allowing the observed wider range of aspect ratios.

3.3. Calculation of the near field

The formulations equipped with interval or surface division are not only able to cope with close surfaces. The calculation of field points that are very close to a boundary surface also benefits from this technique. This application is of importance when the details of the sound field in the vicinity of a surface must be studied. Sound source identification using, for example, sound intensity or nearfield acoustic holography could employ this feature. [26.21]

As an example of the performance of the improved BEM when calculating close field points, the sound pressure in the neighborhood of a rigid sphere of unit radius has been calculated. A plane sound wave coming from the z+ axis is scattered by the sphere. The sound pressure on its surface is presented in Figure 3-11, showing the position of the field points on a line that pierces the sphere's surface. The sound pressure modulus on that line is plotted in Figure 3-12. Note the scale in the abscissas, a range of only 10^{-7} units.

When the surface division technique is used, the pressure is zero inside the sphere, as expected since the calculation domain is exterior. The pressure suddenly rises to the correct value at the other side of the boundary, as it should do. The equivalent calculation without the improved numerical integration shows a complete failure, since the boundary surface is completely missed at this scale.

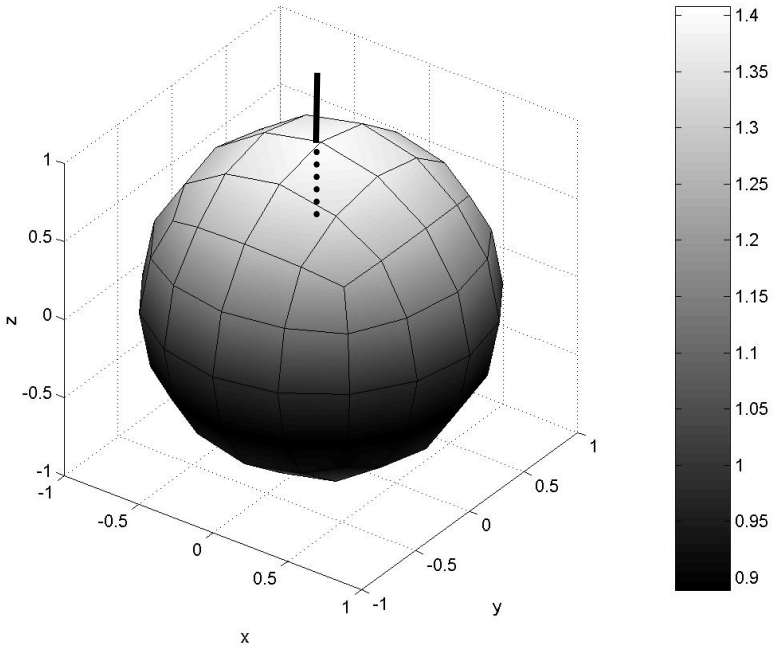

Figure 3-11. Sound pressure modulus on the surface of a rigid sphere of radius R=*1 m with an incident plane wave coming from the z+ direction and k*R=*1. Field points will be calculated along a line on the z axis that crosses the boundary at (0,0,1), as shown.*

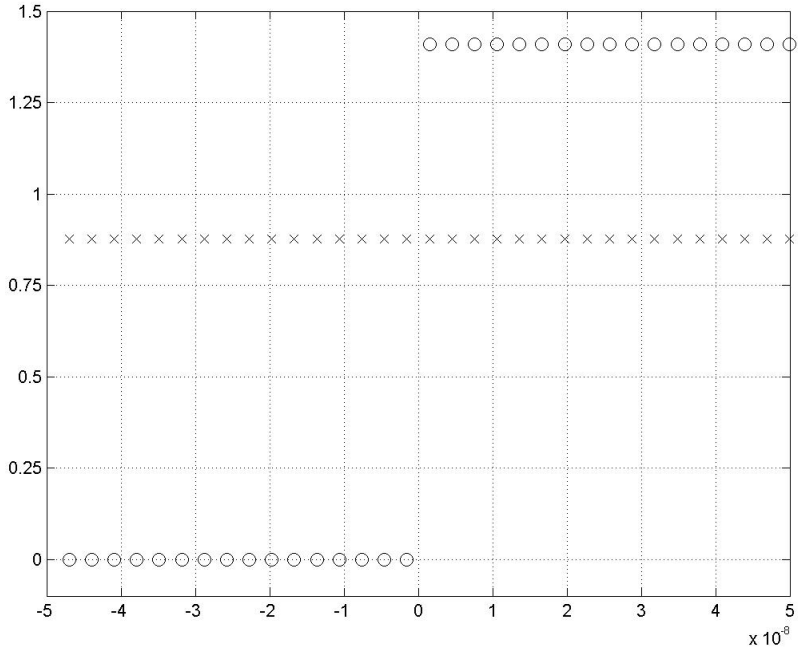

Figure 3-12. Sound pressure modulus calculated on field points in the neighborhood of the surface of the sphere in Figure 3-11. The zero abscissa indicates the position of the boundary at (0,0,1) in Figure 3-11. The improvement of the near-singular integration (circles) and the standard BEM are employed (crosses).

3.4. Discussion

In this chapter a technique has been proposed to overcome the numerical difficulty the BEM has whenever two surfaces are close. The technique has been thoroughly tested using the axisymmetrical BEM formulation. The three-dimensional BEM has also been equipped with this improvement. However, only some tests have been performed in the latter case. It is believed that the conclusions drawn from the axisymmetrical study are applicable to the three-dimensional implementation.

The three-dimensional BEM implementation has been adjusted with the objective of ensuring a good performance. For this reason it is not fully optimized. The calculation of the viscous and thermal modes is more demanding that the ideal fluid equivalent, due to the values of the viscous and thermal wavenumbers. Therefore the thresholds for the automatic near-singular numerical integration and other internal settings have been set with conservative criteria.

An efficient implementation would require a thorough study of the model's performance in a wide range of cases. However, a sufficient number of tests have been run to check the behavior of the method for the cases of interest in this project.

This means that further research on the performance of this formulation is possible and recommended. The calculation of new problems would help to establish this technique as a useful engineering tool.

4. NUMERICAL MODELING OF VISCO-THERMAL FLUIDS

In this chapter the BEM model with viscous and thermal losses for the propagation of sound waves in fluids is described and commented on in detail. This is the central part of the project work where the theory in chapter 2 and the improvements to the BEM in chapter 3 are employed with the purpose of obtaining a working numerical model of a condenser microphone.

We will start with a description of the analytical foundation on which the proposed model is grounded, with a reference to the main precedent, the work by C. Karra. This previous work, together with that of W. M. Beltman, are two of the more successful models in the literature. [1,2,3,23] To the author's knowledge, they are the only ones with a similar objective that have achieved good practical results.

Beltman's work and proposed formulation is not directly related with the development in this thesis but follows a parallel line of research. However, it is obviously relevant here, since it addresses the same physical phenomenon. For this reason it is briefly outlined and discussed in Appendix B.

In the following a formulation will be proposed that includes viscous and thermal effects using the boundary element method. All the important aspects of the development are analyzed. This includes the assembly of the system with viscous and thermal losses and a method to perform a tangential laplacian, needed in the implementation to link tangential and normal boundary conditions for the velocity. The implementation of a coupled membrane is needed to validate the model against the existing analytical model and measurements: the topic is analyzed and a solution is given. The coupled system of equations is described in another section. Finally, the whole implementation is discussed.

4.1. Precedent and analytical development

The main precedent for this project is the doctoral thesis by C. Karra, at Université de Technologie de Compiègne, in France.[22] A number of journal papers and congress communications have also been published as a result of this work.[23,24] The objective of the thesis was the simulation of miniaturized acoustic transducers.

The theoretical background behind Karra's thesis, which is grounded in Bruneau's analysis of visco-thermal fluids already discussed in 2.2, has been analyzed to find ways of extending it and consider viscous losses completely. We will outline here the main features of Karra's formulation. Its description sets into frame the choices made for the present model.

As stated, the theoretical development is taken from Bruneau *et al.*[6] We retake here the discussion about velocity boundary conditions in 2.2.4 and reproduce the expression derived for the normal component of the particle velocity at the boundary (Eq. (2.30)):

$$v_{boundary,\perp} = v_{a,\perp} + v_{h,\perp} + v_{v,\perp} = \phi_a \frac{\partial p_a}{\partial n} + \phi_h \frac{\partial p_h}{\partial n} + v_{v,\perp} \tag{4.1}$$

The first two terms on the right-hand side of this relation constitute the normal component of the irrotational velocity, to which acoustic and thermal modes contribute. The last term $v_{v,\perp}$ is the normal component of the viscous velocity.

The main feature of Karra's development is to assume $v_{v,\perp} = 0$, that is, the normal component of the viscous velocity is neglected. This hypothesis simplifies greatly the calculations because the viscous mode is totally decoupled from the other two, also at the boundaries. The boundary condition for the particle velocity thus becomes:

$$v_{boundary,\perp} = \phi_a \frac{\partial p_a}{\partial n} + \phi_h \frac{\partial p_h}{\partial n} \tag{4.2}$$

which is only a function of the two components of the gradient of the pressure. On the other hand, the pressure boundary condition remains as shown in 2.2.4. Equation (2.11) describing the behavior of the viscous mode is no longer needed, only the pressure is calculated starting with the integral form of equations (2.21) and (2.22).

The numerical implementation is made using an indirect variational formulation of the boundary element method. This formulation has some advantages over the direct collocation formulation. The coefficient matrices are symmetric and the singular integrals are treated analytically. However, it is not very clear whether the near-singular integrals described in chapter 3 are effectively removed or just dealt with. The aspect ratio (relation largest/smallest dimensions) of the setups calculated by Karra is about 10^{-2}, which is still large enough for BEM formulations with conventional numerical integration techniques to handle if a sufficient element density is used.

Furthermore, the final implementation is achieved by means of an axisymmetrical formulation similar to the direct collocation version employed in chapter 3. This allows a much simpler meshing and reduces the computational load. It is the obvious choice for circular microphones with no holes in the backplate, like the miniaturized transducers addressed by Karra's work. However, non-axisymmetrical geometries like microphone backplates with holes or non-circular microphones (like MEMS microphones) would need a three-dimensional version. The implementation could in principle be redone using a three-dimensional BEM code as a basis, at the cost of a complete rebuild.

The membrane is modeled using the Finite Element Method, implemented in a separate program. The coefficient matrices obtained for the membrane are coupled to the rest by means of a least squares minimization.

This work is significant because it is the first serious attempt to implement the theoretical framework laid down by Bruneau *et al.*; it includes thermal losses and there is good agreement with the corresponding analytical models with thermal losses when viscosity effects are removed. The model retains generality and opens paths to be explored; it clearly allows further extensions on the same foundation.

The extension we propose here will be outlined in the following, describing the analytical development that leads to an expression for the normal component of the viscous velocity. A similar development will be repeated in section 4.2 using the BEM implementations of acoustic, thermal and viscous modes.

In order to incorporate the viscous velocity into the model, we must link it with the sound pressure. The tangential part of the vectorial velocity condition must be taken into account. We rewrite here equation (2.31):

$$\vec{v}_{boundary,//} = \phi_a \overrightarrow{grad}_{//} p_a + \phi_h \overrightarrow{grad}_{//} p_h + \vec{v}_{v,//} \tag{4.3}$$

Equation (4.1) above is the normal component and (4.3) is the tangential component of the velocity boundary condition. As we saw, the approach by Karra includes a hypothesis that makes $v_{v,\perp} = 0$, therefore the viscous velocity is not considered. In our formulation $v_{v,\perp}$ is linked to the tangential boundary condition. We recall that the viscous velocity has by definition a null divergence:

$$div\,\vec{v}_v = 0 \tag{4.4}$$

This can be expressed in local coordinates at the boundary in this way:

$$\frac{\partial v_{v,\perp}}{\partial n} + div_{//}\,\vec{v}_{v,//} = 0 \tag{4.5}$$

We assume as well that the boundary does not move in the tangential direction, therefore equation (4.3) can be made equal to zero ($\vec{v}_{boundary,//} = 0$). Applying the differential operator ∇ in the tangential directions on equation (4.3):

$$-div_{//}\,\vec{v}_{v,//} = \phi_a \Delta_{//} p_a + \phi_h \Delta_{//} p_h \tag{4.6}$$

Combining eqs. (4.5) and (4.6) with the thermal boundary condition, eq. (2.24), gives

$$\frac{\partial v_{v,\perp}}{\partial n} = \left(\phi_a - \phi_h \frac{\tau_a}{\tau_h} \right) \Delta_{//}\, p_a \tag{4.7}$$

Equation (4.7) links the acoustic pressure and normal viscous velocity, needed in the boundary condition (4.1) if viscous losses are considered. The numerical implementation does not have to consider explicitly the tangential components of the viscous velocity.

However, to make the solution completely general the geometry of the problem must be included in the development so as to obtain a local coordinate system from the global coordinates.[10,6] Alternatively, one can take advantage of the geometrical characteristics of the setup and the coordinate system; this will be the approach in this thesis.

4.2. Numerical implementation

In order to produce a numerical implementation for the problem under study it is necessary to combine the theoretical developments in 2.2 about thermal and viscous losses in fluids with the three-dimensional boundary element method described in 2.3. A system of equations will be assembled that takes losses into account.

Let us reproduce again the equations describing acoustic, thermal and viscous modes, and the boundary conditions that link them at the boundary. In the following discussion harmonic variation $e^{-i\omega t}$ is assumed. The differential equations are:

$$\left.\begin{aligned} &\left(\Delta + k_a^2\right) p_a = 0 \\ &\left(\Delta + k_h^2\right) p_h = 0 \end{aligned}\right\} \quad \text{where } p = p_a + p_h$$
$$\left(\Delta + k_v^2\right) \vec{v}_v = \vec{0}, \quad \text{where } div\, \vec{v}_v = 0 \tag{4.8}$$

governing acoustic pressure p_a, thermal pressure p_h and viscous velocity $\vec{v}_v$ respectively. These equations are of the Helmholtz form. The expressions for the wavenumbers k_a, k_h and k_v are

given in equations (2.18), (2.19) and (2.20); here we assume that they are constant at any given frequency. The value of k_a is similar to ω/c, the perfect fluid wavenumber. The other two have large values and are complex, indicating a fast decay of thermal and viscous modes. Note again that the viscous velocity has no pressure associated.

The viscous velocity equation is a vector equation; therefore it can be split into three scalar equations in a Cartesian coordinate system:

$$\left(\Delta + k_v^2\right)\vec{v}_v = \vec{0}, \quad \begin{cases} \left(\Delta + k_v^2\right)v_{vx} = 0 \\ \left(\Delta + k_v^2\right)v_{vy} = 0 \\ \left(\Delta + k_v^2\right)v_{vz} = 0 \end{cases} \tag{4.9}$$

The thermal boundary condition relates thermal and acoustic pressures in this way:

$$T = T_a + T_h = \tau_a p_a + \tau_h p_h = 0 \tag{4.10}$$

The continuity of the velocity provides a coupling of all three modes at the boundary:

$$\begin{aligned} \vec{v}_{boundary} &= \phi_a \overrightarrow{grad}\, p_a + \phi_h \overrightarrow{grad}\, p_h + \vec{v}_v \\ &\Rightarrow \begin{cases} v_{boundary,\perp} = \phi_a \dfrac{\partial p_a}{\partial n} + \phi_h \dfrac{\partial p_h}{\partial n} + v_{v,\perp} \\ \vec{v}_{boundary,//} = \phi_a \overrightarrow{grad}_{//}\, p_a + \phi_h \overrightarrow{grad}_{//}\, p_h + \vec{v}_{v,//} \end{cases} \end{aligned} \tag{4.11}$$

We have separated again the normal and the tangential directions at the boundary, as we did in 2.2. If the model should be completely general, the definition of the velocity boundary condition relative to the boundary surface must be linked to the global coordinate system through a transformation that takes the geometry of the problem into account. This is expressed analytically in [6].

However, in a microphone the losses occur in a flat thin layer of air behind the diaphragm. We will take advantage of this fact and make the air layer normal to the z-axis. Figure 4-1

describes a generic microphone geometry with a cavity around the gap, formed by a diaphragm and a backplate. The shape of the cavity is simpler than in a real microphone but it is expected to have a comparable effect.

In such a geometry the viscous and thermal losses in the surrounding annular cavity may be considered negligible, and therefore concentrated in the thin air gap. The x-y coordinates are tangential to the gap's internal surfaces while the z coordinate is normal. The viscous mode will only be calculated inside the gap, simplifying greatly the implementation.

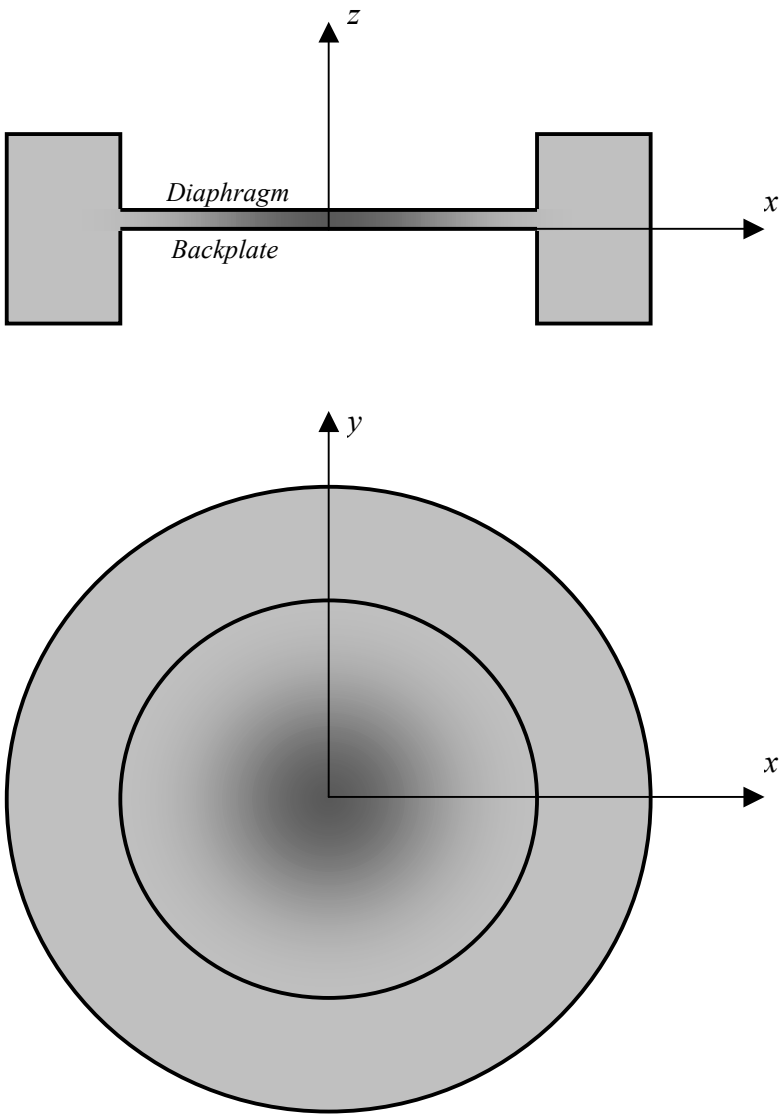

Figure 4-1. Side and top view of a generic microphone geometry.

Let us write now the equations directly in a matrix form, according to the development in 2.3. Equations (4.8) can then be expressed in the same manner as (2.38). There is no incident pressure in the interior of the microphone; the excitation is the movement of the diaphragm. We have:

$$\begin{aligned} \mathbf{A_a} p_a - \mathbf{B_a} \frac{\partial p_a}{\partial n} &= 0 \\ \mathbf{A_h} p_h - \mathbf{B_h} \frac{\partial p_h}{\partial n} &= 0 \\ \mathbf{A_v} \vec{v}_v - \mathbf{B_v} \frac{\partial \vec{v}_v}{\partial n} &= \vec{0} \end{aligned} \tag{4.12}$$

The subscripts *a*, *h* and *v* denote, as before, acoustic, thermal and viscous modes. The matrices *A* and *B* are as described in 2.3. The vector equation for the viscous velocity $\vec{v}_v = \vec{v}_{vx}\hat{x} + \vec{v}_{vy}\hat{y} + \vec{v}_{vz}\hat{z}$, the third of (4.12), can be split into:

$$\begin{aligned} \mathbf{A_v} v_{vx} - \mathbf{B_v} \frac{\partial v_{vx}}{\partial n} &= 0 \\ \mathbf{A_v} v_{vy} - \mathbf{B_v} \frac{\partial v_{vy}}{\partial n} &= 0 \\ \mathbf{A_v} v_{vz} - \mathbf{B_v} \frac{\partial v_{vz}}{\partial n} &= 0 \end{aligned} \tag{4.13}$$

With the geometrical assumption mentioned above, the z-component of the viscous velocity has the same direction as the normal vector *n* for the nodes on the gap surfaces. We can express this with the relation:

$$v_{vz} = \pm v_{v,\perp} = \pm \frac{v_{vn}}{|\mathrm{n}|} \quad \text{in the gap} \tag{4.14}$$

The sign is different on the two sides of the gap, and we normalize by the length of the normal vector. Note also that we call the normal component of the viscous velocity at the surface $v_{v,\perp}$ when it is expressed in global coordinates and v_{vn} when it is based on the local coordinates. We define this local coordinate system relative to the boundary as (ξ,ζ,n) where *n*

is the normal coordinate and the other two are tangential to the surface. By definition the divergence of $\vec{v}_v$ is zero, or, in the local coordinates:

$$\frac{\partial v_{vn}}{\partial n} + \frac{\partial v_{v\xi}}{\partial \xi} + \frac{\partial v_{v\zeta}}{\partial \zeta} = 0 \tag{4.15}$$

where we assume that the surface is flat and the local coordinates are Cartesian; this is our case in the gap. We can then formulate the third equation of (4.13) as:

$$\mathbf{A}_\mathbf{v} v_{vn} + \mathbf{B}_\mathbf{v}\left[\frac{\partial v_{v\xi}}{\partial \xi} + \frac{\partial v_{v\zeta}}{\partial \zeta}\right] = 0 \tag{4.16}$$

It is possible as well to obtain an expression for the local tangential components of the viscous velocity as a function of the pressure, using the tangential velocity boundary condition:

$$\begin{aligned} &\phi_a \overrightarrow{grad}_{//}\, p_a + \phi_h \overrightarrow{grad}_{//}\, p_h + \vec{v}_{v,//} = 0 \quad \Rightarrow \begin{cases} \phi_a \dfrac{\partial p_a}{\partial \xi} + \phi_h \dfrac{\partial p_h}{\partial \xi} + v_{v\xi} = 0 \\ \phi_a \dfrac{\partial p_a}{\partial \zeta} + \phi_h \dfrac{\partial p_h}{\partial \zeta} + v_{v\zeta} = 0 \end{cases} \\ &\Rightarrow \begin{cases} v_{v\xi} = -\dfrac{\partial}{\partial \xi}\left[\phi_a p_a + \phi_h p_h\right] \\ v_{v\zeta} = -\dfrac{\partial}{\partial \zeta}\left[\phi_a p_a + \phi_h p_h\right] \end{cases} \end{aligned} \tag{4.17}$$

where the tangential direction denoted by the symbol // is represented by the (ξ,ζ) coordinates. Combining equations (4.16), (4.14) and (4.17) an expression for the normal component of the viscous velocity as a function of the pressures is found:

$$\begin{aligned} v_{vn} &= \mathbf{A}_\mathbf{v}^{-1}\mathbf{B}_\mathbf{v}\left[\frac{\partial^2}{\partial \xi^2}\left(\phi_a p_a + \phi_h p_h\right) + \frac{\partial^2}{\partial \zeta^2}\left(\phi_a p_a + \phi_h p_h\right)\right] \\ \Rightarrow \quad v_{v,\perp} &= \frac{1}{|n|}\mathbf{A}_\mathbf{v}^{-1}\mathbf{B}_\mathbf{v}\Delta_{//}\left(\phi_a p_a + \phi_h p_h\right) \end{aligned} \tag{4.18}$$

where we define the tangential laplacian operator $\Delta_{//}$. This operator will be treated in the next section. Equation (4.18) is equivalent to (4.7) in section 4.1, but we have managed now to reduce the viscous mode term to local coordinates using the particular geometry of the gap. In the general case, a tangential laplacian in global coordinates would be necessary.

It is now possible to assemble a system of equations with the acoustic pressure as unknown. We take the equations for the acoustic and thermal pressures in (4.12) and the expression just obtained for the normal component of the viscous velocity (4.18) and replace them on the normal velocity boundary condition in (4.11).

$$v_{boundary,\perp} = \phi_a \mathbf{B}_\mathbf{a}^{-1}\mathbf{A}_\mathbf{a} p_a - \phi_h \mathbf{B}_\mathbf{h}^{-1}\mathbf{A}_\mathbf{h} p_h + \frac{1}{|n|}\mathbf{A}_\mathbf{v}^{-1}\mathbf{B}_\mathbf{v}\Delta_{//}\left(\phi_a p_a + \phi_h p_h\right) \qquad (4.19)$$

We use now the remaining equation: the thermal boundary condition that links acoustic and thermal pressures, $T = T_a + T_h = \tau_a p_a + \tau_h p_h = 0$, and finally we arrive to:

$$v_{boundary,\perp} = \left[\phi_a \mathbf{B}_\mathbf{a}^{-1}\mathbf{A}_\mathbf{a} - \phi_h \mathbf{B}_\mathbf{h}^{-1}\mathbf{A}_\mathbf{h}\frac{\tau_a}{\tau_h} + \frac{1}{|n|}\mathbf{A}_\mathbf{v}^{-1}\mathbf{B}_\mathbf{v}\Delta_{//}\left(\phi_a - \phi_h\frac{\tau_a}{\tau_h}\right)\right] p_a \qquad (4.20)$$

The coefficient matrix of this system of equations has three parts, the three terms on the right-hand side of (4.20), which correspond respectively to acoustic, thermal and viscous modes. The system of equations relates acoustic pressure and velocity on the boundary; it is therefore possible to specify any of the two acoustic variables at the boundary and calculate the other. However, the viscous term is only defined inside the gap, according to the geometrical assumption just described. To complete the model of a condenser microphone, the diaphragm must be coupled to the interior. An analytical representation of the membrane will be developed in section 4.4.

The thermal pressure and the normal components of acoustic velocity, thermal velocity and viscous velocity at the boundary can be obtained from the acoustic pressure using respectively:

$$p_h = \frac{\tau_a}{\tau_h} p_a \tag{4.21}$$

$$v_{a,\perp} = \phi_a \mathbf{B_a^{-1}} \mathbf{A_a} p_a \tag{4.22}$$

$$v_{h,\perp} = -\phi_h \mathbf{B_h^{-1}} \mathbf{A_h} \frac{\tau_a}{\tau_h} p_a \tag{4.23}$$

$$v_{v,\perp} = \mathbf{A_v^{-1}} \mathbf{B_v} \Delta_{//} \left(\phi_a - \phi_h \frac{\tau_a}{\tau_h} \right) p_a \tag{4.24}$$

The tangential components of the velocity at the boundary could be calculated by taking a discrete tangential gradient of the acoustic pressure at the boundary, as indicated by the tangential part of the velocity boundary condition (4.11). We will not go further in this direction because these components are not required to test the goodness of the implementation; a discrete tangential gradient could be developed in a similar manner as the tangential laplacian described in 4.3.

With the calculated results at the boundary it is possible to obtain any acoustic variable on any field point in the domain, the interior of the microphone. To do this, new coefficients of the BEM matrices must be calculated and used, together with the solution on the boundary. It is a direct application of the general expression of the Helmholtz integral equation in its discretized form.

If thermal and viscous losses are removed, the system (4.20) reduces to the known form of the Boundary Element Method for perfect fluids with no incident pressure term:

$$v_{boundary,\perp} = \phi_a \mathbf{B_a^{-1}} \mathbf{A_a} p_a \quad \text{or} \quad \mathbf{A}p + ik\rho_0 c\, v_{boundary,\perp} \mathbf{B} = 0 \tag{4.25}$$

In the perfect fluid formulation it sometimes happens that velocity boundary conditions are discontinuous, having two values on the same node belonging to two elements. It must be noted that in a formulation with losses the acoustic variables must be continuous anywhere on the boundary surface, as follows from the vectorial boundary condition for the velocity (4.11).

Non-smoothness of the boundary (i.e. sharp edges) would result in a rapidly varying velocity vector, therefore instability of the calculation.

The phenomenon is shown graphically in Figure 4-2. This problem is not addressed in this project, although it is suspected to have certain effect on a microphone. Measurements done on Brüel & Kjær microphones show that the finishing of the backplate rim and holes has an influence on the device's frequency response. This could be handled by means of small elements on the edge to model the edge shape, if that was necessary.

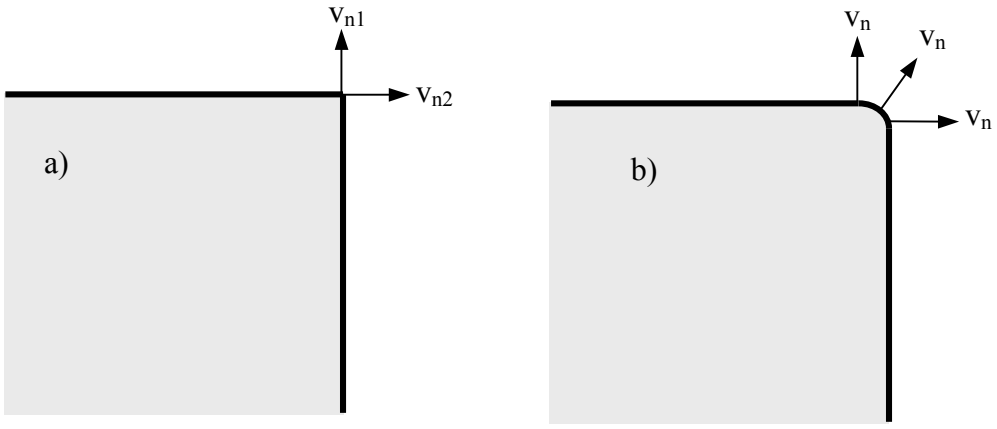

Figure 4-2. Geometrical singularity caused by a sharp edge, a) as seen by a perfect-fluid formulation and b) as it should be when visco-thermal losses are taken into account.

4.3. The discrete tangential laplacian

The matrix equation assembled in the previous section includes a discrete tangential laplacian operator. We will propose here a formulation that uses the values of the acoustic variable on the nodes of the existing boundary element mesh. In this way the system of equations can be assembled easily, although this restriction will limit the quality of the numerical laplacian approximation.

From the theory of finite and boundary element methods we know that the shape functions model the variations of the geometry or the variables within the elements.[43] In general, geometry and variables have a different set of shape functions. For isoparametric formulations, like the one employed in this project, the same shape functions are used for both purposes; we will assume then an isoparametric implementation for the sake of simplicity.

Let us call the shape functions $N_i(\xi,\zeta)$, where (ξ,ζ) are the local coordinates in a surface element. In a general case, we could have another number of local coordinates. It is possible to express the variation of the magnitudes (i.e. acoustic pressure) as a function of the local coordinates in this way:

$$p(\xi,\zeta) = \sum_{i=1}^{n} N_i(\xi,\zeta)\, p_i \tag{4.26}$$

where n is the number of nodes and p_i are the nodal values of the acoustic pressure. In a similar manner it is also possible to express the global coordinates as a function of the local coordinates through the shape functions, like this:

$$\begin{aligned} x &= \sum_{i=1}^{n} N_i(\xi,\zeta) x_i \\ y &= \sum_{i=1}^{n} N_i(\xi,\zeta) y_i \\ z &= \sum_{i=1}^{n} N_i(\xi,\zeta) z_i \end{aligned} \tag{4.27}$$

where x_i, y_i and z_i are the positions of the nodes in global coordinates. Since we assume an isoparametric formulation, the same shape functions appear in (4.26) and (4.27).

Going back to our problem, it is possible to obtain an expression for the tangential laplacian in local coordinates taking second partial derivatives of (4.26):

$$\begin{aligned}\Delta_{//} p(\xi,\zeta) &= \left[\frac{\partial^2 p(\xi,\zeta)}{\partial \xi^2} + \frac{\partial^2 p(\xi,\zeta)}{\partial \zeta^2}\right] = \\ &= \left[\sum_{i=1}^{n} \frac{\partial^2 N_i(\xi,\zeta)}{\partial \xi^2} p_i + \sum_{i=1}^{n} \frac{\partial^2 N_i(\xi,\zeta)}{\partial \zeta^2} p_i\right]\end{aligned} \tag{4.28}$$

We are only interested in the values of the tangential laplacian at the nodal positions, in order to use it in the system of equations. Therefore, the local coordinates (ξ,ζ) can be particularized at the nodes. It is possible to express this in a matrix form:

$$\begin{pmatrix} \Delta_{//} p(\xi_1,\zeta_1) \\ \Delta_{//} p(\xi_2,\zeta_2) \\ \vdots \\ \Delta_{//} p(\xi_n,\zeta_n) \end{pmatrix} = \begin{pmatrix} \frac{\partial^2 N_1(\xi_1,\zeta_1)}{\partial \xi^2} + \frac{\partial^2 N_1(\xi_1,\zeta_1)}{\partial \zeta^2} & \cdots & \frac{\partial^2 N_n(\xi_1,\zeta_1)}{\partial \xi^2} + \frac{\partial^2 N_n(\xi_1,\zeta_1)}{\partial \zeta^2} \\ \vdots & \ddots & \vdots \\ \frac{\partial^2 N_1(\xi_n,\zeta_n)}{\partial \xi^2} + \frac{\partial^2 N_1(\xi_n,\zeta_n)}{\partial \zeta^2} & \cdots & \frac{\partial^2 N_n(\xi_n,\zeta_n)}{\partial \xi^2} + \frac{\partial^2 N_n(\xi_n,\zeta_n)}{\partial \zeta^2} \end{pmatrix} \begin{pmatrix} p_1 \\ p_2 \\ \vdots \\ p_n \end{pmatrix} \tag{4.29}$$

where $(\xi_1,\zeta_1)\ldots(\xi_n,\zeta_n)$ are the local coordinates of the nodes. This matrix has a fixed numeric value for any given element type. As an example, in this project we have used a quadrilateral isoparametric surface element with $n=8$ nodes, as shown in Figure 4-3. The shape functions in this case are:

$$\begin{aligned} N_1(\xi,\zeta) &= \frac{1}{4}(1-\xi)(1-\zeta)(-\xi-\zeta-1) \\ N_2(\xi,\zeta) &= \frac{1}{4}(1+\xi)(1-\zeta)(\xi-\zeta-1) \\ N_3(\xi,\zeta) &= \frac{1}{4}(1+\xi)(1+\zeta)(\xi+\zeta-1) \\ N_4(\xi,\zeta) &= \frac{1}{4}(1-\xi)(1+\zeta)(-\xi+\zeta-1) \\ N_5(\xi,\zeta) &= \frac{1}{2}(1-\xi^2)(1-\zeta) \\ N_6(\xi,\zeta) &= \frac{1}{2}(1-\zeta^2)(1+\xi) \\ N_7(\xi,\zeta) &= \frac{1}{2}(1-\xi^2)(1+\zeta) \\ N_8(\xi,\zeta) &= \frac{1}{2}(1-\zeta^2)(1-\xi) \end{aligned} \tag{4.30}$$

Taking second partial derivatives with respect to ξ and ζ we obtain:

$$\begin{aligned}
\frac{\partial^2 N_1(\xi,\zeta)}{\partial\xi^2} &= \frac{1}{2}(1-\zeta) & \frac{\partial^2 N_5(\xi,\zeta)}{\partial\xi^2} &= (\zeta-1)\\
\frac{\partial^2 N_2(\xi,\zeta)}{\partial\xi^2} &= \frac{1}{2}(1-\zeta) & \frac{\partial^2 N_6(\xi,\zeta)}{\partial\xi^2} &= 0\\
\frac{\partial^2 N_3(\xi,\zeta)}{\partial\xi^2} &= \frac{1}{2}(1+\zeta) & \frac{\partial^2 N_7(\xi,\zeta)}{\partial\xi^2} &= (\zeta-1)\\
\frac{\partial^2 N_4(\xi,\zeta)}{\partial\xi^2} &= \frac{1}{2}(1+\zeta) & \frac{\partial^2 N_8(\xi,\zeta)}{\partial\xi^2} &= 0
\end{aligned} \tag{4.31}$$

$$\begin{aligned}
\frac{\partial^2 N_1(\xi,\zeta)}{\partial\zeta^2} &= \frac{1}{2}(1-\xi) & \frac{\partial^2 N_5(\xi,\zeta)}{\partial\zeta^2} &= 0\\
\frac{\partial^2 N_2(\xi,\zeta)}{\partial\zeta^2} &= \frac{1}{2}(1+\xi) & \frac{\partial^2 N_6(\xi,\zeta)}{\partial\zeta^2} &= (-1-\xi)\\
\frac{\partial^2 N_3(\xi,\zeta)}{\partial\zeta^2} &= \frac{1}{2}(1+\xi) & \frac{\partial^2 N_7(\xi,\zeta)}{\partial\zeta^2} &= 0\\
\frac{\partial^2 N_4(\xi,\zeta)}{\partial\zeta^2} &= \frac{1}{2}(1-\xi) & \frac{\partial^2 N_8(\xi,\zeta)}{\partial\zeta^2} &= (-1-\xi)
\end{aligned} \tag{4.32}$$

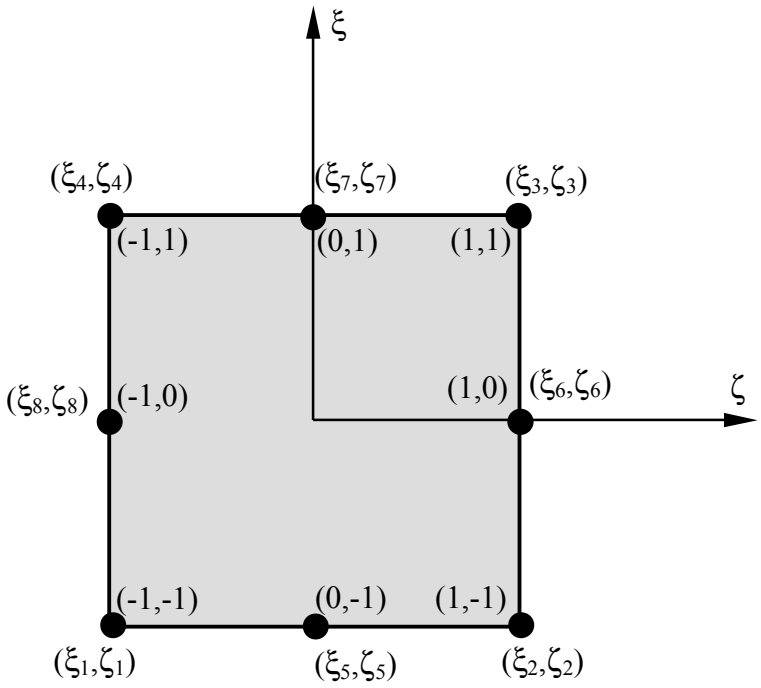

Figure 4-3. Local geometry of a quadrilateral surface element with 8 nodes.

For the element in Figure 4-3, the matrix expression of the tangential laplacian in local coordinates would be:

$$\begin{pmatrix} \Delta_{//} p(\xi_1,\zeta_1) \\ \Delta_{//} p(\xi_2,\zeta_2) \\ \Delta_{//} p(\xi_3,\zeta_3) \\ \Delta_{//} p(\xi_4,\zeta_4) \\ \Delta_{//} p(\xi_5,\zeta_5) \\ \Delta_{//} p(\xi_6,\zeta_6) \\ \Delta_{//} p(\xi_7,\zeta_7) \\ \Delta_{//} p(\xi_8,\zeta_8) \end{pmatrix} = \begin{pmatrix} 2 & 1 & 0 & 1 & -2 & 0 & 0 & -2 \\ 1 & 2 & 1 & 0 & -2 & -2 & 0 & 0 \\ 0 & 1 & 2 & 1 & 0 & -2 & -2 & 0 \\ 1 & 0 & 1 & 2 & 0 & 0 & -2 & -2 \\ 1.5 & 1.5 & 0.5 & 0.5 & -2 & -1 & 0 & -1 \\ 0.5 & 1.5 & 1.5 & 0.5 & -1 & -2 & -1 & 0 \\ 0.5 & 0.5 & 1.5 & 1.5 & 0 & -1 & -2 & -2 \\ 1.5 & 0.5 & 0.5 & 1.5 & -1 & 0 & -1 & -2 \end{pmatrix} \begin{pmatrix} p_1 \\ p_2 \\ p_3 \\ p_4 \\ p_5 \\ p_6 \\ p_7 \\ p_8 \end{pmatrix} \tag{4.33}$$

In the general case described in 4.1 a tangential laplacian as a function of the global coordinates would be needed. To do this, the Jacobian matrix should be used. The Jacobian matrix for second partial derivatives in the case of an element with three coordinates is:

$$J = \begin{pmatrix} \sum_{i=1}^{n} \frac{\partial^2 N_i(\xi,\zeta,n)}{\partial \xi^2} x_i & \sum_{i=1}^{n} \frac{\partial^2 N_i(\xi,\zeta,n)}{\partial \xi^2} y_i & \sum_{i=1}^{n} \frac{\partial^2 N_i(\xi,\zeta,n)}{\partial \xi^2} z_i \\ \sum_{i=1}^{n} \frac{\partial^2 N_i(\xi,\zeta,n)}{\partial \zeta^2} x_i & \sum_{i=1}^{n} \frac{\partial^2 N_i(\xi,\zeta,n)}{\partial \zeta^2} y_i & \sum_{i=1}^{n} \frac{\partial^2 N_i(\xi,\zeta,n)}{\partial \zeta^2} z_i \\ \sum_{i=1}^{n} \frac{\partial^2 N_i(\xi,\zeta,n)}{\partial n^2} x_i & \sum_{i=1}^{n} \frac{\partial^2 N_i(\xi,\zeta,n)}{\partial n^2} y_i & \sum_{i=1}^{n} \frac{\partial^2 N_i(\xi,\zeta,n)}{\partial n^2} z_i \end{pmatrix} \tag{4.34}$$

The coefficients of the matrix on the right-hand side of (4.29) can be converted to partial derivatives with respect to global coordinates using the inverse of the Jacobian matrix (4.34).[43] In practice we will not perform this transformation due to the difficulties caused by having a surface element with two local coordinates and requiring the derivatives at the nodal positions. Besides, the simplified implementation in 4.2 needs only a tangential laplacian in local coordinates and the normalization with the length of the normal vector.

On a surface element, as we have in this implementation, the length of the normal vector is also the determinant of the Jacobian matrix. The normal vector is computed as the vector product:[19]

$$\vec{n} = \frac{\partial^2 \vec{r}(x,y,z)}{\partial \xi^2} \times \frac{\partial^2 \vec{r}(x,y,z)}{\partial \zeta^2} \tag{4.35}$$

These partial derivatives are the first two rows of the Jacobian matrix (4.34). The results of the whole procedure are acceptable as long as the surface elements are not too distorted in the boundary element mesh.

The actual implementation of the tangential laplacian needs to combine the calculations on the nodes from every element in a global result. The nodes in the elements of the type depicted in Figure 4-3 and used in this project are shared by two, three or four adjacent elements. An average of the contributions from all adjacent elements is performed at every node.

The technique described in this section has a resemblance with numerical differentiation by finite differences, except for the fact that meshing in BEM does not generally result in perfect Cartesian grids. It is convenient at this point to summarize some of the difficulties inherent to numerical differentiation in order to understand its limitations.

First of all, numerical differentiation is intrinsically unstable. Contrarily to numerical integration, it tends to amplify the errors in the input data. Secondly, the size of the increment h between function samples has to be chosen properly: too small values exaggerate the effect of rounding errors, while a large h fails to estimate the derivative.[14] Furthermore, the performance of the technique strongly depends on the function's behavior, its smoothness and variation.

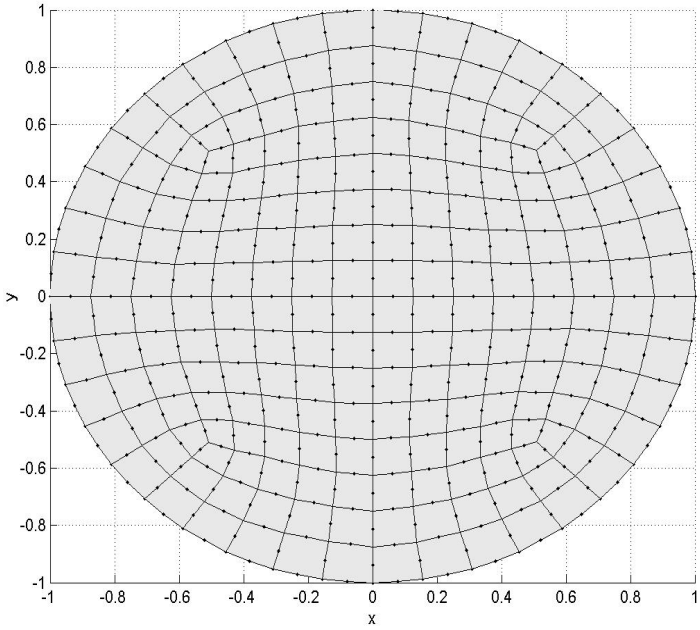

Figure 4-4. Mesh of a disc with quadrilateral elements.

In order to examine the properties of the algorithm, its performance and limitations, an example is shown in Figure 4-5. It is calculated with a test routine that produces results having a resemblance with the problem at hand, the acoustic transducer, using the tangential laplacian implementation. A circular surface has been meshed with quadrilateral elements as shown in Figure 4-4.

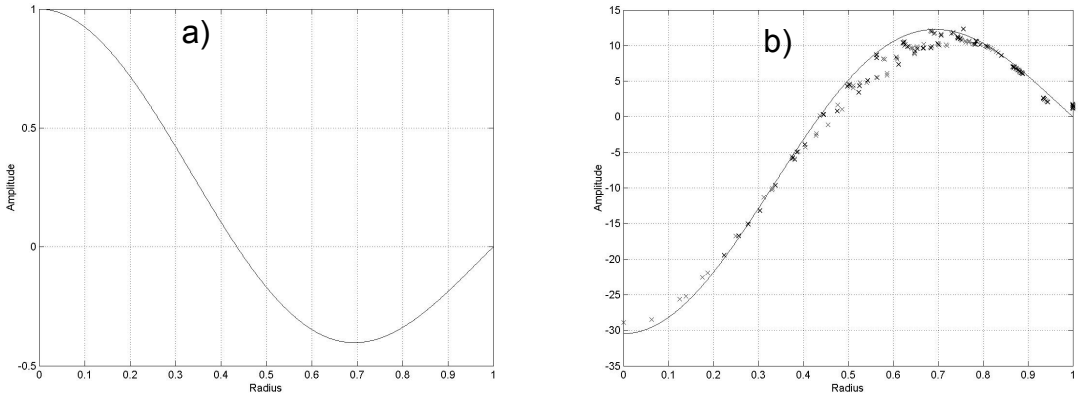

Figure 4-5. Example of tangential laplacian calculation over the disc in Figure 4-4: a) Bessel function J_0 imposed on the circular surface, b) tangential laplacian, analytical (solid line) and numerical (crosses).

A Bessel function of the first kind and order zero has been used and its two-dimensional laplacian has been calculated analytically for comparison. A zero of the function is forced at the rim of the disc, resembling a vibration mode of a circular membrane clamped at the rim. The comparison of analytical solution and calculation in Figure 4-5 (b) gives an idea of the algorithm's performance.

The result is only computed at the nodes and a tangential laplacian matrix is obtained. This matrix can be used directly on the nodal values of the pressure, as required in order to assemble the system in (4.20). The price to pay is a lack of control on the positions of the surface points where the algorithm takes function samples because of the dependence on the BEM mesh, which might be inadequate for the tangential laplacian in some cases. Therefore, some attention should be paid to the performance of the numerical tangential laplacian on every particular calculation.

4.4. Membrane formulation

The coupling exterior-membrane-interior is very strong in condenser microphones. This means that it is not possible to construct a model of this device if the interaction between its parts is not considered. Nevertheless, for simplicity one can remove the coupling with the exterior medium by assuming a uniform excitation acting on the membrane surface. In this way only the coupling membrane-interior remains. This assumption is valid for measurements made with an electrostatic actuator, as described in 2.1.3, and also for the analytical model employed.

In chapter 5 we will use an analytical model for validation that is defined on a very simplified geometry, a thin cylinder that contains the thin layer of air, with the sides representing membrane and backplate.[34] This geometry is depicted in Figure 5-1 and the model is reviewed in chapter 5 and Appendix A. The rim around the gap is taken care of by imposing a pressure release boundary condition $p = 0$, in the understanding that this is the effect of the microphone's back cavity.

Since our validation reference has a coupled membrane, we must also incorporate it to the numerical model in order to validate the calculations. The geometry of the analytical model just described was tried for the numerical model under development, adopting the same analytical solution for the membrane included in the analytical reference. Let us explain this membrane representation in more detail.

We will assume harmonic wave motion in the following. The non-homogeneous differential equation for the movement of a membrane is:[31]

$$T\left(\Delta + K^2\right)\varepsilon = p_{inc} - p \tag{4.36}$$

where $K^2=\rho_s\omega/T$, T is the tension of the membrane, ρ_s is the membrane's surface density, ω is the angular frequency, ε is the normal displacement, p_{inc} the incident pressure on one side, and p is the reacting pressure on the other side. It is assumed that the membrane only moves in the normal direction, reducing the problem to two dimensions.

If we particularize equation (4.36) for a circular membrane held on its rim, like in cylindrical condenser microphones, we can express it in polar coordinates and have:

$$\frac{\partial^2\varepsilon}{\partial r^2} + \frac{1}{r}\frac{\partial\varepsilon}{\partial r} + K^2\varepsilon = \frac{p_{inc}}{T} - \frac{p}{T} \tag{4.37}$$

with $\varepsilon(R) = 0$, where R is the membrane radius and r the radial coordinate. We also suppose the problem is fully axisymmetrical, that is, there is no variation in the circumferential direction.

We can find the solution to this equation as a modal expansion in Bessel functions if we combine the homogeneous solutions with particular solutions for the incident pressure p_{inc} and the internal reacting pressure p. We must however find an expression for p in order to obtain its corresponding particular solution, and this will be, like in the analytical solution in Appendix A, a modal expansion with modes that match those of the membrane:

$$p = \sum_{n=1}^{\infty} A_n J_0(k_n r) \tag{4.38}$$

where A_n are the expansion coefficients and the products Rk_n are the zeros of the Bessel function J_0. Note that we are in fact imposing a $p = 0$ condition with this expression of the reacting pressure in the gap. This condition will be incorporated in the membrane formulation and constitute an important limitation, as we will see.

If we obtain the particular solutions corresponding to p_{inc} and p, add them to homogeneous solutions of the form $\varepsilon = A\, J_0(Kr)$ and impose the boundary condition $\varepsilon(R) = 0$, then we obtain a solution for the normal displacement ε:

$$\varepsilon(r) = \frac{p_{inc}}{TK^2}\left[1 - \frac{J_0(Kr)}{J_0(KR)}\right] + \sum_{n=1}^{\infty} \frac{A_n}{T\left(k_n^2 - K^2\right)} J_0(k_n r) \tag{4.39}$$

Unfortunately, it was not possible to validate the numerical model in this manner. It was found that in a general case of a microphone with viscous and thermal losses the assumptions made for the analytical solution do not hold, except at high frequencies. As was mentioned above, a pressure release condition $p = 0$ is assumed at the rim of the gap between membrane and backplate, instead of a surrounding cavity as in actual microphones. This turned out to be problematic for a numerical model with viscous losses. We elaborate further on this issue in the discussion in 4.6.

In order to overcome this problem, several geometries with an annular reservoir at the periphery were tried for the numerical model, like those shown in Figure 5-5. In this way the $p=0$ boundary condition was not imposed to the numerical formulation of the interior domain. This partially solved the problem, but the numerical model was still fitted with the membrane formulation outlined above and, as a result, the coupled model could only perform acceptably above 50 kHz for ¼ inch microphones. We will see this in the results later. This is because of the assumptions taken for the membrane that in fact limit the performance of the coupled numerical model in a similar manner, especially the proposed particular solution for

the pressure acting on the back side of the membrane (4.38). It is an expansion in Bessel functions J_0 that makes the pressure zero at the rim.

Therefore, the next step would be to implement a membrane for the numerical formulation using the Finite Element Method. The calculation of the stiffness matrix that relates the excitation (the pressure difference on both sides of the membrane) with the displacement can be done using a standard FEM package. The stiffness matrix thus obtained can be coupled with the visco-thermal model of the interior of the microphone.

However, the FEM model of the membrane could not be accomplished within the duration of this project. Some difficulties for extracting the stiffness matrix from the FEM package available (ANSYS) delayed this solution. The results shown in chapter 5 correspond to the numerical model with a cavity around, but the membrane is still modeled using the analytical expression with limiting hypotheses. Further extensions of this project could address the task of a FEM model for the membrane.

4.5. Coupled system of equations

The numerical implementation obtained in 4.2 for the interior of the microphone and the analytical solution for the membrane described in 4.4 must be combined in a coupled system of equations. In particular, we impose equation (4.20) in the fluid, equation (4.38) for the pressure behind the membrane, and equation (4.39) for the membrane displacement. It is important to note again, as we have just done in the last section, that imposing the modal expansion (4.38) for the reacting pressure is a limitation that will in fact restrict the model's frequency range. The resulting system has this form:

$$\begin{pmatrix} J_0(k_n r_j) & \left(1-\frac{\tau_a}{\tau_h}\right) \\ -i\omega\frac{J_0(k_n r_j)}{T(k_n^2-K^2)} & \phi_a \mathbf{B_a^{-1}A_a} - \phi_h \mathbf{B_h^{-1}A_h}\frac{\tau_a}{\tau_h} + \mathbf{A_v^{-1}B_v}\Delta_{//}\left(\phi_a - \phi_h\frac{\tau_a}{\tau_h}\right) \end{pmatrix} \begin{pmatrix} \vdots \\ A_n \\ \vdots \\ p_{aj} \\ \vdots \end{pmatrix} = \begin{pmatrix} \vdots \\ 0 \\ \vdots \\ \vdots \\ i\omega\frac{p_{inc}}{TK^2}\left[1-\frac{J_0(Kr_j)}{J_0(KR)}\right] \\ \vdots \end{pmatrix} \quad (4.40)$$

where the index *n* indicates membrane mode number and the index *j* a node on the internal surface of the microphone. The modal expansion should contain enough modes to represent the membrane movement with sufficient accuracy within the frequency range of interest. For example, in most calculations for ¼ inch microphones five modes were used; there was not much improvement with a higher number. Since all the other surfaces are supposed to be rigid, the normal velocity is only different from zero on the membrane.

The system (4.40) is overdetermined. The unknowns are the modal coefficients for the membrane and the pressures for the acoustic mode on all nodes, but we have one equation per node for the fluid (lower part of the coefficient matrix) and one equation per membrane node (upper part of the coefficient matrix). The number of nodes on the membrane is generally much larger that the membrane modes considered in the expansion, therefore the number of equations will be larger than the number of unknowns.

In order to obtain a system with the same number of equations than unknowns, a technique must be applied to fit the unknowns to the modal expansion model of the membrane. [35] This is a linear least squares problem, where the goodness of the expansion's fit is measured by a merit function of this sort:

$$\chi^2 = \sum_{j=1}^{M} \left[p_j - \sum_{n=1}^{N} A_n J_0(k_n r_j) \right]^2 \tag{4.41}$$

The problem is said to be linear because the modal expansion is a linear combination of modes. There are various techniques available to find the parameters A_n that minimize χ^2. We will make use here of the normal equations, obtained taking the derivatives of χ^2 with respect to all A_n and equating them with zero. The normal equations are a square system that we can combine with the BEM equations to obtain a full system. With these manipulations the overdetermined system (4.40) becomes:

$$\left(\begin{array}{c|c} \left[J_0(k_n r_j)\right]^T J_0(k_n r_j) & \left[J_0(k_n r_j)\right]^T \left(1 - \dfrac{\tau_a}{\tau_h}\right) \\ \hline -i\omega \dfrac{J_0(k_n r_j)}{T(k_n^2 - K^2)} & \phi_a \mathbf{B}_\mathbf{a}^{-1}\mathbf{A}_\mathbf{a} - \phi_h \mathbf{B}_\mathbf{h}^{-1}\mathbf{A}_\mathbf{h} \dfrac{\tau_a}{\tau_h} + \mathbf{A}_\mathbf{v}^{-1}\mathbf{B}_\mathbf{v}\Delta_{//}\left(\phi_a - \phi_h \dfrac{\tau_a}{\tau_h}\right) \end{array}\right) \left(\begin{array}{c} \vdots \\ A_n \\ \vdots \\ p_{aj} \\ \vdots \end{array}\right) = \left(\begin{array}{c} \vdots \\ 0 \\ \vdots \\ \hline \vdots \\ i\omega \dfrac{p_{inc}}{TK^2}\left[1 - \dfrac{J_0(Kr_j)}{J_0(KR)}\right] \\ \vdots \end{array}\right) \tag{4.42}$$

The solution of this system is a set of modal coefficients An and the values of the acoustic pressure p_a on the nodes. Other acoustic variables can be calculated using the expressions (4.21), (4.22), (4.23) and (4.24).

4.6. Discussion

A numerical model for fluids with viscous and thermal losses, and its use on condenser microphones is developed in this chapter. The model uses the direct collocation formulation

of the Boundary Element Method. We will discuss here some of the topics related with the previous development.

Viscous mode implementation

One of the main contributions of this project, together with the developments in chapter 3, is that the viscous mode has been fully implemented without taking restrictive hypotheses. Its inclusion meant a more complicated formulation than a formulation that only considers thermal losses, like the one described in [22]. The vectorial nature of the viscous velocity adds three more equations that are linked to the rest through the velocity boundary condition, which is also expressed in a vectorial form.

This work took some advantage of the particular geometry of microphones with a thin layer of air, where the losses occur, defined on a plane. In this manner the equations could be built with no need to consider in a general way the geometry of the setup when transforming from local coordinates referred to the boundary to the global coordinate system. Such change would be needed in a general case because the boundary conditions are defined locally, while the acoustic variables are expressed in the global reference system.

However, if one wants to avoid a full implementation in global coordinates, it is still possible to attack other sets of problems with typical geometries. The assumption taken in 4.2 to allow the normal component of the viscous velocity match the z-direction (equation (4.14)) could be reproduced in a similar way in other coordinate systems. A typical example would be the calculation of visco-thermal losses in narrow tubes, where the normal direction to the boundary could match the radial coordinate direction in a cylindrical coordinate system, thus simplifying the development. Figure 4-6 shows how the normal vector would fit in the narrow tube setup.

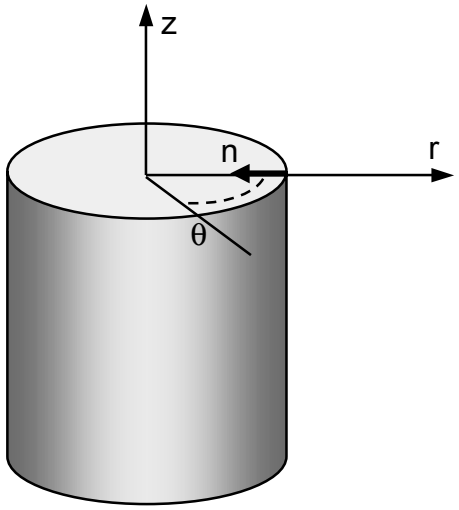

Figure 4-6. Schematic representation of a narrow tube, where the normal vector to the inner surface follows the radial direction in cylindrical coordinates.

Three-dimensional implementation

Most authors dealing with this problem propose axisymmetrical geometries that are certainly good enough to represent some microphones.[34,3] In our case, however, the model is intended to be applied to *any* microphone design, including standard condenser microphones with holes on the backplate and MEMS (Micro Electro-Mechanical Systems) silicon microphones, which are not circular in most cases. Moreover, measurements made at Brüel & Kjær have shown that small geometrical details that are not considered in simplified models have an influence on the device's performance, which is precisely what the model, once developed, should address. For this reason it was decided to develop a three-dimensional BEM formulation, even though an axisymmetrical version of the BEM was previously available.

This generality means heavier calculations, on the one hand, and a more complex mathematical development, on the other. The implementation of the viscous mode could have been simplified in 4.2 by using cylindrical coordinates and, since axisymmetrical BEM would be employed, the tangential laplacian in 4.3 could have been reduced to the radial direction on the generator's linear elements. Additionally, mesh generation on three-dimensional surfaces becomes too complicated to be done directly, like in axisymmetrical BEM, and mesh generation software is needed.

Membrane implementation

It would be interesting to extend the model by including a numerical implementation of the membrane using finite elements and couple it to the fluid, as was stated in 4.4. The present coupled model uses an analytical solution for the membrane that prevents it from performing properly below around 50 kHz, in the case of ¼ inch microphones studied here. In particular, it is the assumption about the reacting pressure acting on the back side of the membrane (eq. (4.38)) that prevents the coupled model from working properly at low frequencies. This assumption is imposed in the present form of the coupled system, as we saw. Some results in chapter 5 will illustrate this situation. In any case, this limitation is not inherent to the BEM model with visco-thermal losses developed here; it is a consequence of the coupling with a membrane represented analytically. The coupling is needed for a complete microphone model and, even more important, there is no easy way to validate the visco-thermal BEM alone due to the lack of analytical models or measurements without coupling to compare with.

Tangential laplacian

The tangential laplacian developed here is expressed as a matrix transformation that is easily included in the viscous mode part of the combined matrix in equation (4.20). To be able to do this, the values of the acoustic pressure on the nodes of the existing BEM mesh must be used. This introduces small errors in the laplacian calculation, due to the slight distortion of the surface elements, whose local coordinate system can only approximately be considered Cartesian. The distortion is unavoidable in a circular microphone setup meshed with square elements but, since the meshing software usually imposes an adjustable maximum distortion limit as a meshing requirement, this effect is under control.

On the other hand, some extra care must also be taken when choosing element sizes and it must be kept in mind that they will also be used for the laplacian calculation. The size of the interval between function evaluations, which in our case is the distance between nodes, is important for a good performance of any numerical differentiation algorithm.

It is of course possible to implement a more elaborate numerical differentiation scheme. However, in this project, an acceptably good solution is enough to prove the feasibility of the visco-thermal implementation that has been developed, and would probably suffice in most practical calculations. A more sophisticated laplacian would require a new solution strategy for the visco-thermal system of equations, probably an iterative procedure.

Surrounding cavity

The use of a real cavity around the gap in the numerical implementation is justified if we consider the difficulties that imposing a $p = 0$ boundary condition at the rim would create to this implementation. If we recall the theory of visco-thermal fluids in section 2.2, we saw that the viscous velocity had no pressure associated. This means that a direct relationship between pressure and velocity at the boundary no longer exists, as it did in the perfect fluid formulation or even in formulations with thermal losses like [22]. The viscous velocity at the rim is not completely defined with just a pressure release boundary condition; some other restriction should be added, as it is proposed in reference [7]. It is therefore more realistic and easier to add the surrounding cavity.

Alternative solution using iteration

The solving of the coupled system of equations in 4.5 could also be possible by adopting an iterative solution strategy. We briefly outline here this method, since further extensions of this project could make this approach necessary. The iteration computes consecutively, in a loop, the membrane and the fluid formulations producing solutions that, if the procedure works properly, should converge to the desired coupled result. The iterative process is stopped when the improvement in the solution, computed as a difference between the last and the previous values of the sound pressure, falls below a given threshold. The process is represented in Figure 4-7. Iteration might also be needed in the viscous mode implementation if a more demanding version of the tangential laplacian is introduced.

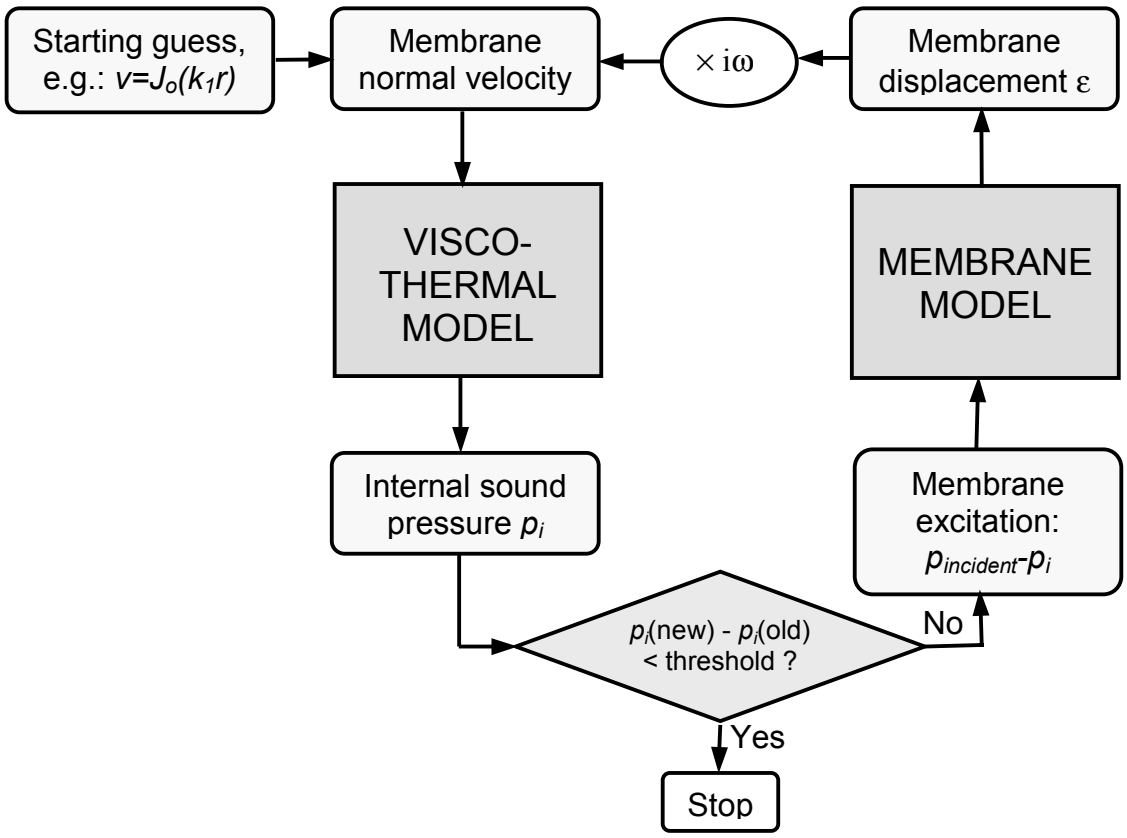

Figure 4-7. Iterative calculation of the coupling membrane-interior of the microphone .

5. RESULTS

A set of calculations has been run using the model developed in this project with the purpose of validating it against data available and evaluating its performance. An analytical model and actual measurements on commercial Brüel & Kjær ¼ inch microphones have been used for validation; they are described and discussed in section 5.1.

Section 5.2 presents results from the analytical model and the numerical implementation in the microphone interior. In section 5.3 frequency responses are shown, with data from measurements, analytical model and numerical model.

Finally, all the results that were only plotted the in previous sections are discussed in 5.4.

5.1. Review of the analytical model and measurements

The usual procedure when validating a numerical calculation is to compare with an exact analytical solution for simple geometries. A good agreement normally implies that the model can handle more complicated cases for which no analytical solutions are available. Measurements can also be used for validation, but they are subject to measurement errors and cannot provide exact values. In our case, however, there are two difficulties: i) the analytical model employed is based on assumptions that are not valid at low frequencies, therefore its results cannot be trusted for comparison in that range, as we will see in the following, and ii) the numerical visco-thermal implementation is coupled to a membrane modeled analytically that actually prevents the viscous part from working well at low frequencies and spoils the coupled result; this was discussed in chapter 4 and we will come back to it in the comments of the results. These limitations of analytical and numerical implementations impose, in practice, a lower limiting frequency of about 50 kHz for the comparison using ¼ inch microphones.

The analytical model

The analytical solution in reference [34] used here for validation considers losses, assumes a uniform excitation and a coupling membrane-interior for a thin gap of air trapped between a membrane and a backplate. It provides a complete description of the sound field inside the gap, including acoustic and thermal pressures, acoustic, thermal and viscous velocities and membrane displacement, all expressed in modal expansions. A summary of this analytical development with mathematical expressions is given in Appendix A.

This analytical model is developed for the simplest microphone geometry conceivable: a cylindrical thin gap between a membrane and a backplate of the same radius, as shown in Figure 5-1. The boundary conditions are: zero velocity on the backplate, pressure release at the rim and coupling with the membrane, which moves in the normal direction and is clamped at its rim.

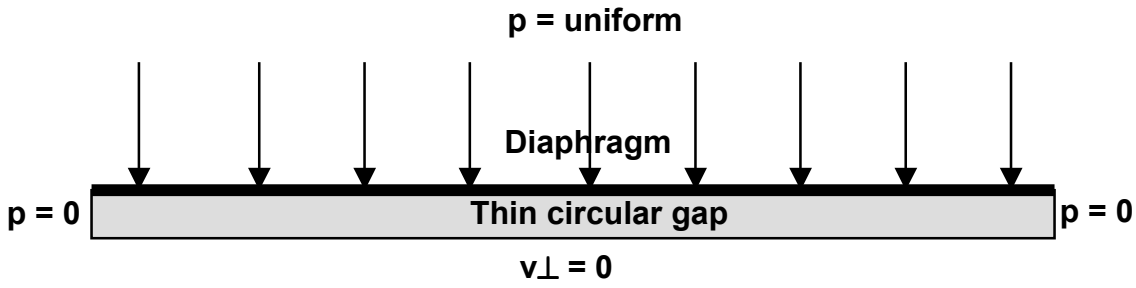

Figure 5-1. Microphone geometry for the analytical solution in reference [34]. The setup is circular. The gap width is exaggerated for clarity.

The frequency range of use for this model is said to be between 50-100 kHz by the authors. The reason for this lays in the pressure release boundary condition $p=0$ imposed at the gap's rim. As a consequence of it, the representations of the sound pressures (acoustic and thermal) and normal components of the velocity (acoustic, thermal and viscous) turn out to be expansions of Bessel functions of order zero with a zero at the rim, as shown in Appendix A.

This condition is in principle correct within the mentioned frequency range, where we can assume that the surrounding cavity can be replaced by a pressure release condition. At lower frequencies, however, the pressure has time to equalize inside the microphone and tends, in the limit of low frequencies, to be uniform. Let us demonstrate this with a simple calculation and some results from analytical and numerical models at 1 kHz.

At frequencies as low as 1 kHz, the membrane governs the microphone behavior. The reaction of the interior is too weak by comparison to have an influence; therefore the coupling is negligible. We can describe the normal displacement of the membrane ε with a simplified version of equation (4.39)

$$\varepsilon(r) = \frac{p_{inc}}{TK^2}\left[1 - \frac{J_0(Kr)}{J_0(KR)}\right] \tag{5.1}$$

where $K^2=\rho_s\omega/T$, T is the tension of the membrane, ρ_s is the membrane's surface density, p_{inc} the uniform incident pressure on the external side, R the radius of the setup and r the radial coordinate. We have removed the term that corresponds to the internal reaction.

The volume velocity of the membrane can be calculated by integrating the normal velocity of the membrane, which is the time derivative of the normal displacement, over the membrane surface:

$$Q = \int_S \frac{\partial \varepsilon(r)}{\partial t} dS = -\frac{i\omega p_{inc}}{TK^2}\int_0^R \left[1 - \frac{J_0(Kr)}{J_0(KR)}\right] dS = -\frac{i\omega p_{inc}\pi R^2}{TK^2}\frac{J_2(KR)}{J_0(KR)} \tag{5.2}$$

On the other hand, the ideal acoustic impedance of a cavity at low frequency is:

$$Z_{aVol} = -\frac{\rho_o c^2}{i\omega V} \tag{5.3}$$

where V is the volume of the cavity, ρ_0 is the density of the air and c is the speed of sound in air. We assume here that the fluid has no losses. It is then possible to calculate the pressure in the microphone's interior, assumed uniform, with the expression:

$$p_{\text{int}} = Q\, Z_{aVol} = \frac{i\omega p_{inc} \pi R^2}{TK^2} \frac{J_2(KR)}{J_0(KR)} \frac{\rho_o c^2}{i\omega V} \tag{5.4}$$

The sound pressure in Figure 5-2 is calculated with the analytical and the numerical models at 1 kHz and removing the effect of viscous losses. Thermal losses are supposed very small at this frequency, therefore the result should approximate to the expression (5.4) for perfect fluids.

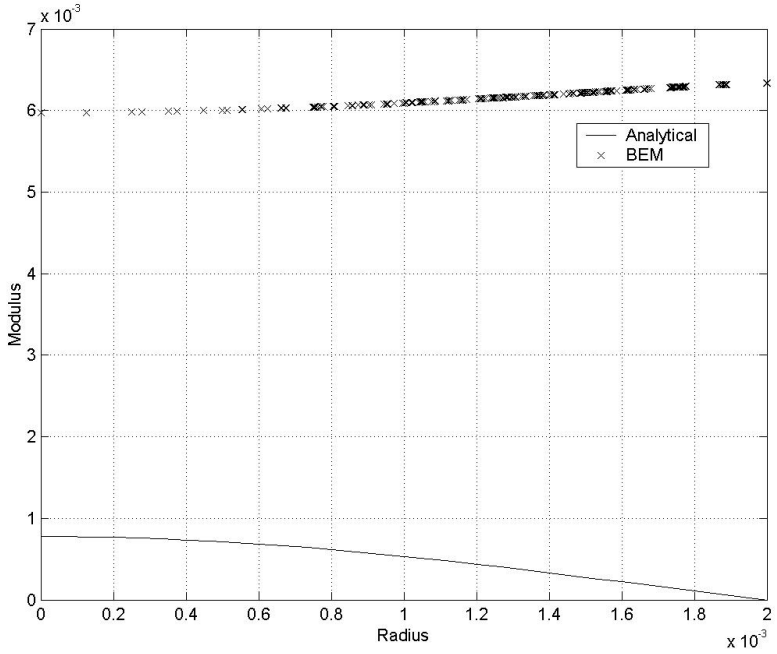

Figure 5-2. Sound pressure behind the membrane of a B&K.4938 microphone at 1 kHz, with the viscous losses removed.

We can now use the parameters of the microphone B&K 4938 and the dimensions of the volume of the surrounding cavity in the numerical calculation to compute the pressure in the interior. The volume of the cavity is $3.17 \cdot 10^{-8}$ m^3, the incident pressure is 1 Pascal, the frequency is 1 kHz, the radius is 2 mm, the membrane tension utilized is 4000 N/m and the surface density of the membrane is 0.0577 Kg/m^3.

With these values equation (5.4) gives an internal sound pressure of 0.0067 Pascal, which is quite similar to the almost uniform value obtained with the numerical model in Figure 5-2. The analytical model result is not uniform; it cannot be, unless it was zero everywhere, because it is a sum of Bessel functions with a zero at the rim.

This shows that the values of the acoustic variables at low frequencies provided by the analytical model are not correct. The membrane movement is nevertheless still correctly calculated, since it is not influenced by the microphone's interior at low frequencies.

On the other hand, in the high range of frequency the cavity can effectively be assumed to behave as a pressure release element, as long as no cavity resonances are present. The authors state that they intend to use their model for miniaturized acoustic transducers in the frequency range 50-100 kHz; therefore a good performance at low frequencies is not expected.

It must be mentioned that reference [7] addresses the shortcomings of this analytical model and proposes some ideas to overcome them analytically. It is not, however, an alternative model that we can use here.

Measurements

We use as well frequency responses measured with an electrostatic actuator on commercial B&K microphones. The microphones chosen are ¼ inch B&K models 4938 and 4939. Table 5-1 lists their technical specifications and Figure 5-3 shows their external appearance. Both analytical solution and numerical calculation are fitted with dimensions and parameters that can resemble these microphones.

The measurements give an indication of the model performance, but they cannot provide a good description of the phenomena in the interior of the microphone or the movement of the membrane. It is practically impossible to measure acoustic parameters inside a microphone; only the study of actual membrane movement has been tried using laser vibrometers, although the data available are still scarce and unreliable. Therefore we use here the electrical output

from the microphone, which is a function of the mean membrane displacement. Figure 5-4 shows the actuator frequency responses of the chosen microphones.

Type Number	4938	4939
Diameter (inch.)	1/4	1/4
Optimised	Pressure-field	Free-field
Nominal open-circuit sensitivity (mV/Pa)	1,6	4
Polarization voltage	200	200
Optimised frequency response +/- 2dB	4 Hz to 70 kHz	4 Hz to 100 kHz
Dynamic range with preamplifier	42dB(A)-172 dB (2670)	35dB(A)-164 dB (2670)
Inherent noise dB (A)	30	28
Capacitance pF	6,1	6,1
Venting	Side	Side
Lower Limiting Frequency (-3dB)	0.3Hz-3Hz	0,3Hz-3Hz

Table 5-1. Technical specifications of B&K microphones 4938 and 4939 (B&K microphone catalogue).

Figure 5-3. Brüel & Kjær measurement microphones 4938 (pressure field) and 4939 (free field).

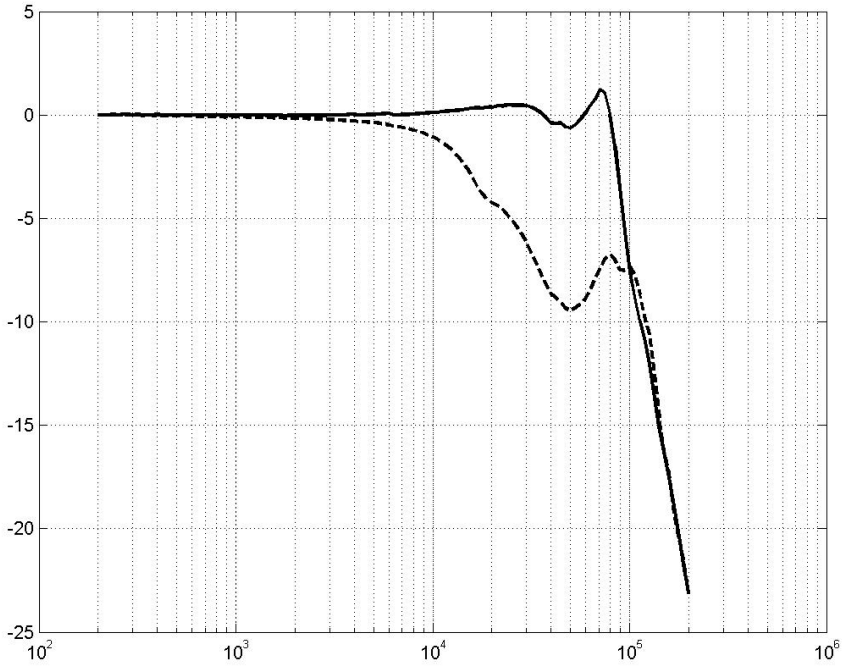

Figure 5-4. Actuator frequency responses of Brüel & Kjær measurement microphones 4938 (solid) and 4939 (dashed).

The microphone model 4938 is designed for pressure-field conditions such as found in acoustic couplers, while model 4939 is adjusted for free-field conditions as we find when measuring direct sound from a source. This explains the differences in their frequency responses. Model 4939 uses the damping in the air gap to compensate for the increase caused by the scattering of its body in free-field conditions. Under such conditions its frequency response varies very little within its working bandwidth.

We need an additional set of characteristics of the microphones for the analytical and numerical models. They have been requested and obtained from the designers and are summarized in Table 5-2.

Type Number	4938	4939
Membrane radius (mm)	2	2
Backplate radius (mm)	1,75	1,75
Gap thickness (μm)	18	18
Membrane tension (N/m)	3128	1039
Membrane density (kg/m^3)	8300	8300
Membrane thickness (μm)	6,95	2,35

Table 5-2. Design parameters of B&K microphones 4938 and 4939.

These parameters describe roughly the interior of the microphone and the membrane. There is complete documentation for all the microphones' parts, but such a level of detail is not needed for our validation purposes. It should only be noted that microphones 4938 and 4939 have no holes in the backplate, thus facilitating the modeling and comparison with the analytical solution.

5.2. Comparison with analytical results: microphone interior

Two simplified geometries that resemble the microphones described above have been used for numerical calculation with the visco-thermal implementation. They are shown schematically in Figure 5-5. Setup *a)* has a membrane radius that is larger than the backplate's and is more similar to the actual microphone. Setup *b)*, however, has a closer similarity to the simplified geometry of the analytical solution in Figure 5-1, only with a surrounding cavity added.

Calculation results are very similar for the two geometries. We will only show results from setup *b)*; they are sufficient for the purpose of examining the model's performance. Figure 5-6 presents the meshes that correspond to the setups in Figure 5-5. The meshes are created by means of the mesh generator incorporated in the FEM package ANSYS, using one of the pre-defined shell elements. They are manipulated afterwards in Matlab to check their integrity, prepare them to be used by the BEM code and resize them to the desired microphone dimensions.

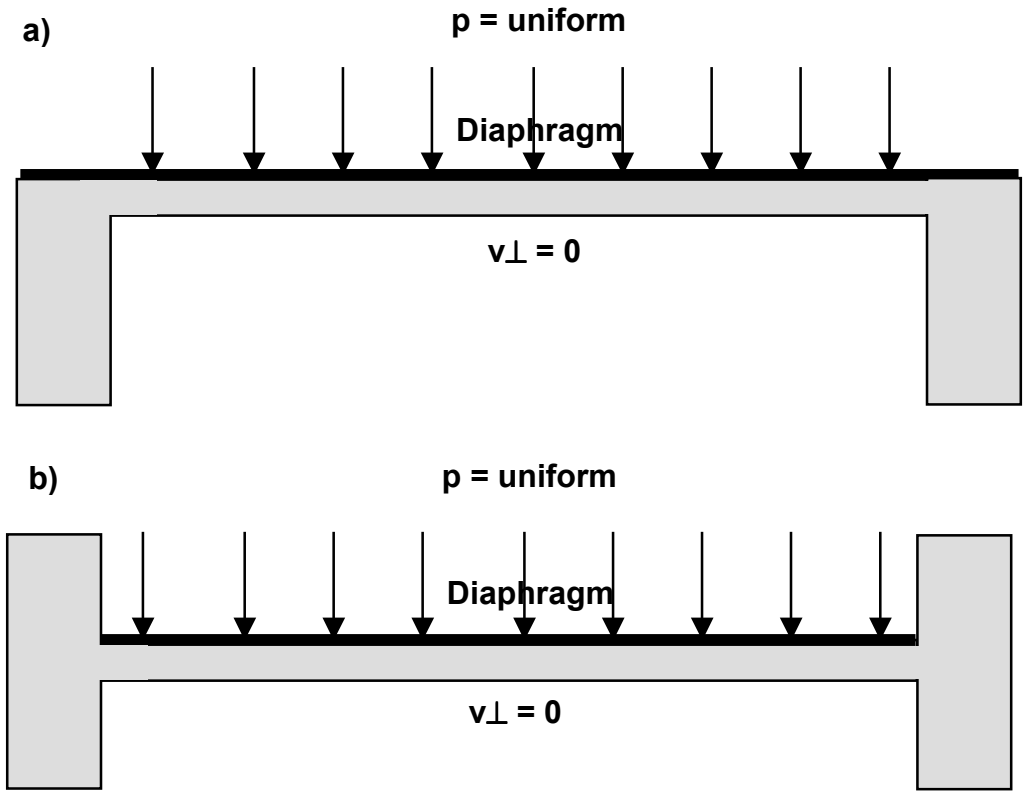

Figure 5-5. Microphone geometries used for the numerical model. The setup is circular. The gap width is exaggerated for clarity.

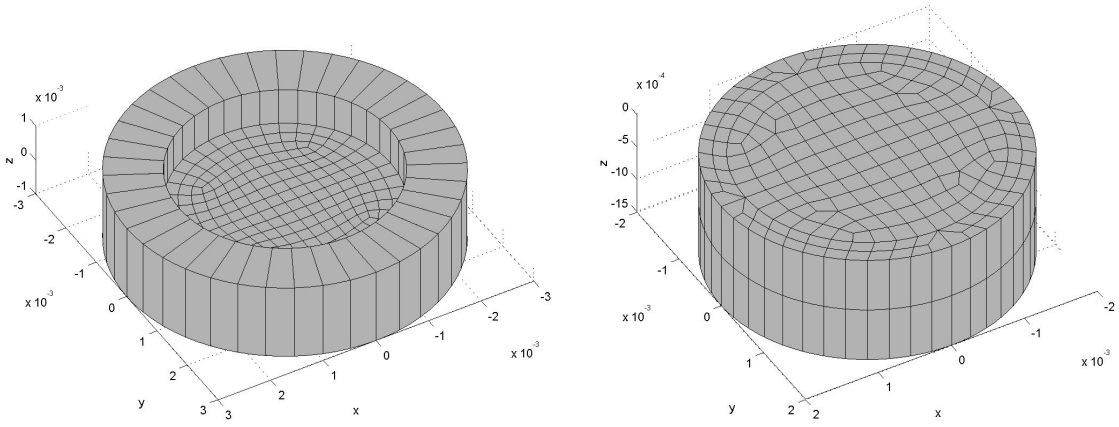

Figure 5-6. Three-dimensional surface meshes used for the numerical model. They correspond to the geomertries shown in Figure 5-5.

Figure 5-7 to Figure 5-16 are representations of acoustical parameters just behind the microphone membrane, calculated with the analytical model and using the coupled BEM method with visco-thermal losses developed in this project. The two microphones B&K 4938 and B&K 4939 are shown in separate figures.

The parameters represented are: total sound pressure and normal components of the total velocity, of the viscous velocity, of the thermal velocity and of the acoustic velocity. Although the raw data contains also phase information, only the modulus is represented; it suffices to show the model's performance. The analytical model gives a solution that is a function of the radius (2 mm in our case). All the nodal values on the membrane nodes are accumulated and represented with the radial coordinate; for this reason some points have very similar positions in the plots, since they have a similar radius but at different membrane positions.

The six frequencies chosen are: 50, 63, 80, 100, 126 and 160 kHz. They are separated by one-thirds octaves. As stated in previous chapters, frequencies below 50 kHz give poor results due to the imperfect coupling with the membrane.

The microphones are excited in the models with a uniform pressure of 1 Pascal. The magnitudes shown in the graphs, in Pascal for the acoustic pressure and in m/s for the velocities, are the result of this excitation.

The discussion of the results is left to section 5.4.

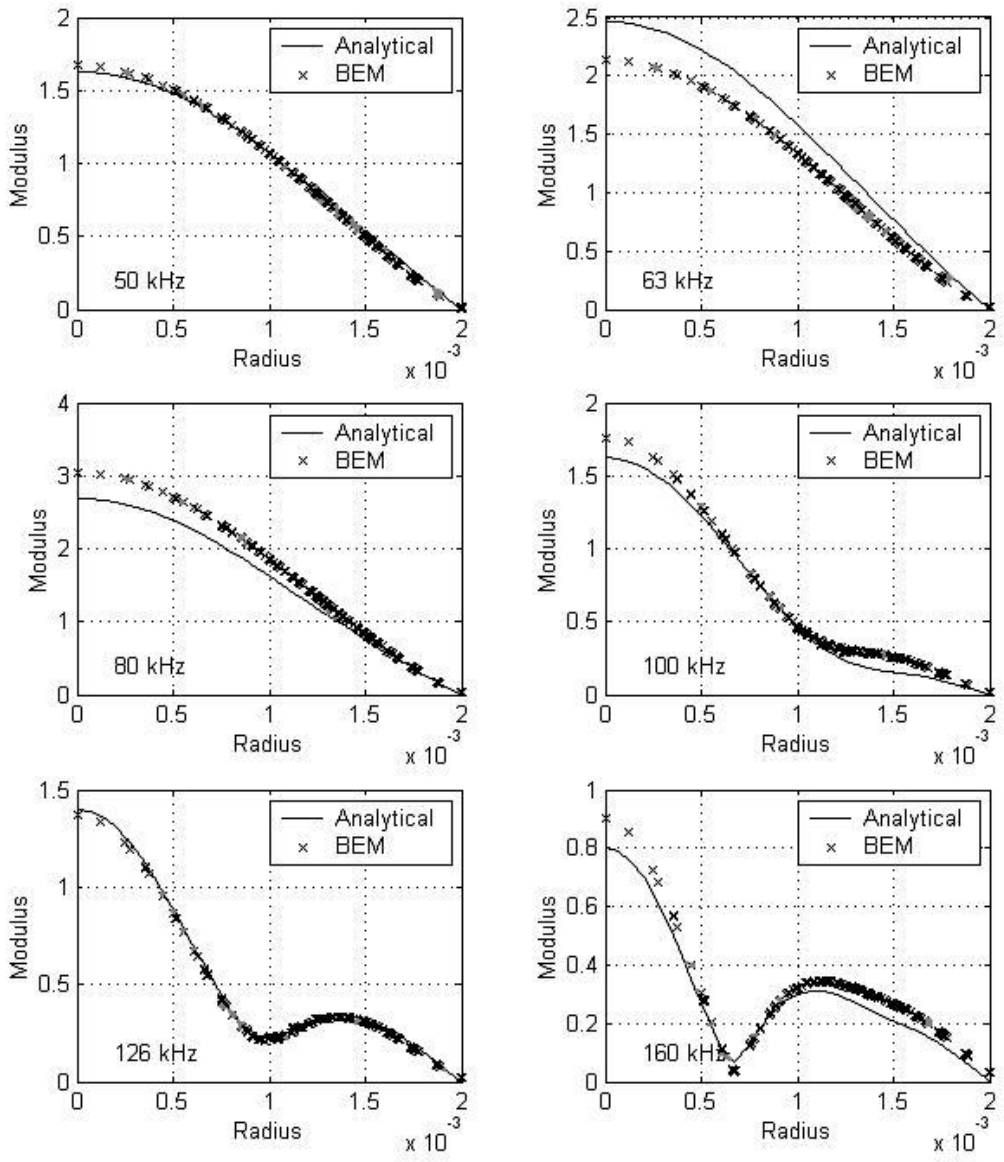

Figure 5-7. Sound pressure behind the membrane of microphone BK 4938 at six 1/3 octave frequencies. Results from the analytical model (solid) and the BEM with visco-thermal losses (crosses) are shown.

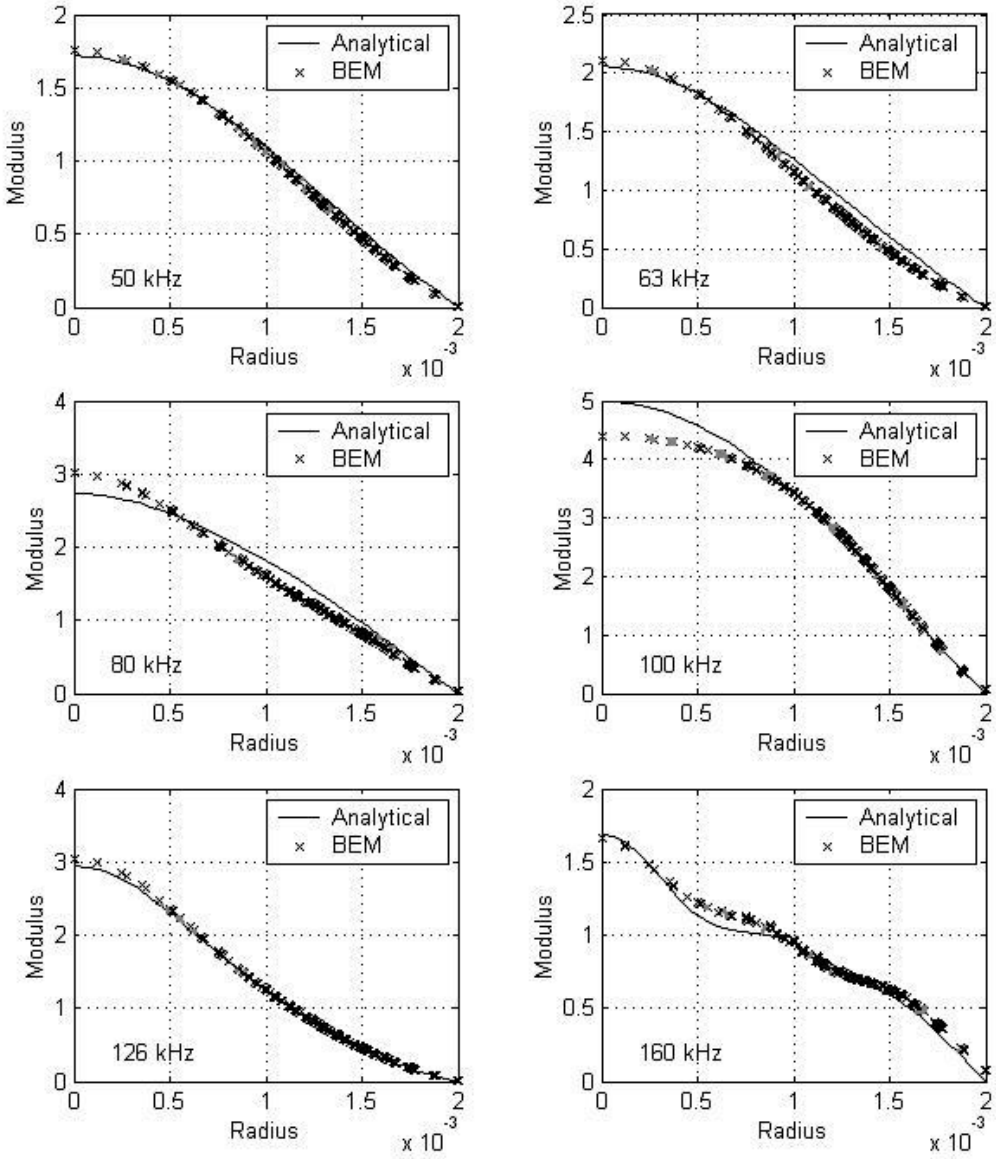

Figure 5-8. Sound pressure behind the membrane of microphone BK 4939 at six 1/3 octave frequencies. Results from the analytical model (solid) and the BEM with visco-thermal losses (crosses) are shown.

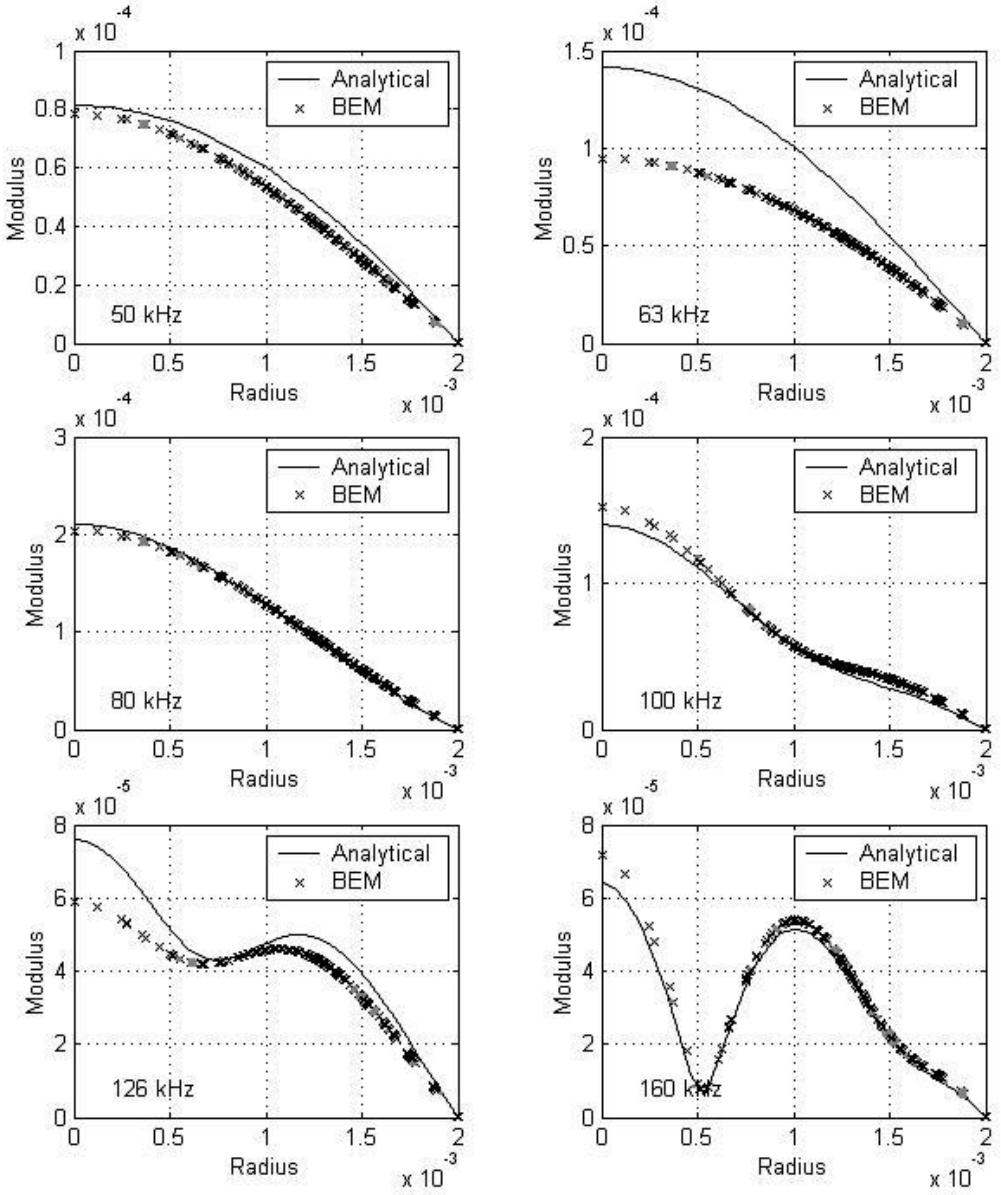

Figure 5-9. Total normal velocity of the membrane of microphone BK 4938 at six 1/3 octave frequencies. Results from the analytical model (solid) and the BEM with visco-thermal losses (crosses) are shown.

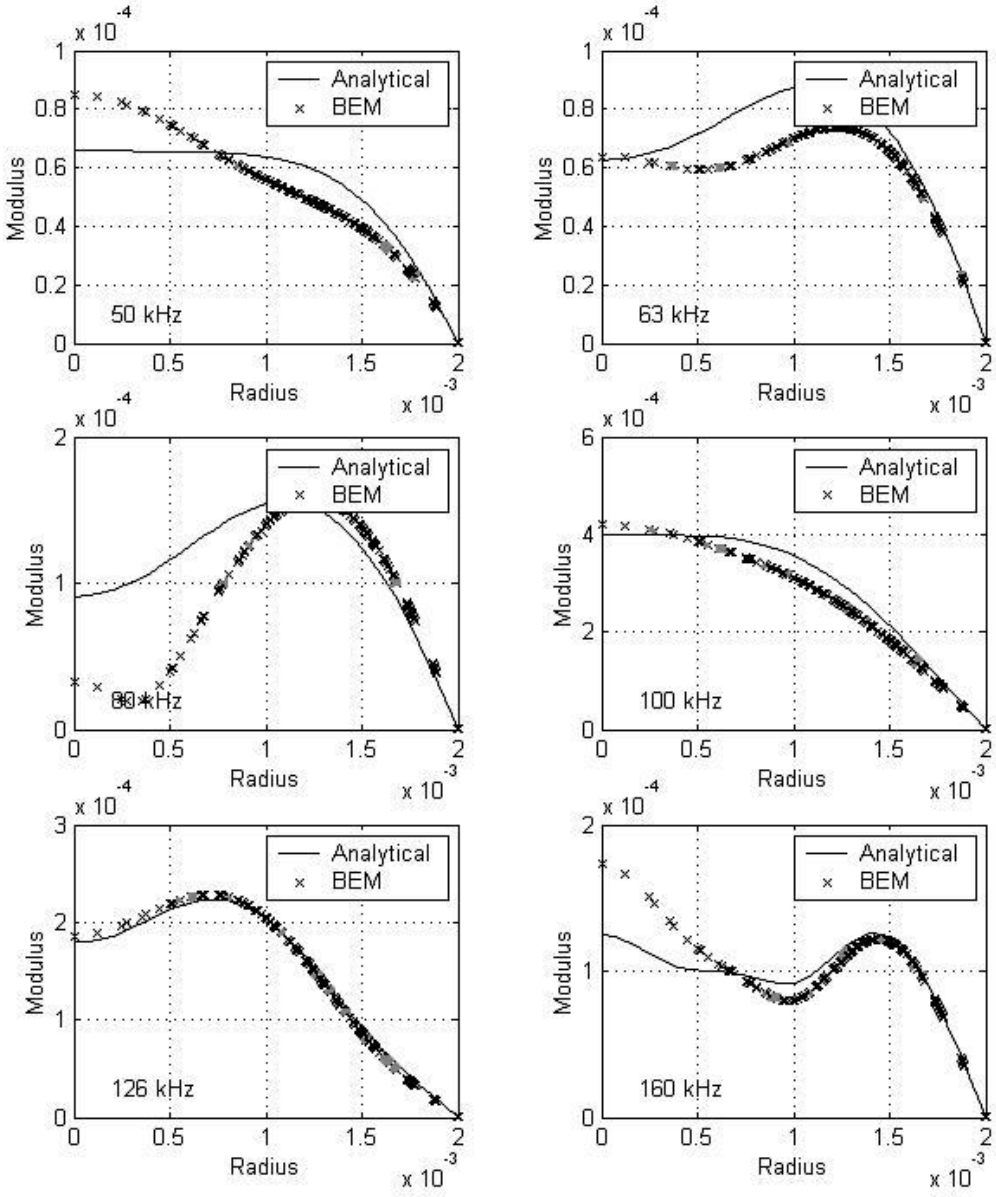

Figure 5-10. Total normal velocity of the membrane of microphone BK 4939 at six 1/3 octave frequencies. Results from the analytical model (solid) and the BEM with visco-thermal losses (crosses) are shown.

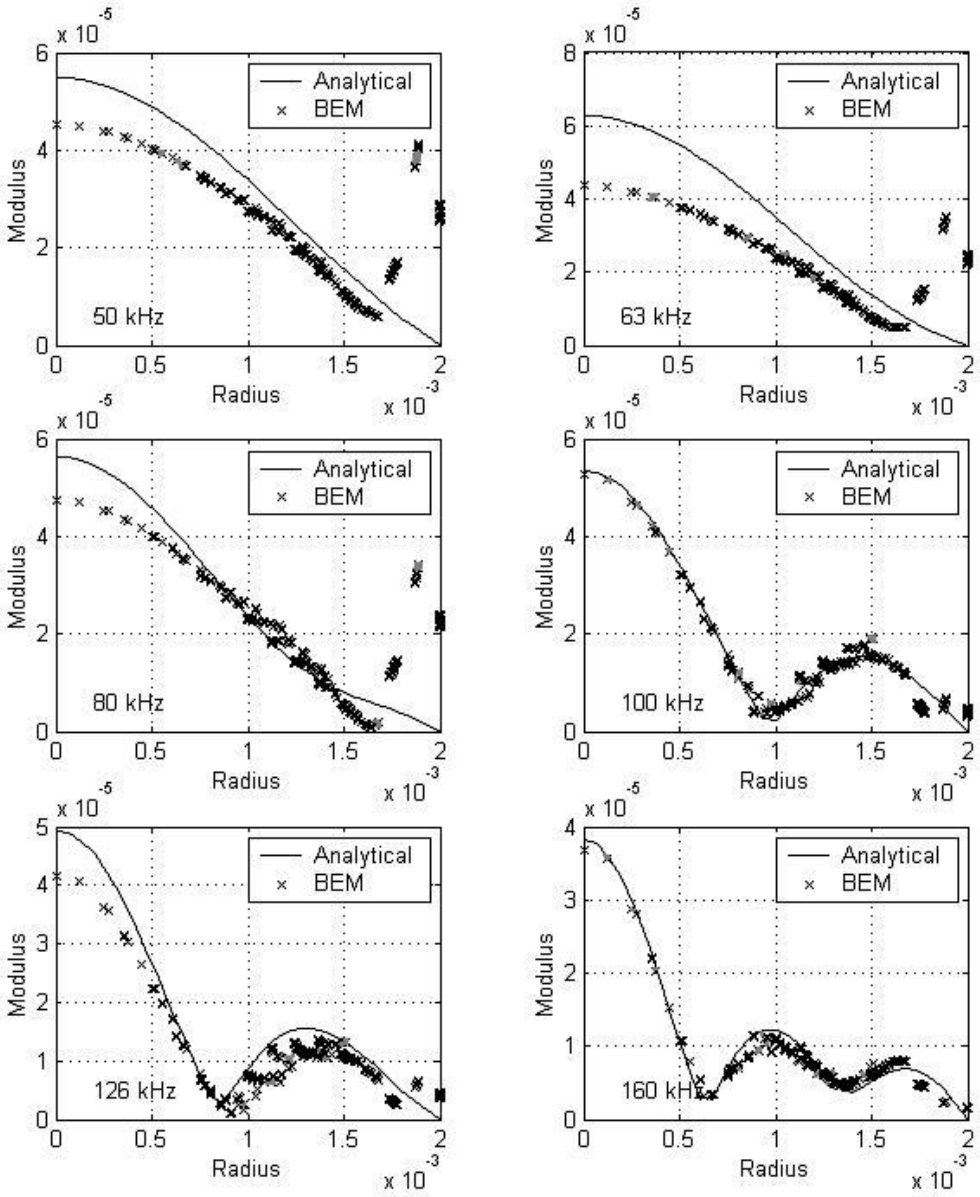

Figure 5-11. Normal viscous velocity behind the membrane of microphone BK 4938 at six 1/3 octave frequencies. Results from the analytical model (solid) and the BEM with visco-thermal losses (crosses) are shown.

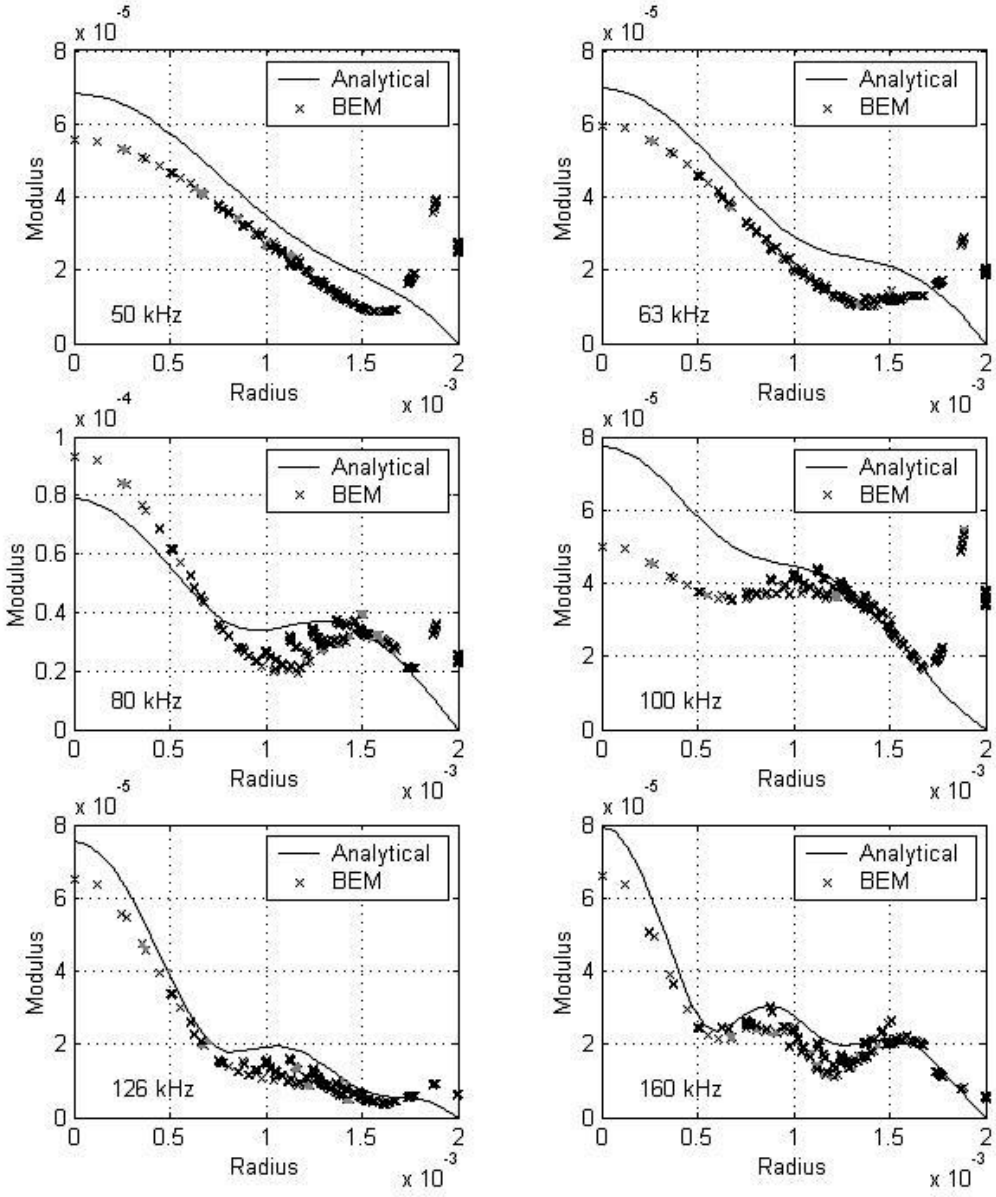

Figure 5-12. Normal viscous velocity behind the membrane of microphone BK 4939 at six 1/3 octave frequencies. Results from the analytical model (solid) and the BEM with visco-thermal losses (crosses) are shown.

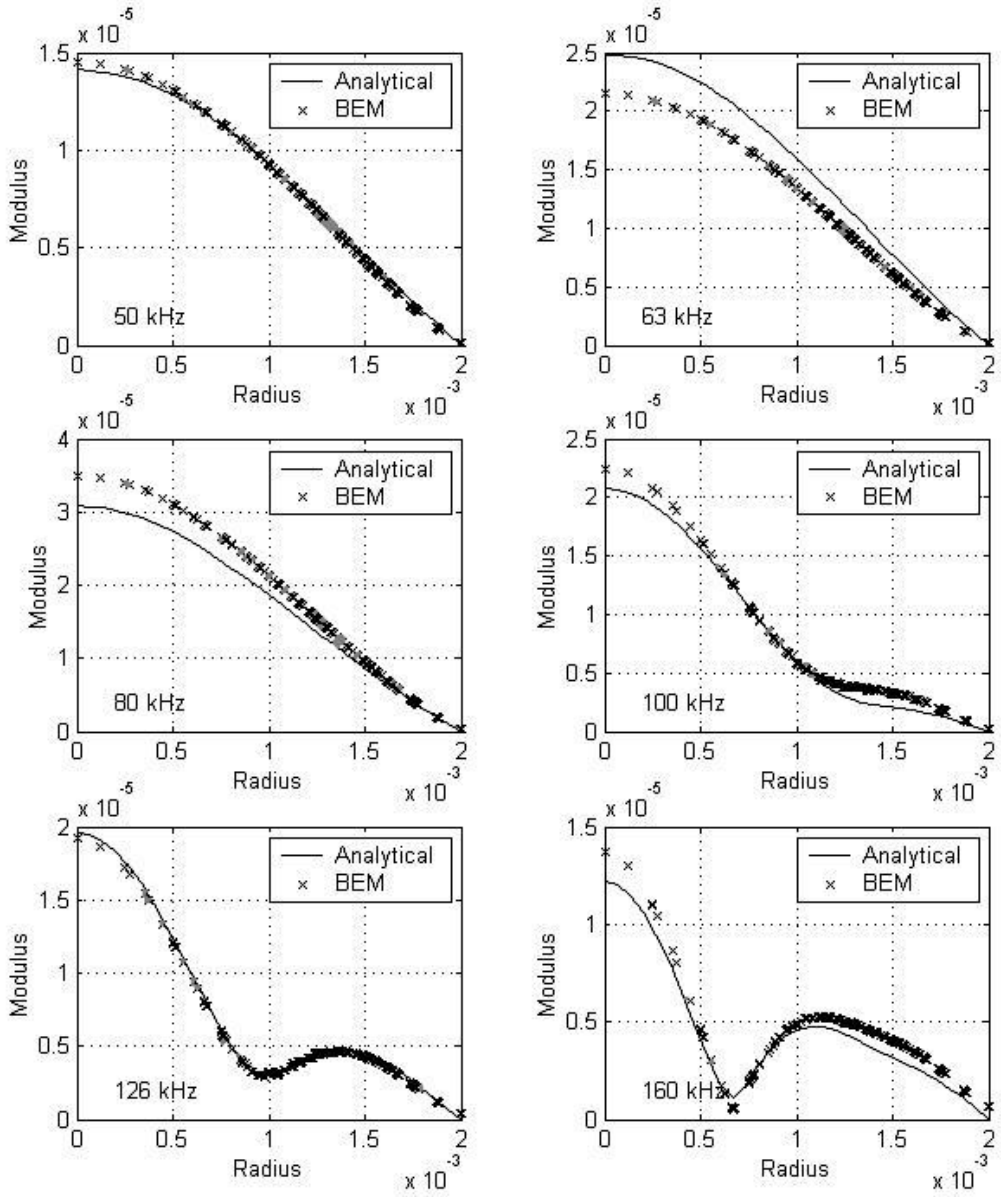

Figure 5-13. Normal thermal velocity behind the membrane of microphone BK 4938 at six 1/3 octave frequencies. Results from the analytical model (solid) and the BEM with visco-thermal losses (crosses) are shown.

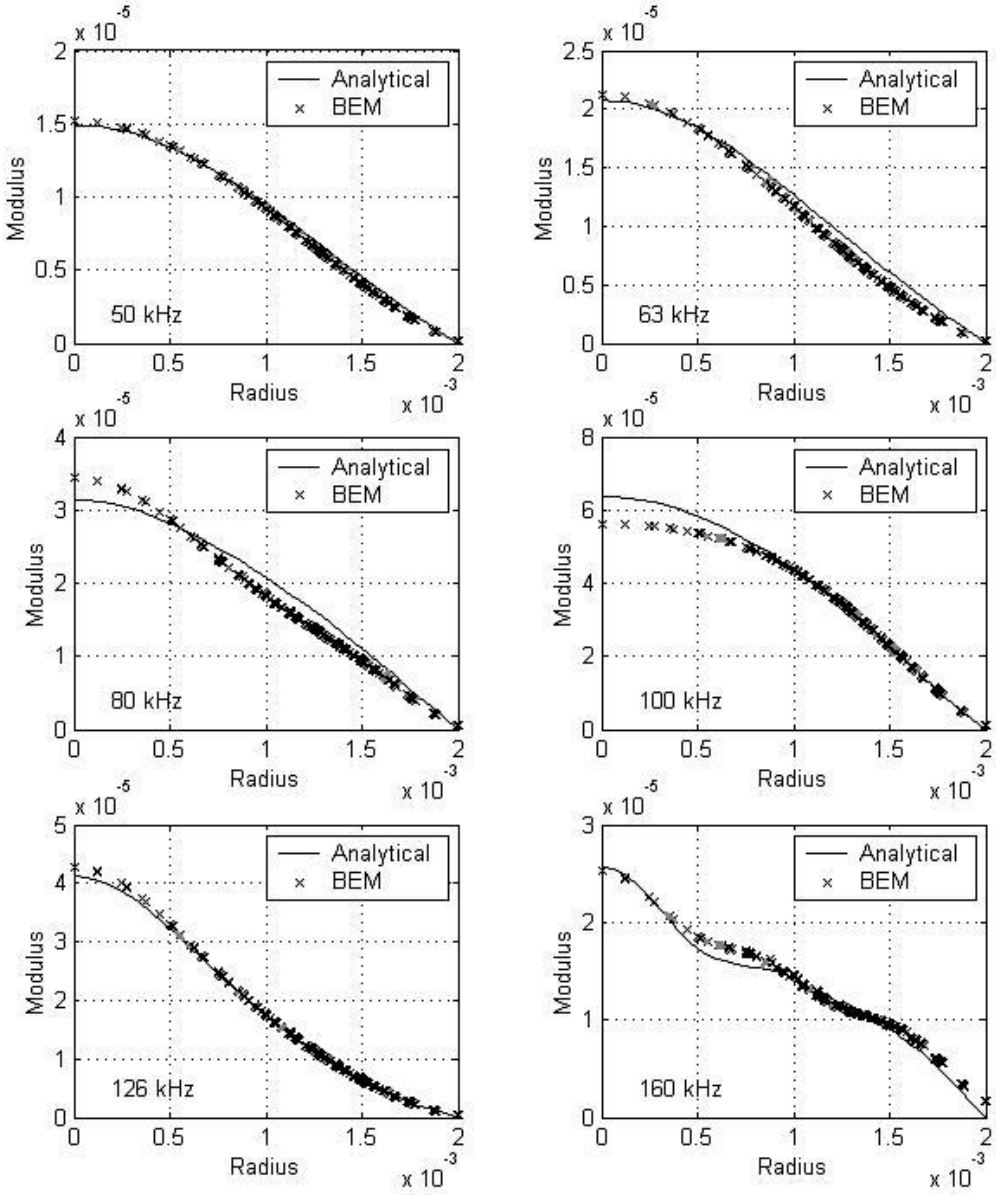

Figure 5-14. Normal thermal velocity behind the membrane of microphone BK 4939 at six 1/3 octave frequencies. Results from the analytical model (solid) and the BEM with visco-thermal losses (crosses) are shown.

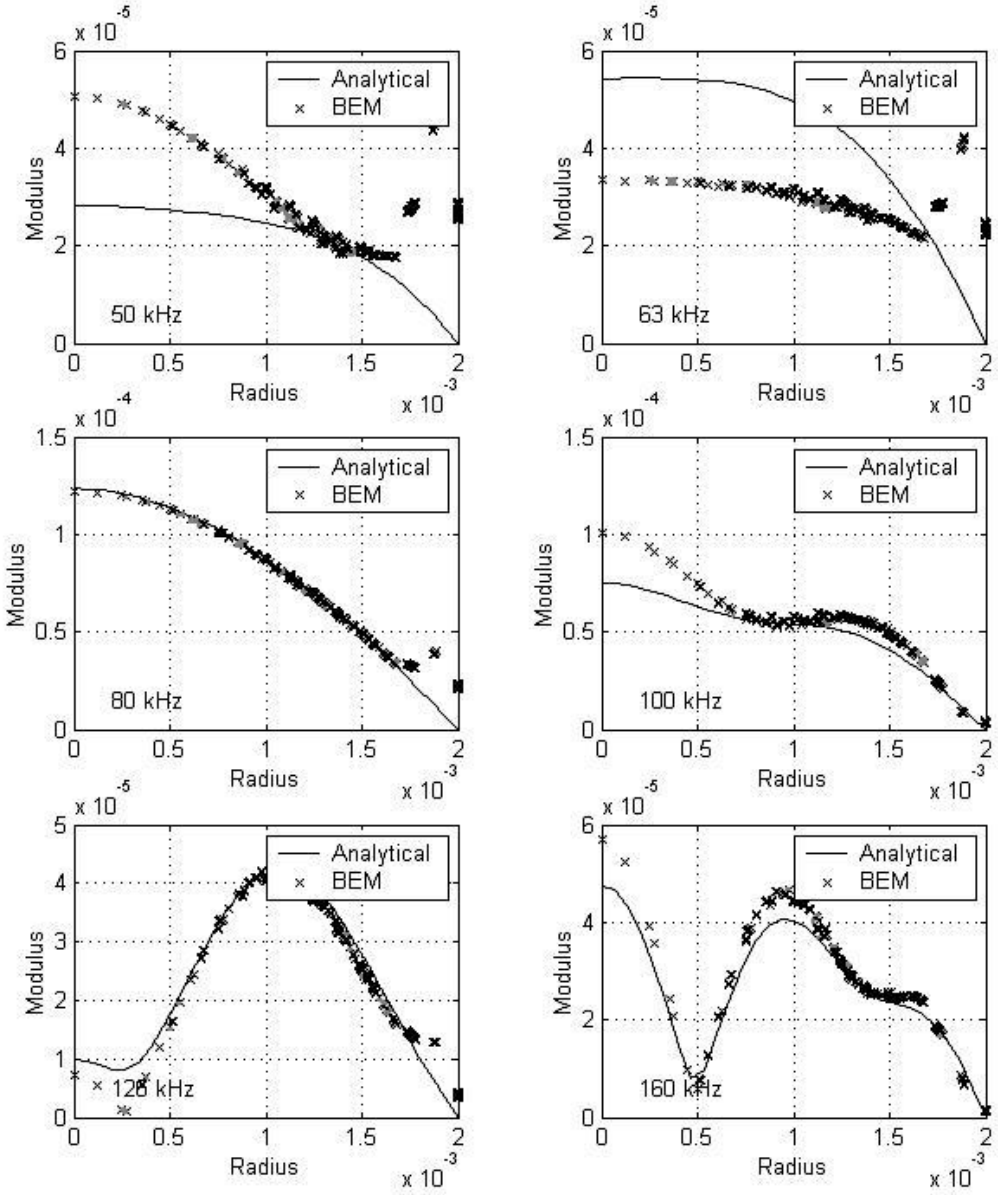

Figure 5-15. Normal acoustic velocity behind the membrane of microphone BK 4938 at six 1/3 octave frequencies. Results from the analytical model (solid) and the BEM with visco-thermal losses (crosses) are shown.

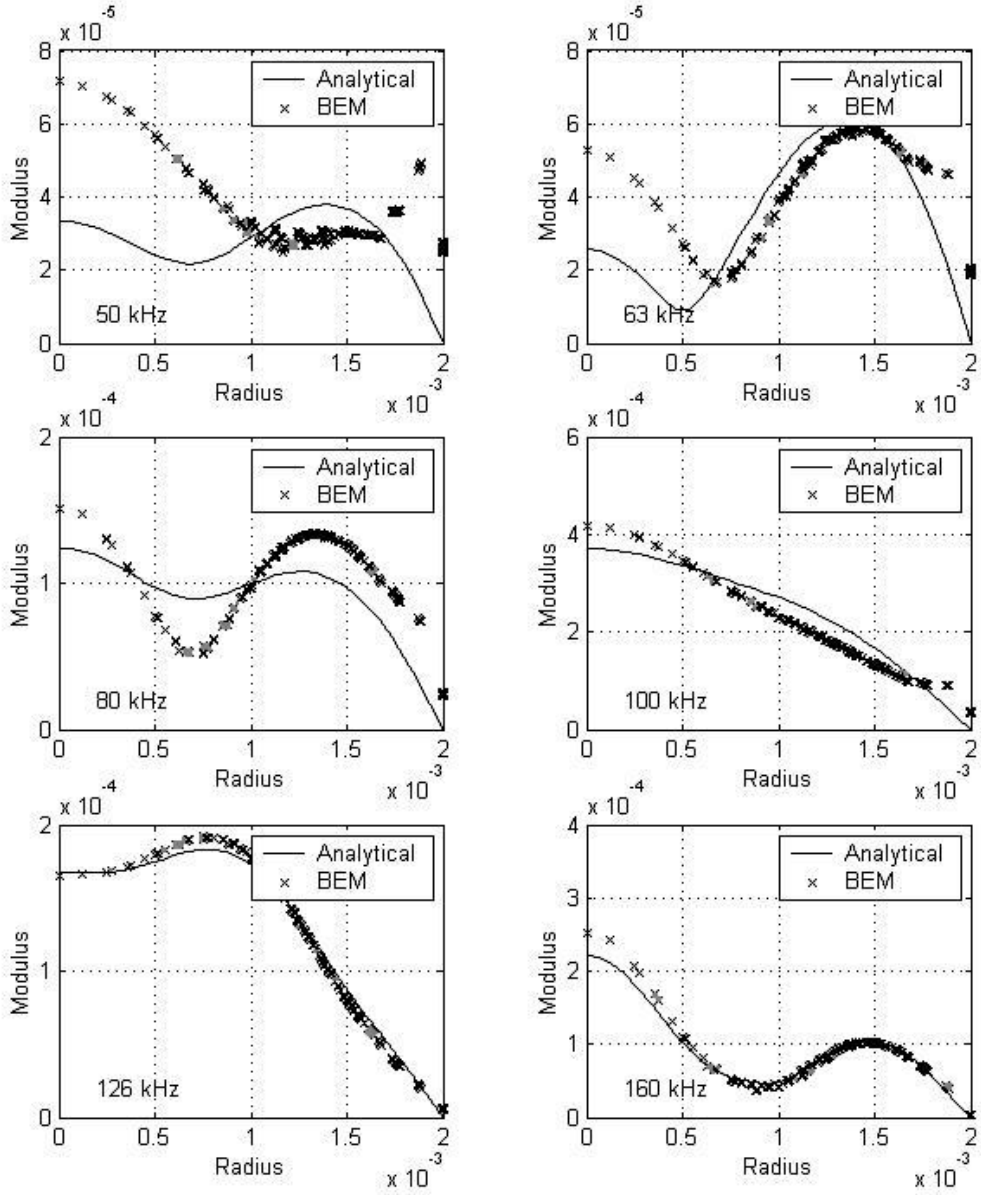

Figure 5-16. Normal acoustic velocity behind the membrane of microphone BK 4939 at six 1/3 octave frequencies. Results from the analytical model (solid) and the BEM with visco-thermal losses (crosses) are shown.

Let us introduce now new figures, equivalent to the previous set, but without viscosity. Since the new development in this thesis is the introduction of viscosity in the numerical calculation, it would perhaps be interesting to observe what is the effect of its absence in the results.

It is possible to reduce the influence of viscosity in the analytical model by reducing the coefficient of viscosity. In the BEM model, one can completely remove the viscosity by neglecting the last term in equation (4.20).

Figure 5-17 to Figure 5-24 represent this calculation without viscosity; the presentation is equivalent to the previous set of figures with viscosity, but there are, obviously, no plots for the viscous velocity.

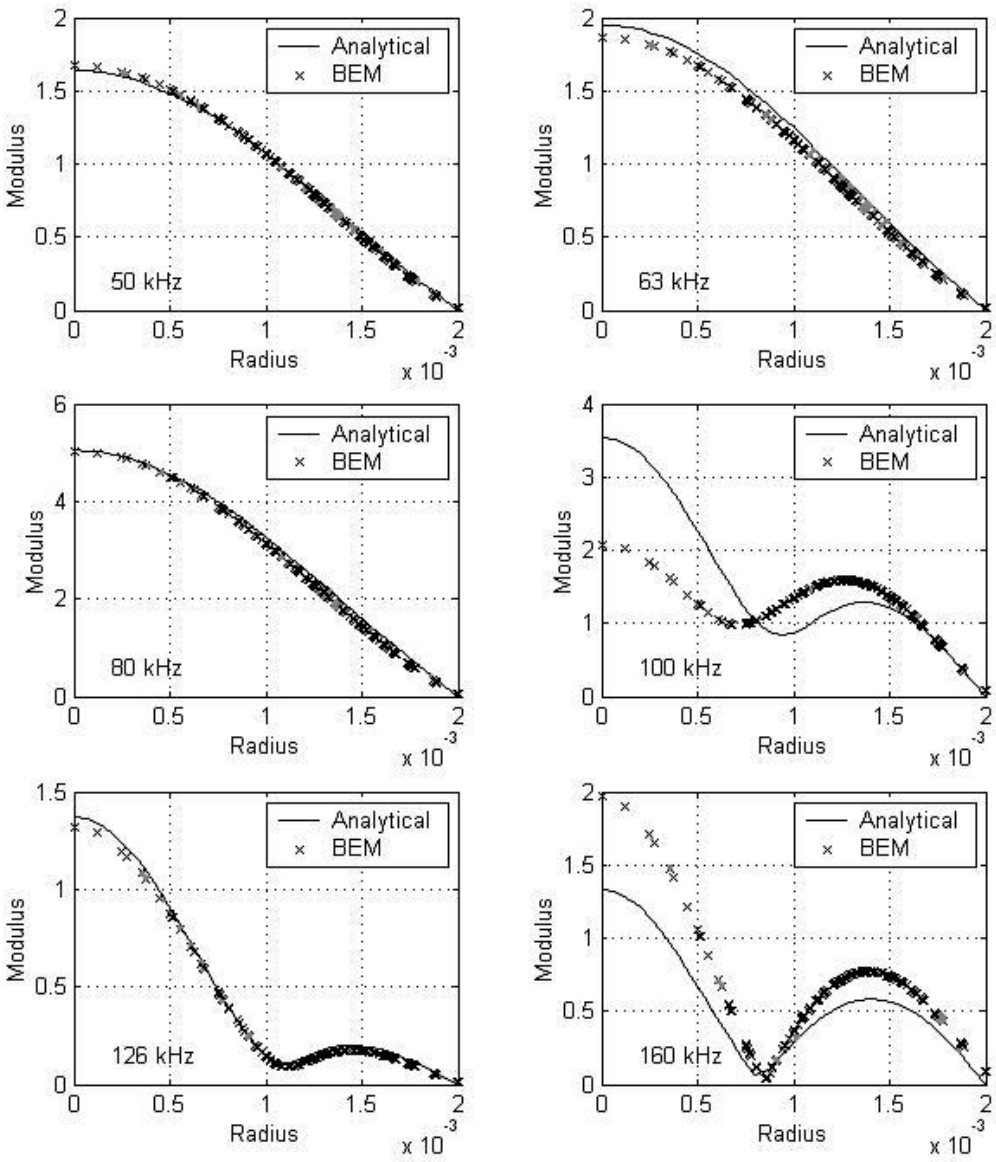

Figure 5-17. Sound pressure behind the membrane of microphone BK 4938 at six 1/3 octave frequencies. Results from the analytical model with reduced viscosity (solid) and the BEM with thermal losses only (crosses) are shown.

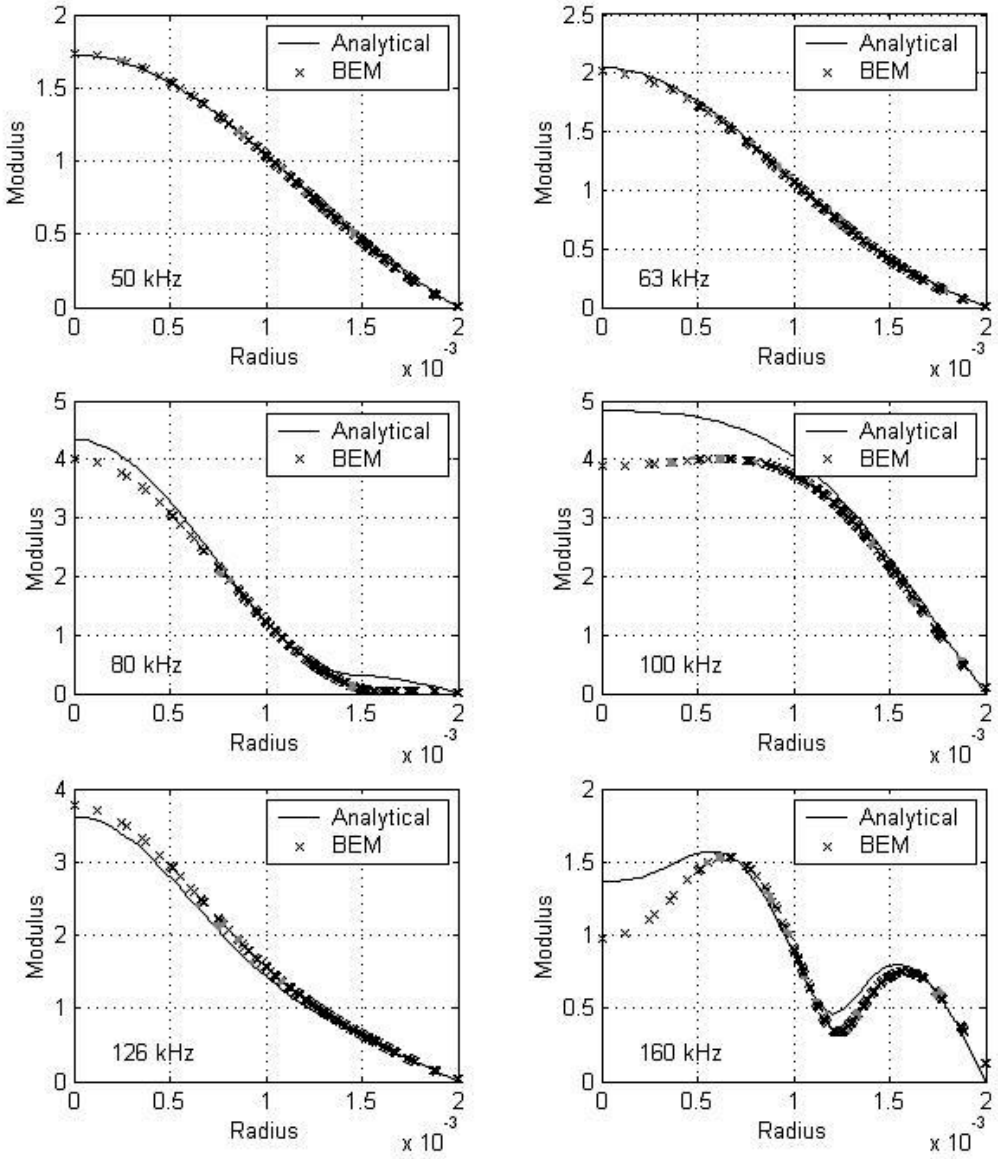

Figure 5-18. Sound pressure behind the membrane of microphone BK 4939 at six 1/3 octave frequencies. Results from the analytical model with reduced viscosity (solid) and the BEM with thermal losses only (crosses) are shown.

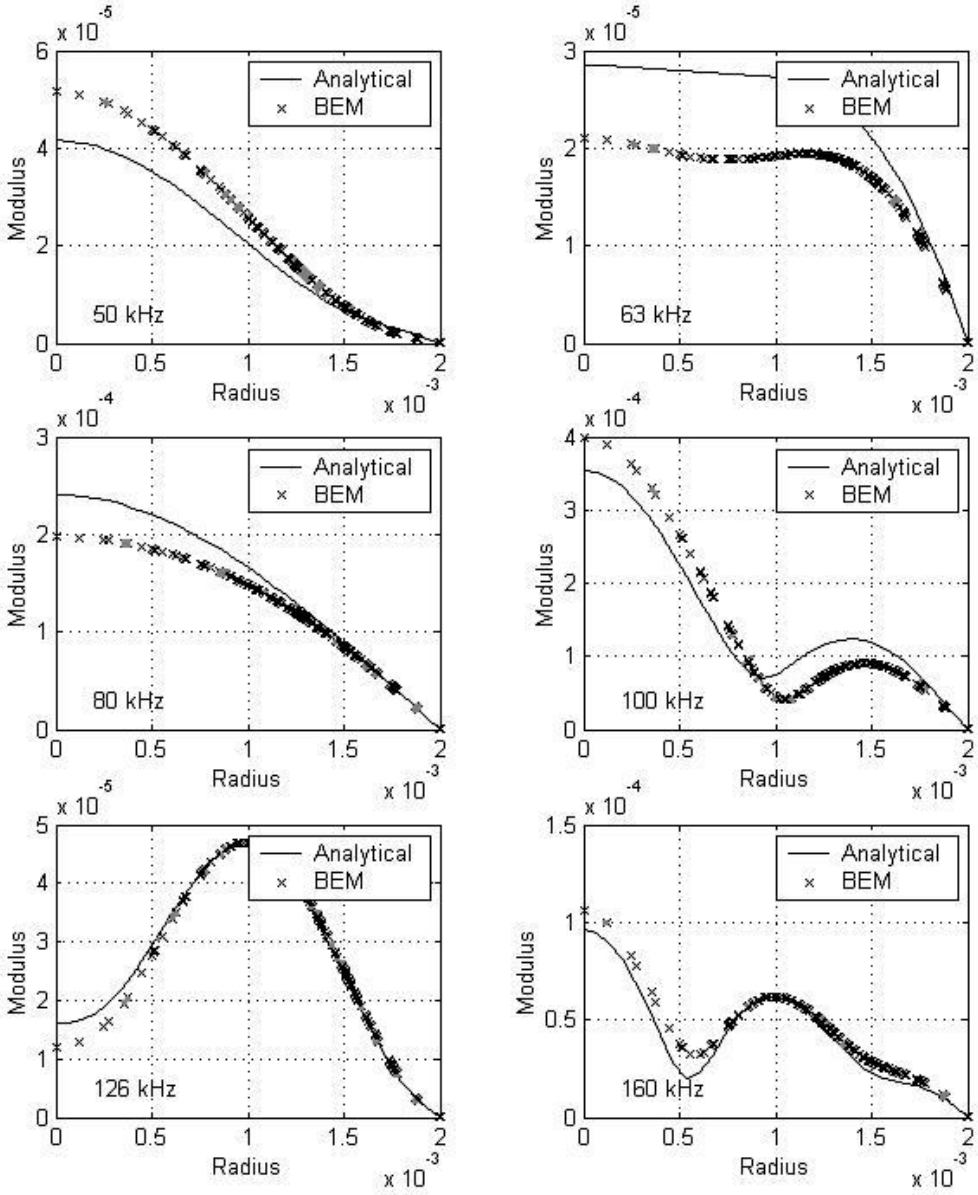

Figure 5-19. Total normal velocity of the membrane of microphone BK 4938 at six 1/3 octave frequencies. Results from the analytical model with reduced viscosity (solid) and the BEM with thermal losses only (crosses) are shown.

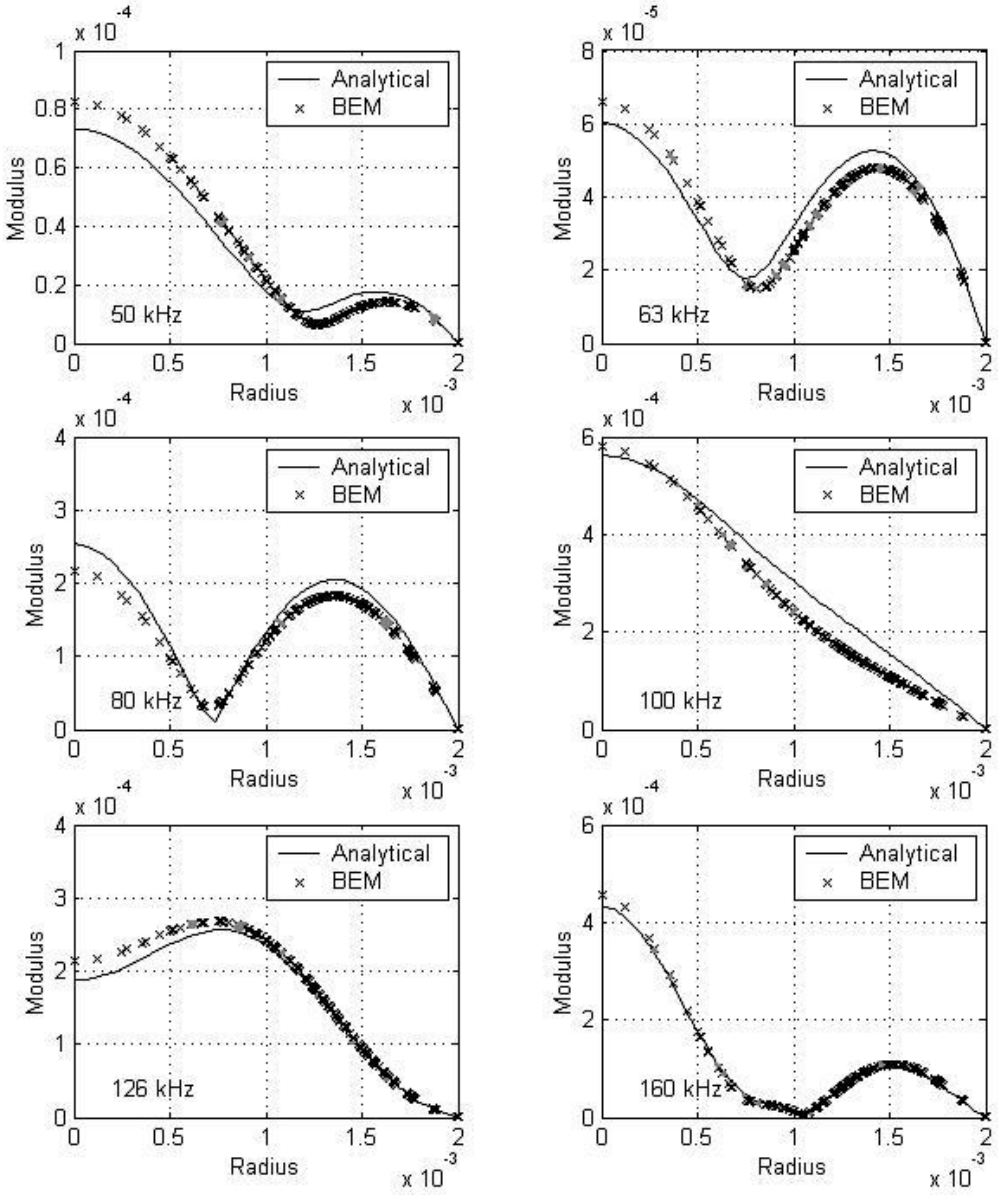

Figure 5-20. Total normal velocity of the membrane of microphone BK 4939 at six 1/3 octave frequencies. Results from the analytical model with reduced viscosity (solid) and the BEM with thermal losses only (crosses) are shown.

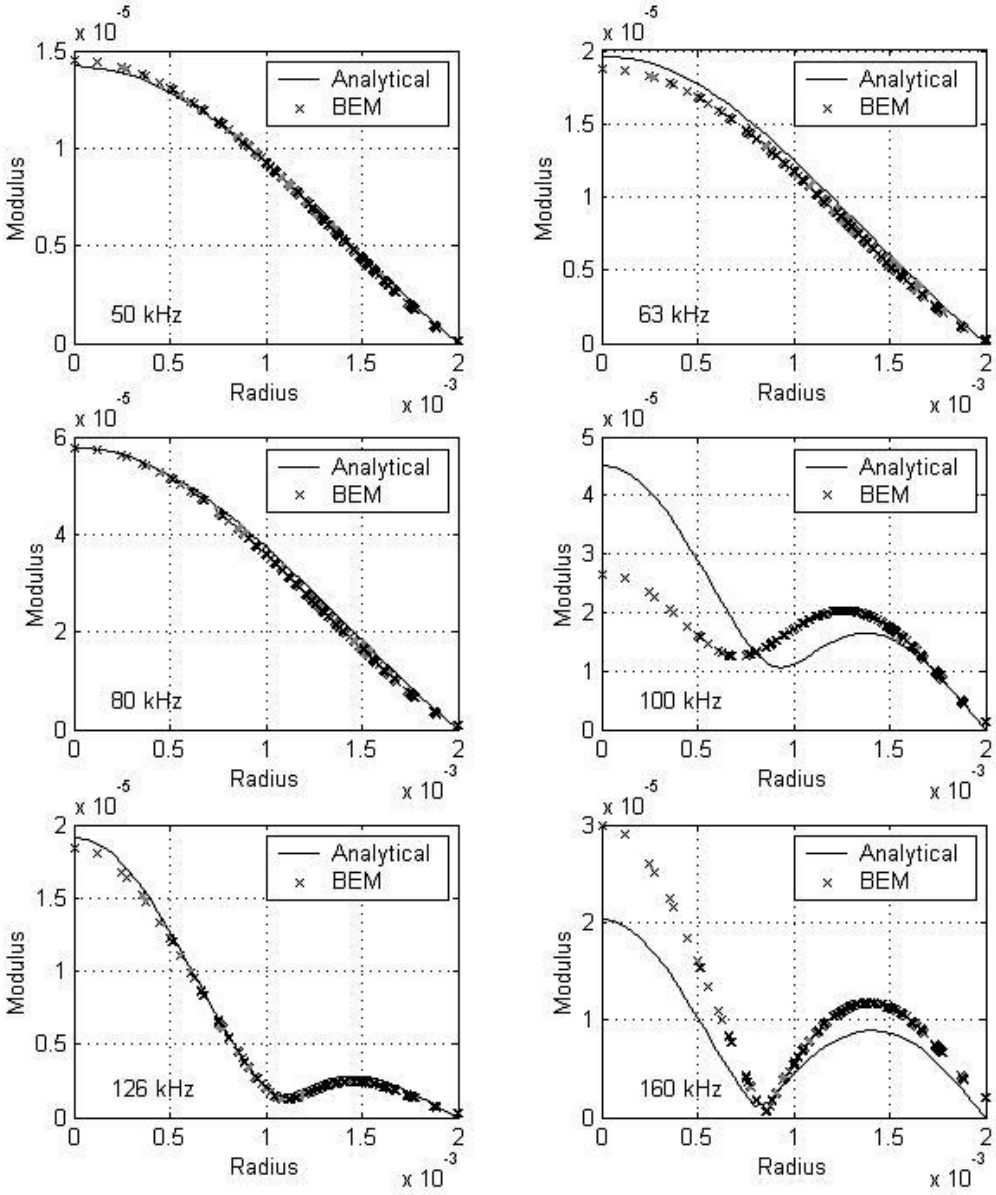

Figure 5-21. Normal thermal velocity behind the membrane of microphone BK 4938 at six 1/3 octave frequencies. Results from the analytical model with reduced viscosity (solid) and the BEM with thermal losses only (crosses) are shown.

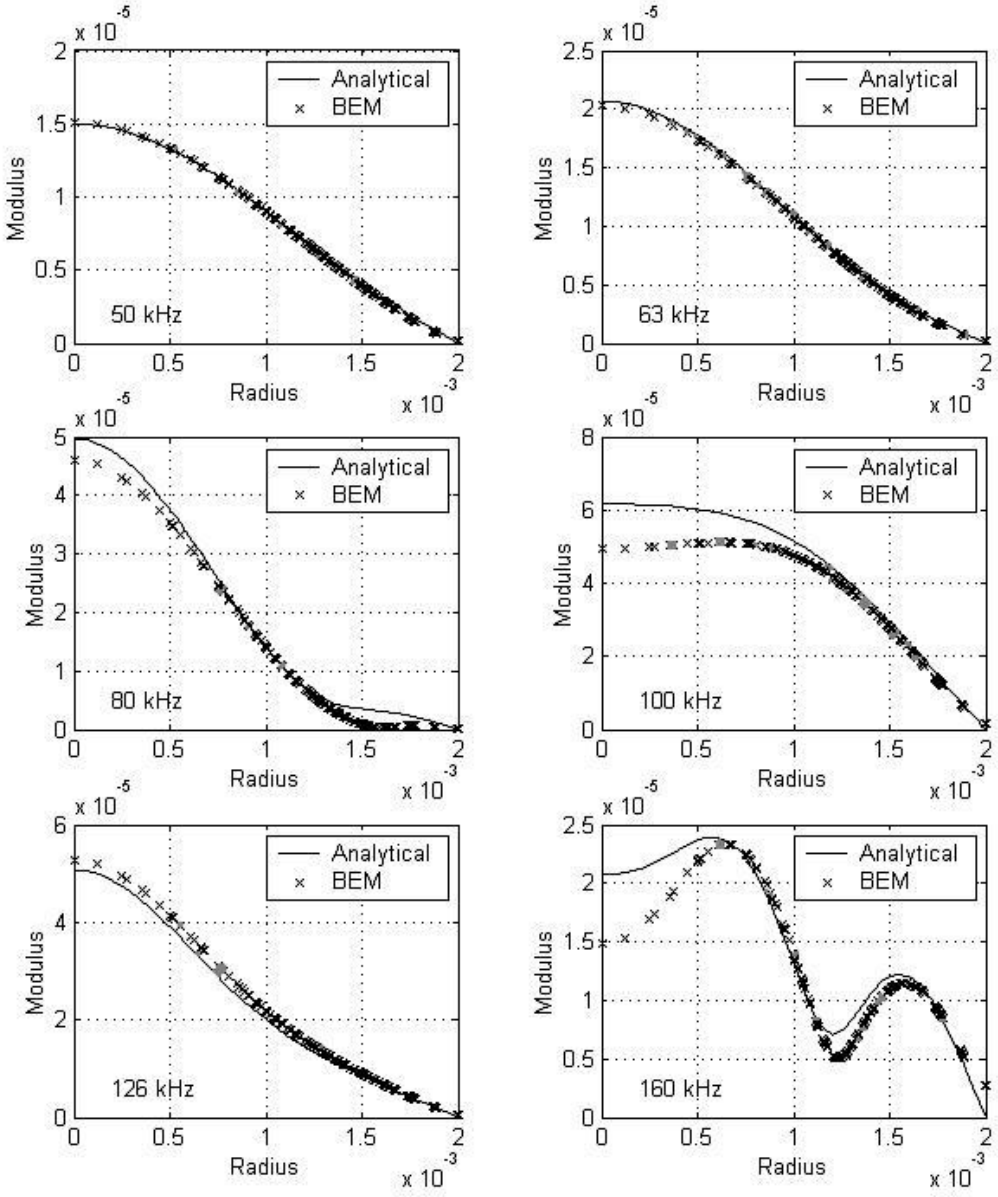

Figure 5-22. Normal thermal velocity behind the membrane of microphone BK 4939 at six 1/3 octave frequencies. Results from the analytical model with reduced viscosity (solid) and the BEM with thermal losses only (crosses) are shown.

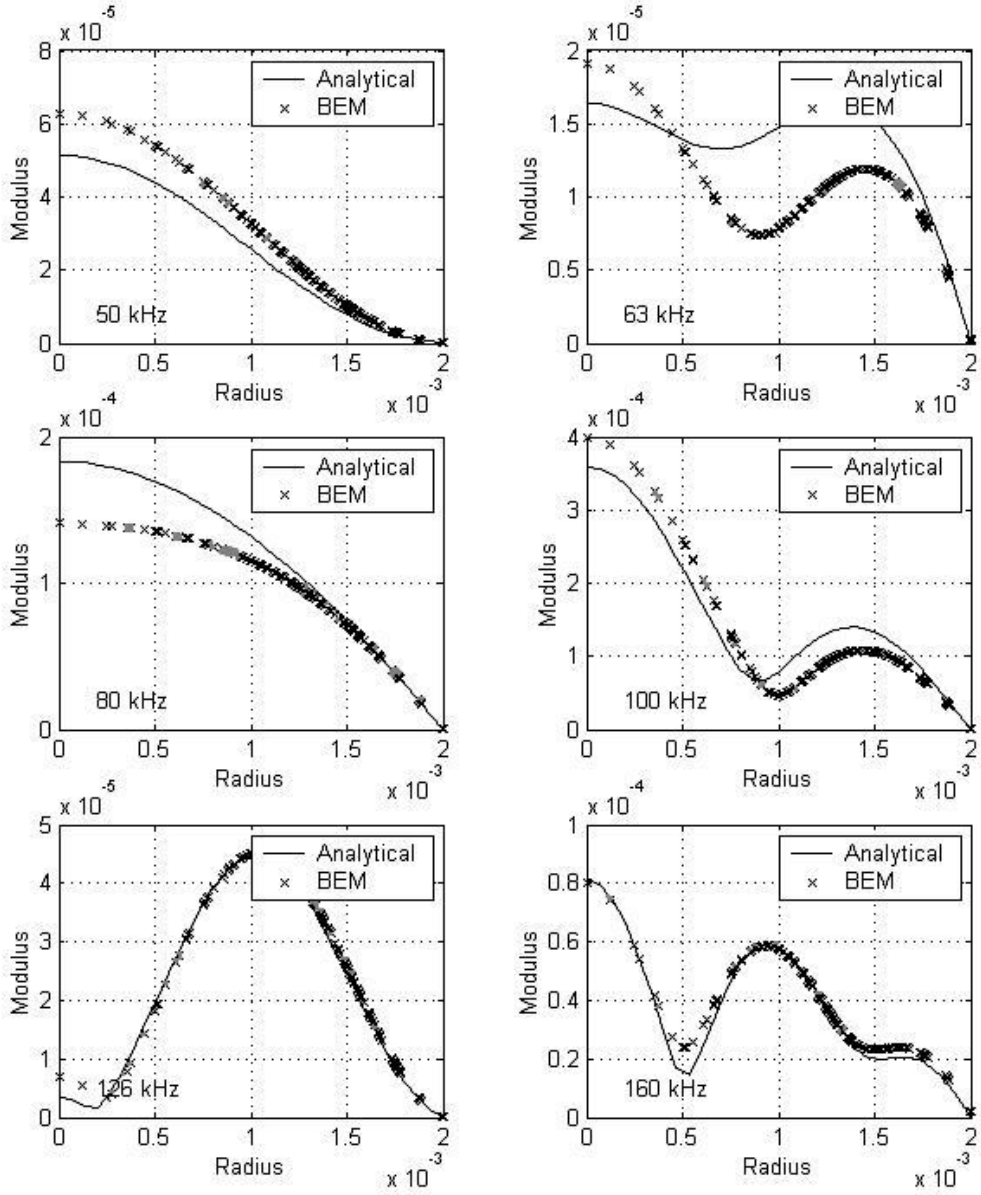

Figure 5-23. Normal acoustic velocity behind the membrane of microphone BK 4938 at six 1/3 octave frequencies. Results from the analytical model with reduced viscosity (solid) and the BEM with thermal losses only (crosses) are shown.

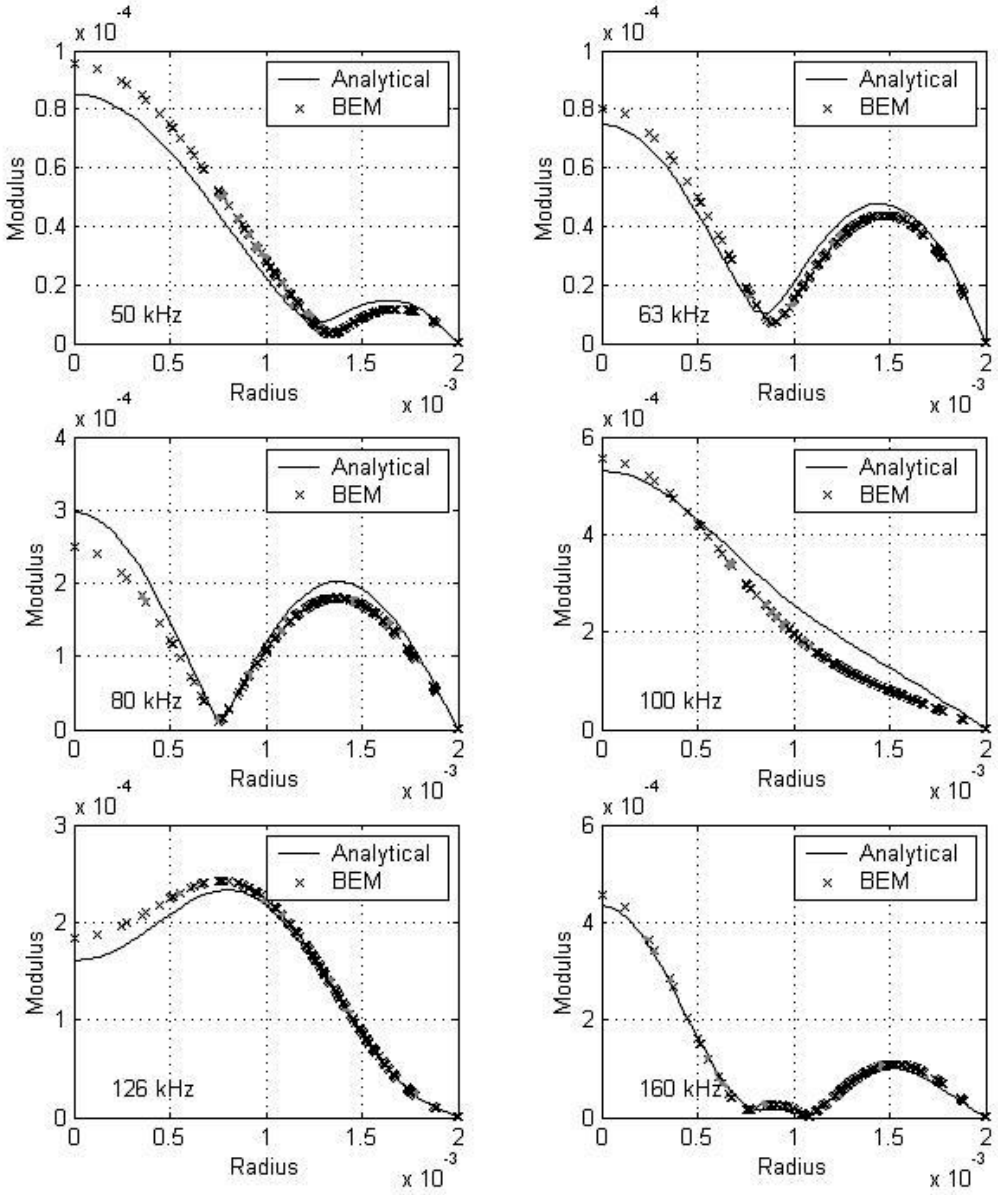

Figure 5-24. Normal acoustic velocity behind the membrane of microphone BK 4939 at six 1/3 octave frequencies. Results from the analytical model with reduced viscosity (solid) and the BEM with thermal losses only (crosses) are shown.

5.3. Comparison with measurements: frequency responses

In this section we present the data in the form of frequency responses. The graphs are normalized with the values at 1 kHz.

Figure 5-25 presents the normalized frequency response of the two microphones under study. It includes data from measurements made with an electrostatic actuator and results from the numerical and analytical models. The mean displacement of the membrane, proportional to the microphone's output, was calculated to obtain a result from the models.

Figure 5-26 shows a normalized frequency response with the viscous losses removed. If we compare this figure with the previous one it is possible to see the effect of the viscous losses.

The frequencies chosen do not follow an exact linear or logarithmic spacing. They were selected during the research so as to study some parts of the spectra in more detail. This is the case of the frequency range 50-100 kHz, where 13 frequencies were calculated.

The results are discussed in the next section.

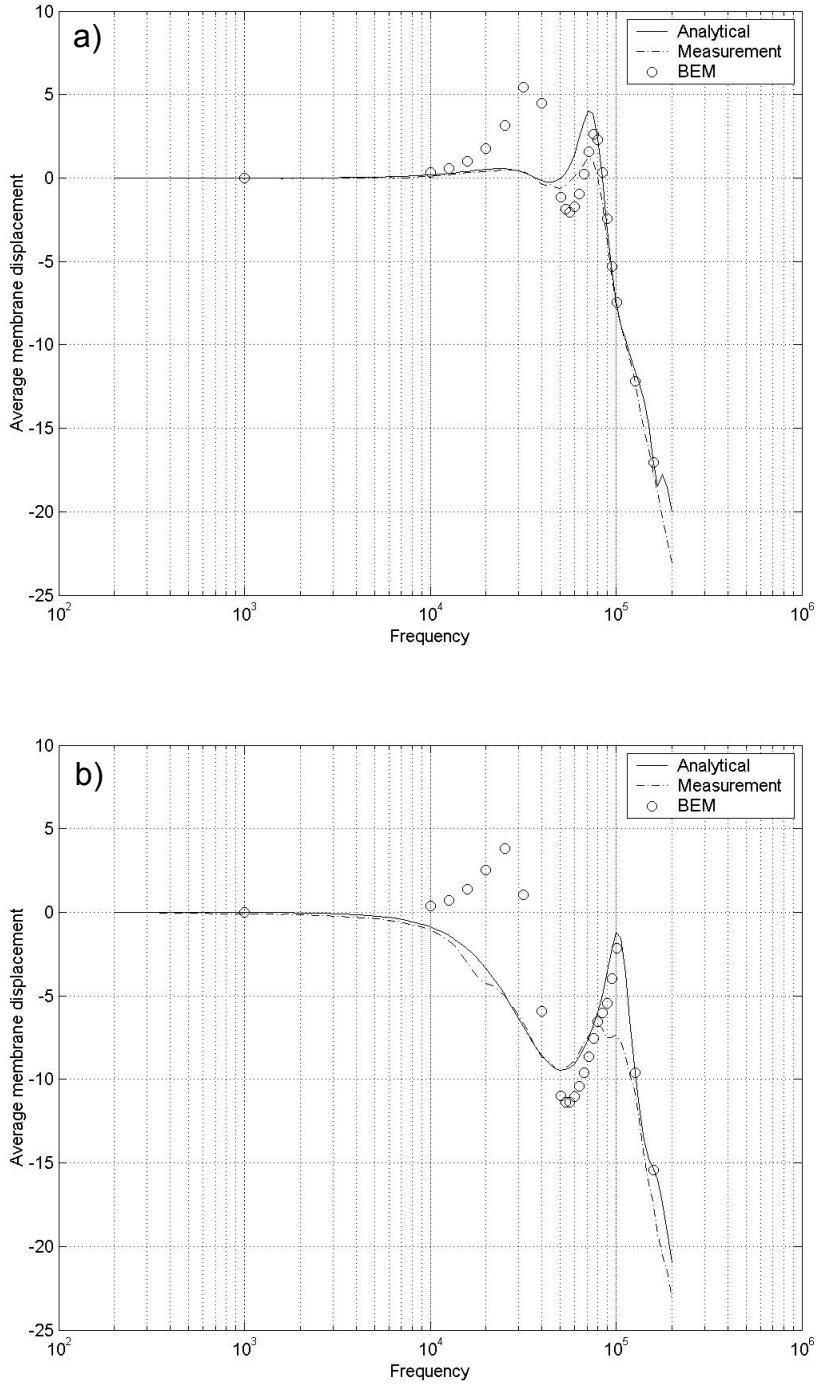

Figure 5-25. Normalized frequency response of the two microphones. Results from the analytical model, the BEM model with visco-thermal losses and measurements. a) BK 4938, b) BK 4939.

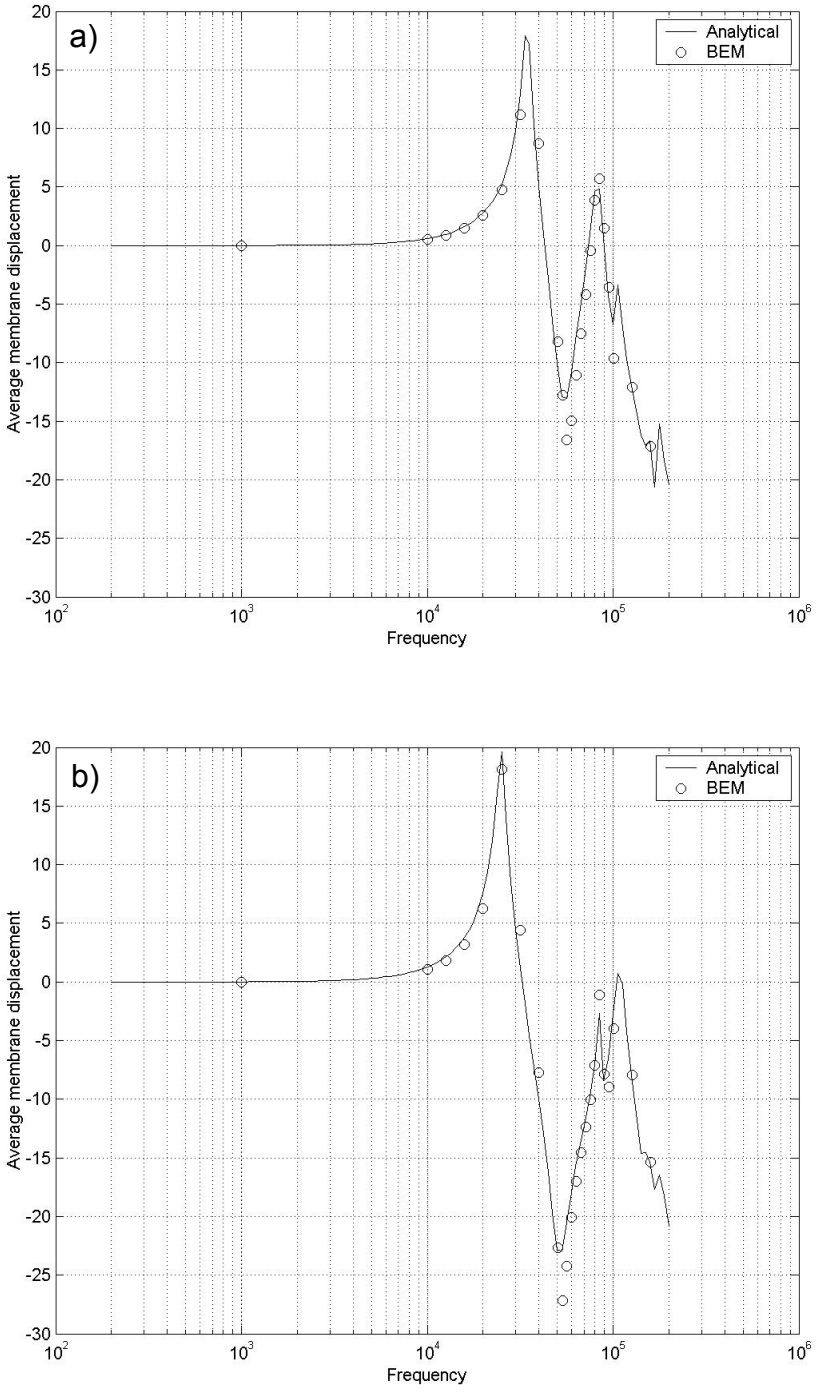

Figure 5-26. Normalized frequency response of the two microphones. Results from the analytical model and the BEM model. Viscous losses have been removed from all the calculations. a) BK 4938, b) BK 4939.

5.4. Discussion

The results presented here have been selected from the large volume of data available. For example, we only show results on the boundary surface, but the BEM model allows the calculation of any acoustical variable anywhere in the domain, that is, in the microphone's interior. Other frequencies have been calculated as well. However, the results shown are considered sufficient to observe the main features of the model developed here.

The matching of the results from the two models represented in section 5.2 is in most cases good in the frequency range considered. But let us first summarize some facts about the numerical model and the analytical model used for validation, most of them already touched upon in previous discussions:

1. The numerical model is fitted with a surrounding annular cavity that the analytical model only simulates with a pressure release boundary condition. The match between the two models can therefore only be reached when the two conditions at the rim are equivalent.

2. The analytical model assumes that the membrane's modes of vibration match one by one the modes inside the microphone, and that there is no influence between modes. They are calculated, in fact, independently. The numerical model, at least within the microphone, makes no assumptions of this sort; only the membrane is modeled using a modal expansion.

3. As was already discussed in 5.1, the analytical model's results at low frequencies for the acoustic variables in the interior are erroneous. The question here is to know above what frequency these results can be considered reliable and suitable for validating another model. Unfortunately, this question does not have a clear answer, since the transition is smooth. Besides, we do not have more models or measurements to compare with and find what results are acceptable.

4. The membrane representation in the numerical model is likely to spoil the coupling at low frequencies, since a modal expansion of the pressure behind the membrane is imposed in the coupled system, as we mentioned in chapter 4. This representation of the pressure is erroneous at low frequencies, as we have seen with an example in 5.1 in the study of the analytical solution. The situation is in fact similar for the two models, since they use the same membrane representation. In the case of the numerical model, however, it is also the incompatibility between membrane and fluid representations that causes difficulties.

5. The viscous mode is calculated in the numerical model using a tangential laplacian of the pressure, therefore it depends on a second derivative operator and in consequence the pressure representation should also be reliable down to its second derivative; it is not clear whether this is true for the modal expansion imposed by the membrane.

Under such conditions, the match observed in the results at high frequencies is quite good. The total pressure is certainly similar with the two models at high frequencies, if we observe Figure 5-7 and Figure 5-8.

The total normal component of the velocity in Figure 5-9 and Figure 5-10 is in general in good agreement, but there are some exceptions. At 63 kHz for the 4938 microphone, for example, the normal velocity is underestimated in the numerical model with respect to the corresponding analytical result. In other cases, like 50 and 80 kHz for the 4939 microphone, the total pressure seems in good agreement, but the corresponding velocity has a poorer match. The reason can be seen in Figure 5-8 where the pressure at these frequencies has a different "curvature", or second derivative, and the calculation of the viscous mode depends on this as we saw. This could perhaps be a consequence of the membrane formulation mentioned in point 4 above.

Let us observe now, for comparison with the figures just analyzed, the corresponding ones without viscosity, which are Figure 5-17, Figure 5-18, Figure 5-19 and Figure 5-20. The total pressure predicted by the analytical solution is sometimes different in magnitude than the

numerical result, in this case because the viscosity cannot be removed completely from the analytical solution. Other calculations with different values of the viscosity coefficient supplied to the analytical calculation prove this.

Let us analyze now the different parts of the normal component of the velocity: acoustic, thermal and viscous. Figure 5-11 and Figure 5-12 show the normal viscous velocity and one can observe the effect of the discrete tangential laplacian in the blurred aspect of the numerical result: there are some boundary elements that are slightly more distorted at a radius of 1-1.5 mm, and this is apparent in the figures.

The reason for the behavior of the viscous component in the neighborhood of the rim is more difficult to explain. One should expect physically a null normal viscous velocity at the rim, as reference [7] maintains. This sudden increase of the modulus of the normal viscous velocity at the rim could be due to several reasons: i) the tangential laplacian at the rim's nodes ($r=R$) is calculated using the sound pressure at membrane nodes with $r<R$., while in other nodes the tangential laplacian is a function of the sound pressure at all neighboring nodes in all directions, ii) the corner is not modeled properly because only losses in the gap are considered, and iii) the membrane formulation in the numerical model mentioned in point 4 above could manifest its incompatibility with the BEM calculation in the fluid with special difficulties at the rim. We cannot know for sure which of these explanations is correct. Further investigation should address this topic. The author has the impression that the membrane representation (listed iii) above) could be the reason since this behavior at the rim is more obvious the lower the frequency, where this problem shows more clearly. If the other explanations were correct the rim's discrepancy should not, in principle, depend on the frequency.

If we observe the normal components of the thermal and acoustic velocities in Figure 5-13, Figure 5-14, Figure 5-15 and Figure 5-16, we see that the acoustic velocity has the same "blurring" the viscous velocity had, but it is not present in the thermal velocity. At the same time, the thermal velocity does not show any of the "rim effects" just commented. This can be explained physically considering that the thermal velocity is almost negligible in the direction tangential to the surface.[30] The calculation of the viscous component is based, as we saw, on

imposing the no-slip boundary condition in the tangential direction, and this means that the tangential components of the acoustic and viscous velocities must be balanced and therefore behave in a similar manner. This also shows in the normal components.

We can now move again to the calculation without viscosity to compare the behavior of the thermal and acoustic modes. Note that no viscous mode result exits, since we removed the viscosity. This corresponds to Figure 5-21, Figure 5-22, Figure 5-23 and Figure 5-24. None of the effects mentioned above ("blurring" of the data, mismatch at the rim) are present here. This proves that such effects are a consequence of the viscous mode implementation, as was maintained. There are however discrepancies at some frequencies, perhaps due to the vicinity of a resonance, that the two models are likely to hit differently. This becomes apparent by observing the sharp peaks in the frequency response without viscosity in Figure 5-26

We have not shown results at frequencies below 50 kHz in section 5.2. As discussed above, neither the analytical reference nor the numerical calculation can be trusted in this range. However, we include in Figure 5-27 an example of the total sound pressure behind the membrane for one of the microphones at some frequencies up to 53 kHz.

The lowest frequency, 1 kHz, has a similar behavior as in Figure 5-2, where the viscous losses were removed. In the present case the numerically calculated pressure at 1 kHz is forced to a low value, presumably by the membrane's formulation coupled to the BEM in the interior. The following plots at progressively higher frequencies show that this effect is slowly diminished, until a match of the pressures is achieved at 53 kHz. This behavior seems to support the conclusions maintained in this thesis about the need of a better model, probably using FEM, of the membrane to be coupled to the numerical calculation in the microphone's interior.

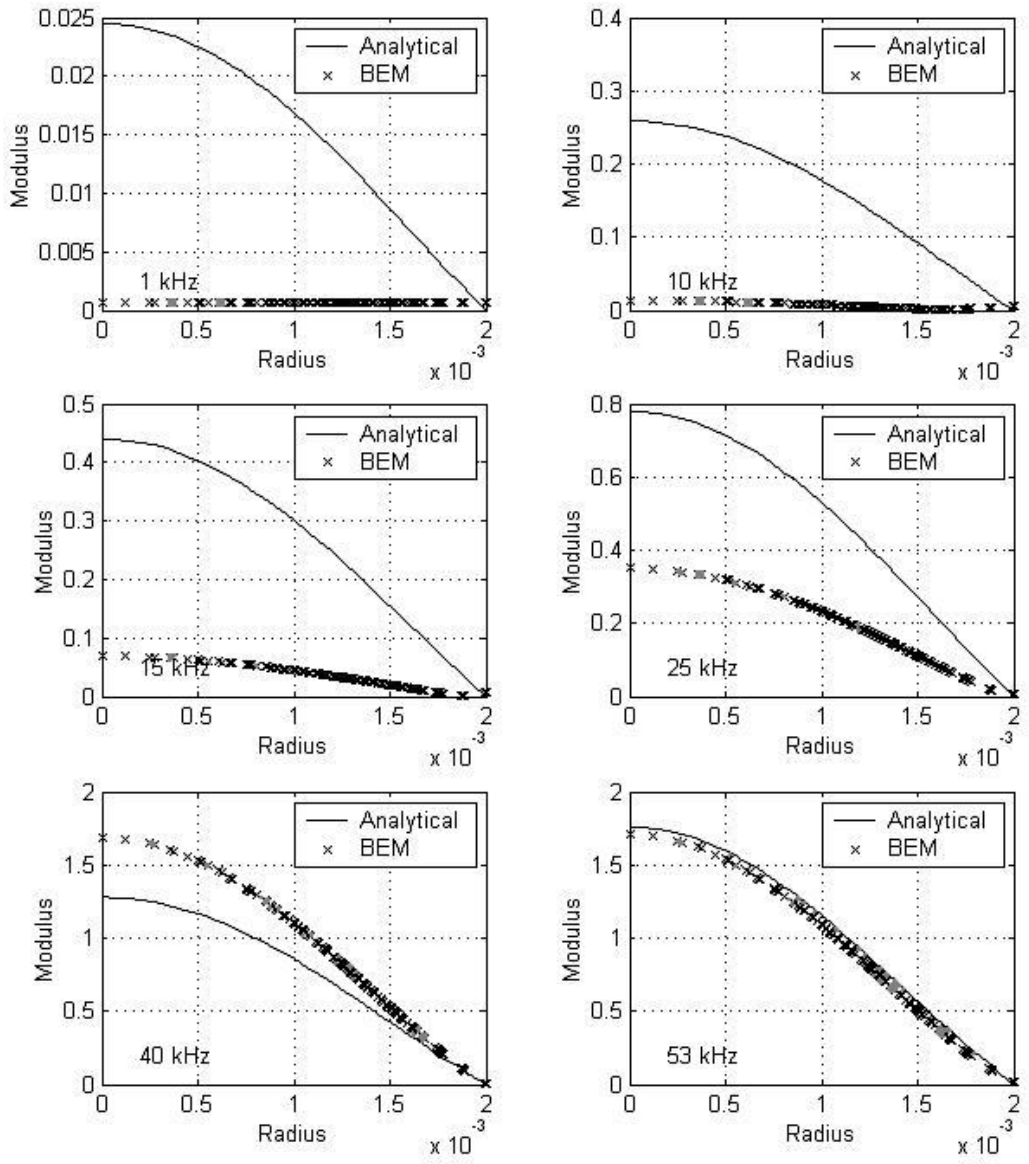

Figure 5-27. Sound pressure behind the membrane of microphone BK 4938 at six frequencies. Results from the analytical model (solid) and the BEM with visco-thermal losses (crosses) are shown.

The observation of the frequency responses in section 5.3 (Figure 5-25) shows also the failure of the numerical calculation at frequencies below around 50 kHz, where the calculated viscous losses are not able to damp the first resonance of the membrane. At even lower frequencies,

the membrane dominates the behavior of the setup and the errors in the calculation do not show. Above around 50 kHz, however, the three sets of results look more similar, as expected.

Figure 5-26 presents results with only thermal losses, and in this case the agreement is excellent. In this case no measurements are shown since it is not possible to measure without viscosity. One can conclude that the limitations imposed to the numerical model by the analytical formulation of the membrane coupled to it are only apparent when the viscosity is included.

6. DISCUSSION AND SUGGESTIONS FOR FUTURE WORK

In this thesis the phenomenon of the propagation of sound waves in fluids with viscous and thermal losses has been addressed, with the objective of examining the feasibility of a numerical model that can be used to simulate the behavior of measurement condenser microphones and help with the design process.

To do this it was necessary to acquire sufficient knowledge about three different fields: i) the manufacturing and operation of measurement condenser microphones and the tools used for their design and testing, ii) the physical phenomenon of viscous and thermal losses of sound waves in fluids and iii) numerical methods, the Boundary Element Method in particular.

The standard direct collocation formulation of the Boundary Element Method is not in principle able to cope with thin bodies or narrow gaps. The problem was studied and a interval division integration technique was found that could be incorporated to the method to improve its performance to the point of being able to cope with gaps much narrower than the microphone's, thus allowing the use of this numerical formulation in the project. The improved version of the method was thoroughly tested to establish its performance and suitability. The technique has other possible applications apart from transducer modeling: it can be used whenever the setup studied with BEM has very close meshed surfaces or when the calculation of the sound field at a point very close to a boundary is required.

This modification of the BEM to deal with close surfaces was fitted in an axisymmetrical formulation and in a standard three-dimensional formulation. The latter was finally employed in the development of the microphone model.

The available literature on viscous and thermal losses of sound waves in fluids has been searched for ways to combine it with numerical methods and produce a model. The theoretical work by Bruneau *et al.* and the numerical implementation by Karra and Ben Tahar have been fundamental to approach the task.[6,7,23,22]

Bruneau's theoretical formulation of the Navier-Stokes equations for visco-thermal fluids with no flow and linear variation sets an adequate framework for numerical implementations. The theory was used for extending the work by Karra and Ben Tahar to include viscous losses. The main difficulty was the correct implementation of the velocity boundary conditions, which have a vector nature when viscosity is considered.

The numerical implementation developed here has been validated against measurements and analytical results. The validation, however, was problematic for three reasons: i) the analytical solution used for comparison is not reliable in the lower part of the frequency spectrum, ii) the measurements only allow the comparison of frequency responses, not the sound fields inside the microphone, and iii) the numerical model was fitted with a membrane, coupled to it, that in its present analytical form hinders its performance at frequencies below around 50 kHz. In any case, the model could be validated in the high frequency range and it is expected that further extensions make it suitable to cover the whole bandwidth.

This project leaves several paths of research open for further investigation. Let us list some of them:

- The implementation of the special integration technique for narrow gaps in the three-dimensional BEM can be extended to cope with any close collocation point, not only those that are close to the nodes. In this way the close meshes would not necessarily have to be matched node by node.

- The improved three-dimensional BEM should be tested thoroughly to establish its convergence properties, its stability, the influence of the mesh densities and the behavior of the different types of surface elements. In the present work such a study was accomplished for the axisymmetrical case (see the journal paper in Appendix D) and its results extrapolated to the three-dimensional case. From the calculations that were run during the development it is believed that the three-dimensional version could perform considerably better than the axisymmetrical one when coping with close surfaces.

- A possible future line of work would be a full implementation of the viscous and thermal losses with the axisymmetrical BEM formulation. Although this formulation limits the range of cases that can be simulated, it would be much more suitable for the study of possible improvements that could be later incorporated to the full three-dimensional version. The three dimensional version takes considerable time and computer storage to run; therefore its development is necessarily slow. Some of the possible improvements to be added using the axisymmetrical formulation are the generalization of the viscous mode to any non-flat surface and the treatment of the geometrical singularity at the corners.

- A new formulation for the membrane using the Finite Element Method is very much needed. The corresponding stiffness matrix of the membrane thus obtained can be coupled to the BEM formulation with visco-thermal losses using an iterative procedure. This development can be done either in the three-dimensional implementation or in an axisymmetrical version, if that is developed.

- A suitable method for validation at low frequencies should be found. Once the FEM implementation of the membrane is achieved, the performance of the model at low frequency could only be compared with measured frequency responses.

The numerical model developed in this project, in its present form or after new improvements, can be useful to understand the phenomenon of visco-thermal losses and attack new problems different from the original objective, the condenser microphone. It could for example be used to improve the performance of acoustic transducers mounted in mobile telephones, by calculating the losses in the narrow openings left for the sound to pass through.

7. CONCLUSIONS

The thesis work described in this report has reached several objectives, with some findings of interest. They can be briefly summarized in the following conclusions:

1. Existing work has been analyzed and considered as a foundation for the thesis. In particular the theoretical development of Bruneau *et al.* and the numerical models by Karra and Beltman have been a source of inspiration.

2. A numerical implementation using the standard collocation formulation of the Boundary Element Method has been developed using the equations that govern the physics of the propagation of sound waves in fluids with viscous and thermal losses. A method of calculating a discrete tangential laplacian on a surface has been created to the effect of introducing viscous losses.

3. This visco-thermal implementation has been applied to the modeling of measurement condenser microphones. To do this, it has been defined in a microphone-like geometry and it has been coupled to a membrane. The coupled model, however, was not taken to the final stage of development since the membrane formulation limits its use to high frequencies. However, the coupled model could be validated in that range.

4. The Boundary Element Method used in this work has been fitted with a new integration technique applied to the near-singular integrals that appear in the standard formulation whenever two surfaces are very close. The technique was developed especially for the purpose of making the BEM suitable for the modeling of condenser microphones, but it is presumed to have a much wider range of applications.

5. An analytical model taken from the literature has been implemented. It was used for the validation of the numerical implementation with viscous and thermal losses. The suitability of this analytical model for the validation task has been analyzed and some aspects of its performance at low frequency clarified.

8. REFERENCES

[1] W. M. Beltman, P. J. M. van der Hoogt, R. M. E. J. Spiering and H. Tijdeman, "Implementation and experimental validation of a new viscothermal acoustic finite element for acousto-elastic problems." *Journal of Sound and Vibration* **216** (1998), 159-185.

[2] W. M. Beltman, "Viscothermal wave propagation including acousto-elastic elastic interaction, part I: theory." *Journal of Sound and Vibration* **227** (1999), 555-586.

[3] W. M. Beltman, "Viscothermal wave propagation including acousto-elastic elastic interaction, part I: applications." *Journal of Sound and Vibration* **227** (1999), 587-609.

[4] L.L. Beranek. *Acoustics*. Acoustical Society of America. New York, 1954.

[5] J. J. Bowman, T. B. A. Senior and P. L. E. Uslenghi, *Electromagnetic and acoustic scattering by simple shapes*. North-Holland Publishing Company, Amsterdam, 1969.

[6] M. Bruneau, Ph. Herzog, J. Kergomard and J. D. Polack. "General formulation of the dispersion equation in bounded visco-thermal fluid, and application to some simple geometries." *Wave Motion* 11 (1989), 441-451.

[7] M. Bruneau, A. M. Bruneau and P. Hamery. "An improved approach to modeling the behavior of thin fluid films trapped between a vibrating membrane and a backing wall and surrounded by a reservoir at the periphery." *Acta Acustica* 1 (1993), 227-234.

[8] *B&K microphone handbook*. Brüel & Kjær Sound & Vibration A/S, Nærum (Denmark), 1996.

[9] A. J. Burton and G. F. Miller, "The Application of Integral Equation Methods to the Numerical Solutions of Some Exterior Boundary Value Problems." *Proceedings of the Royal Society of London Series A* **323** (1971), 201-210.

[10] É. Cartan. *Leçons sur la géométrie des espaces de Riemann*. Gauthier-Villars, Paris 1946.

[11] C. Y. R. Cheng, A. F. Seybert, and T. W. Wu, "A Multidomain Boundary Element Solution for Silencer and Muffler Performance Prediction." *Journal of Sound and Vibration* **151** (1991), 119-129.

[12] R.D. Ciskowski and C.A. Brebbia (eds.). *Boundary Element Methods in Acoustics*. Elsevier Applied Science, London, 1991.

[13] V. Cutanda, P.M. Juhl and F. Jacobsen, "On the modeling of narrow gaps using the standard boundary element method." *Journal of the Acoustical Society of America* **109** (2001), 1296-1303.

[14] J. E. Dennis, jr. and R. B. Schnabel. *Numerical methods for unconstrained optimization and nonlinear equations*. Prentice Hall, New Jersey, 1983.

[15] F. J. Fahy. *Sound Intensity (2nd edition)*. E & FN Spon, London, 1995.

[16] C. Flammer, *Spheroidal wave functions*. Stanford University Press, 1957.

[17] E. Frederiksen. "Condenser microphones used as Sound Sources." *B&K Technical Review* nr. 3 (1977), 3-23.

[18] F. Jacobsen, V. Cutanda and P.M. Juhl, "A numerical and experimental investigation of the performance of sound intensity probes at high frequencies." *Journal of the Acoustical Society of America* **103** (1998), 953-961.

[19] P. M. Juhl. *The Boundary Element Method for Sound Field Calculations*. Doctoral Thesis. Department of Acoustic Technology, Technical University of Denmark, 1993.

[20] P.M. Juhl, "An axisymmetric integral equation formulation for free space non-axisymmetric radiation and scattering of a known incident wave." *Journal of Sound and Vibration* **163** (1993), 397-406.

[21] S.C. Kang and J.G. Ih, "On the accuracy of nearfield pressure predicted by the acoustic boundary element method." *Journal of Sound and Vibration* **233** (2000), 353-358.

[22] C. Karra. *Formulation variationelle par équations intégrales pour la résolution des problèmes de couplage vibro-acoustique dans un fluide thermovisqueux*, Thèse UTC, 1997.

[23] C. Karra and M. Ben Tahar. "An integral equation formulation for boundary element analysis of propagation in viscothermal fluids." *Journal of the Acoustical Society of America* **102** (1997), 1311-1318.

[24] C. Karra and M. Ben Tahar. "Modélisation par elements finis de frontiers du comportement vibratoire d'une membrane couplée à une couche de fluide thermoconducteur." *C. R. Acad. Sci. Paris* (1998), t. 326 série II b, 733-739.

[25] L. E. Kinsler, A. R. Frey, A. B. Coppens and J. V. Sanders. *Fundamentals of Acoustics (3rd edition)*. John Wiley & sons, New York, 1980.

[26] B.U. Koo, B.C. Lee and J.G. Ih, "A non-singular boundary integral equation for acoustic problems." *Journal of Sound and Vibration* **192** (1996), 263-279.

[27] G. Krishnasamy, F. J. Rizzo, and Y. Liu, "Boundary Integral Equations for Thin Bodies." *International Journal for Numerical Mehods in Engineering* **37** (1994), 107-121.

[28] Y. Liu and F. J. Rizzo, "Scattering of elastic waves from thin shapes in three dimensions using the composite boundary integral equation formulation." *Journal of the Acoustical Society of America* **102** (1997), 926-932.

[29] R. Martinez, "The thin-shape breakdown (TSB) of the Helmholtz integral equation." *Journal of the Acoustical Society of America* **90** (1991), 2728-2738.

[30] P.M. Morse and K.U. Ingard. *Theoretical Acoustics*. McGraw-Hill, NewYork, 1968.

[31] P. M. Morse. *Vibration and Sound*. The American Institute of Physics. 1983.

[32] M. Möser, "Damping of structure borne sound by the viscosity of a layer between two plates." *Acustica* **46** (1980), 210-217.

[33] A. D. Pierce. *Acoustics. An Introduction to Its Physical Principles and Applications*. Acoustical Society of America, New York, 1989.

[34] G. Plantier and M. Bruneau, "Heat conduction effects on the acoustic response of a membrane separated by a very thin air film from a backing electrode." *Acoustique* **3** (1990), 243-250.

[35] W. H. Press, S. A. Teukolsky, W. T. Vetterling and B. P. Flannery. *Nuumerical recipes in C. The art of scientific computing (2nd Ed.)*. Cambridge University Press, New York, 1992.

[36] A.F. Seybert, B. Soenarko, F.J. Rizzo, and D.J. Shippy, "An advanced computational method for radiation and scattering of acoustic waves in three dimensions." *Journal of the Acoustical Society of America* **77** (1985), 362-368.

[37] A.F. Seybert, "The uses and abuses of virtual experimentation." *International Journal of Acoustics and Vibration* **Vol 6, nr. 1** (2001), 2.

[38] A.Trochidis, "Vibration damping due to air or liquid layers." *Acustica* **51** (1982), 201-212.

[39] G. S. K. Wong and T. F. W. Embleton (eds.). *AIP handbook of condenser microphones. Theory, Calibration and Measurements.* American Institute of Physics, NewYork, 1996.

[40] T.W. Wu and G.C. Wan, "Numerical modeling of acoustic radiation and scattering from thin bodies using a Cauchy principal integral equation." *Journal of the Acoustical Society of America* **92** (1992), 2900-2906.

[41] T.W. Wu, "A direct boundary element method for acoustic radiation and scattering from mixed regular and thin bodies." *Journal of the Acoustical Society of America* **97** (1995), 84-91.

[42] S. Zhang and J. Jin, *Computation of special functions*. John Wiley, 1996.

[43] O.C. Zienkiewicz and R.L. Taylor. *The Finite Element Method (Fourth Edition)*. McGraw-Hill, New York, 1989-91. (Two volumes.)

APPENDIX A - PLANTIER'S ANALYTICAL MODEL

The analytical model for a thin layer of air between a membrane and a backplate summarized in this appendix is taken from reference [34] and it is used for validation in this project. The model is based on the equations for visco-thermal fluids in reference [6] that have been reviewed in section 2.2 of this thesis. For this reason we will go directly into the equations of the model.

The model is defined in a simplified microphone geometry, as shown in Figure 5-1. It is a circular thin gap, with a membrane on one side and a rigid boundary (zero velocity) on the other. The rim of the gap is characterized by a pressure release boundary condition ($p = 0$). A cylindrical coordinate system (r,θ,z) is defined with the origin in the center of the gap and with the z coordinate as normal to its sides, being $z=0$ placed at the rigid side. The thickness of the gap is d and the radius of the setup is R. the dependence with θ is omitted; the model is considered fully axisymmetrical.

The wavenumbers for the acoustic (k_a), thermal (k_h) and viscous (k_v) modes are the same defined in equations (2.18), (2.19) and (2.20) in section 2.2. Harmonic wave motion is assumed; note, however, that the convention in reference [34] is $e^{j\omega t}$, but $e^{-j\omega t}$ is used in this project. The wavenumbers are split in radial and normal directions (r and z directions), where the radial wavenumbers are obtained by imposing $J_0(k_n R)=0$ and assumed equal for all the three modes. The result is:

$$\left.\begin{aligned} k_a^2 &= k_{azn}^2 + k_n^2 \\ k_h^2 &= k_{hzn}^2 + k_n^2 \\ k_v^2 &= k_{vzn}^2 + k_n^2 \end{aligned}\right\} \rightarrow \left.\begin{aligned} k_{azn}^2 &= k_a^2 - k_n^2 \\ k_{hzn}^2 &= k_h^2 - k_n^2 \\ k_{vzn}^2 &= k_v^2 - k_n^2 \end{aligned}\right\} \tag{A.1}$$

Under these conditions the solution for the sound pressure is expressed:

$$p = p_a + p_h$$
$$= \sum_{n=1}^{\infty} J_0(k_n r)\left[\frac{1}{\tau_a}\left(A_{an}\cos k_{azn} z + B_{an}\sin k_{azn} z\right) + \frac{1}{\tau_h}\left(A_{hn}\cos k_{hzn} z + B_{hn}\sin k_{hzn} z\right)\right] \quad \text{(A.2)}$$

where the total sound pressure is the sum of acoustic p_a and thermal p_h sound pressures. The irrotational velocity $v_l = v_a + v_h$ is the sum of acoustic and thermal velocities, and is expressed in this model as:

$$v_l\big|_r = v_a\big|_r + v_h\big|_r$$
$$= -\sum_{n=1}^{\infty} k_n J_1(k_n r)\left[\frac{\phi_a}{\tau_a}\left(A_{an}\cos k_{azn} z + B_{an}\sin k_{azn} z\right) + \frac{\phi_h}{\tau_h}\left(A_{hn}\cos k_{hzn} z + B_{hn}\sin k_{hzn} z\right)\right] \quad \text{(A.3)}$$

$$v_l\big|_z = v_a\big|_z + v_h\big|_z$$
$$= -\sum_{n=1}^{\infty} J_0(k_n r)\left[\frac{\phi_a}{\tau_a} k_{azn}\left(A_{an}\sin k_{azn} z - B_{an}\cos k_{azn} z\right) + \frac{\phi_h}{\tau_h} k_{hzn}\left(A_{hn}\sin k_{hzn} z - B_{hn}\cos k_{hzn} z\right)\right] \quad \text{(A.4)}$$

where (A.3) and (A.4) are respectively the radial and normal components. The viscous velocity is obtained as:

$$v_v\big|_r = \sum_{n=1}^{\infty} \frac{k_{vzn}}{k_n} J_1(k_n r)\left[A_{vn}\sin k_{vzn} z - B_{vn}\cos k_{vzn} z\right] \quad \text{(A.5)}$$

$$v_v\big|_z = \sum_{n=1}^{\infty} J_0(k_n r)\left[A_{vn}\cos k_{vzn} z + B_{vn}\sin k_{vzn} z\right] \quad \text{(A.6)}$$

The implementation of the membrane has been commented in detail in 4.4, we only reproduce here the expression of its normal displacement ε, adapted to this case:

$$\varepsilon = \frac{p_{inc}}{TK^2}\left[1 - \frac{J_0(Kr)}{J_0(KR)}\right] + \frac{1}{T}\sum_{n=1}^{\infty}\left[\frac{\frac{1}{\tau_a}\left(A_{an}\cos k_{azn}z + B_{an}\sin k_{azn}z\right) + \frac{1}{\tau_h}\left(A_{hn}\cos k_{hzn}z + B_{hn}\sin k_{hzn}z\right)}{k_n^2 - K^2} J_0(k_n r)\right] \quad \text{(A.7)}$$

where $K^2=\rho_s\omega/T$, T is the tension of the membrane, ρ_s is the membrane's surface density, ω is the angular frequency and p_{inc} the uniform incident pressure on the outer side.

There are six infinite series of constants to determine: A_{an}, B_{an}, A_{hn}, B_{hn}, A_{vn} and B_{vn}. To do this, the boundary conditions are imposed to equations (A.2) to (A.7) and the following system of six equations is obtained for every mode:

$$A_{an} + A_{hn} = 0 \quad \text{(A.8)}$$

$$A_{an}\cos k_{azn}d + B_{an}\sin k_{azn}d + A_{hn}\cos k_{hzn}d + B_{hn}\sin k_{hzn}d = 0 \quad \text{(A.9)}$$

$$B_{an}\frac{\phi_a}{\tau_a}k_{azn} + B_{hn}\frac{\phi_h}{\tau_h}k_{hzn} + A_{vn} = 0 \quad \text{(A.10)}$$

$$A_{an}\frac{\phi_a}{\tau_a}k_n + A_{hn}\frac{\phi_h}{\tau_h}k_n + B_{vn}\frac{k_{vzn}}{k_n} = 0 \quad \text{(A.11)}$$

$$\begin{aligned} &-A_{an}\frac{\phi_a}{\tau_a}k_n\cos k_{azn}d - B_{an}\frac{\phi_a}{\tau_a}k_n\sin k_{azn}d - A_{hn}\frac{\phi_h}{\tau_h}k_n\cos k_{hzn}d \\ &-B_{hn}\frac{\phi_h}{\tau_h}k_n\sin k_{hzn}d + A_{vn}\frac{k_{vzn}}{k_n}\sin k_{vzn}d - B_{vn}\frac{k_{vzn}}{k_n}\cos k_{vzn}d = 0 \end{aligned} \quad \text{(A.12)}$$

$$A_{an}\left[\frac{i\omega\cos k_{azn}d}{\tau_a T(k_n^2-K^2)}+\frac{\phi_a}{\tau_a}k_{azn}\sin k_{azn}d\right]+B_{an}\left[\frac{i\omega\sin k_{azn}d}{\tau_a T(k_n^2-K^2)}-\frac{\phi_a}{\tau_a}k_{azn}\cos k_{azn}d\right]$$
$$+A_{hn}\left[\frac{i\omega\cos k_{hzn}d}{\tau_h T(k_n^2-K^2)}+\frac{\phi_h}{\tau_h}k_{hzn}\sin k_{hzn}d\right]+B_{hn}\left[\frac{i\omega\sin k_{hzn}d}{\tau_h T(k_n^2-K^2)}-\frac{\phi_h}{\tau_h}k_{hzn}\cos k_{hzn}d\right] \quad \text{(A.13)}$$
$$-A_{vn}\cos k_{vzn}d-B_{vn}\sin k_{vzn}d=\frac{2i\omega p_{inc}}{T(k_n^2-K^2)k_n R J_1(k_n R)}$$

The last equation (A.13) introduces the coupling with the membrane, since it represents the velocity boundary condition on the membrane surface.

The model is programmed in a Matlab function, as shown in Appendix C. The mean membrane displacement must be calculated in order to obtain a frequency response, by integrating it in the radial direction, using this expression:

$$\varepsilon_{mean}=\frac{1}{\pi R^2}\int_0^R \varepsilon(r)2\pi r dr \quad \text{(A.14)}$$

In practice, $\varepsilon(r)$ is evaluated on a finite number of radial positions r_i, and the integral (A.14) becomes a summation:

$$\varepsilon_{mean}=\frac{1}{\pi R^2}\left\{\varepsilon(1)\pi\left(\frac{r_1+r_2}{2}\right)^2+\sum_{i=2}^{N-1}\varepsilon(i)\pi\left[\left(\frac{r_{i+1}+r_i}{2}\right)^2-\left(\frac{r_i+r_{i-1}}{2}\right)^2\right]\right.$$
$$\left.+\varepsilon(N)\pi\left[R^2-\left(\frac{R^2+r_{N-1}}{2}\right)^2\right]\right\} \quad \text{(A.15)}$$

where the positions r_i where $\varepsilon(r)$ is calculated are N consecutive values of r, starting with $r=0$ at the center of the membrane and ending with $r=R$ at the rim.

APPENDIX B – FORMULATION BY BELTMAN

The series of papers published by W.M. Beltman from University of Twente in the Netherlands are focused on the problem of acoustics in visco-thermal fluids.[1,2,3] In particular, references [2] and [3] contain a comprehensive review of the various theoretical approaches that have appeared over the years dealing with this topic, as well as practical implementations.

In [2], a set of dimensionless parameters is used to express the methods, study their properties and establish their range of use. The five parameters are named shear wave number *s*, reduced frequency *k*, square root of the Prandtl number σ, and viscosity ratio ξ:

$$\begin{aligned} s &= l\sqrt{\rho_0 \omega/\mu} & \sigma &= \sqrt{\mu C_p/\lambda} \\ k &= \omega l/c_0 & \xi &= \eta/\mu \end{aligned} \qquad \text{(B.1)}$$

They are functions of the the air density ρ_0, the viscosity coefficient μ, the angular frequency ω, thermal conductivity coefficient λ and bulk viscosity η. In the case of *s* and *k*, they are also a function of the quantity *l*, which is called *length scale* and represents a geometrical length that characterizes the setup. In the case of microphones, for example, *l* would be the gap width. This way of expressing the main parameters is advantageous for the kind of models Beltman recommends in most cases, the so-called *low reduced frequency models*, as we will see.

Expressing the various models as a function of these parameters, Beltman divides the methods in three groups:

- *Full linearized Navier-Stokes model*: this class is represented by the model outlined in section 2.2, in which this thesis is based and was originated by the work by M. Bruneau *et al.*[6]

- *Simplified Navier-Stokes model*: there are two models described under this class, the Trochidis model and the Möser model.[38,32] The former assumes the gas to be incompressible, and the latter considers compressibility only partially, and the process to be adiabatic. Their range of use is limited due to the restrictive hypotheses.

- *Low reduced frequency model*: its main assumption is that the wavelength is large compared with the length scale *l*, gap width in our case, and boundary layer thickness. As a consequence, the reduced frequency *k* defined above satisfies $k<<1$, therefore the name. This allows simplifications in the equations that facilitate the calculation. The use of dimensionless parameters containing the length scale *l* is also justified by the hypothesis. The geometrical coordinates are divided into *propagation directions* and *other directions*, and the equations split with them. The so-called *other directions* are the cross-sectional or thickness directions, the normal to the membrane-backplate gap in the microphone case. The sound pressure is assumed constant across that direction.

Beltman maintains that the low reduced frequency model approach can successfully replace the full linearized Navier-Stokes model in most cases. Some analytical solutions are presented and, in another paper, a new class of finite element is developed in order to handle complicated geometries using this method.[1] The finite element formulation is two-dimensional, since the non-propagational normal direction is removed under the hypotheses. It can however handle different values of the removed dimension as a parameter in the simplified differential equation for the pressure.

Among the analytical solutions presented in [3], there is a simplified circular microphone. The analytical solution based in the so-called *full linearized model* in reference [34] is used to compare with Beltman's *low reduced frequency* version. This analytical solution is the same used in this project for validation. Beltman, however, only compares the impedance of the microphone, which depends on the mean membrane displacement. Both solutions assume a pressure release boundary condition at the membrane/backplate rim.

Since Beltman's formulation is based on the Finite Element Method, it has the advantage of an easy coupling with a membrane modeled in the same manner. On the other hand, the geometrical simplification that removes the pressure variations in the direction normal to the membrane could perhaps be too restrictive if the objective is the understanding of the acoustical phenomena inside a condenser microphone in order to help with its design. The effects at the boundaries of the thin gap of air (holes and backplate rims) play an important part in this device.

However, to the author's notice, there is not by the moment an implementation available of a condenser microphone using Beltman's FEM formulation. It would be interesting to observe the performance of such implementation; this line of research looks promising and deserves attention.

APPENDIX C - MODEL IMPLEMENTATION

The main phases of the numerical calculation are described in this appendix, and some of the implemented Matlab functions are described and listed. The entire project, except mesh generation, has been programmed using Matlab.

The three-dimensional Boundary Element Method code on which the visco-thermal formulation is based is part of a set of BEM formulations in Matlab that includes also axisymmetrical and two-dimensional formulations. The set is called OpenBEM.[19]

In particular, the 3-D BEM part of OpenBEM was produced during this project and it incorporates some improvements, like the developments shown in chapter 3 for computation of very close meshes, especially developed for this occasion. Some adjustments were also needed to compute the integrals in the calculation of the viscous and thermal coefficient matrices, due to the values of the viscous and thermal wavenumbers.

The three-dimensional mesh is generated using the built-in mesh generator in ANSYS, a Finite Element Method commercial package. The mesh is then exported to Matlab, where it is checked and adapted for the calculation.

The calculation flowchart in Figure C-1 describes the whole calculation process of the numerical model of a microphone with viscous and thermal losses.

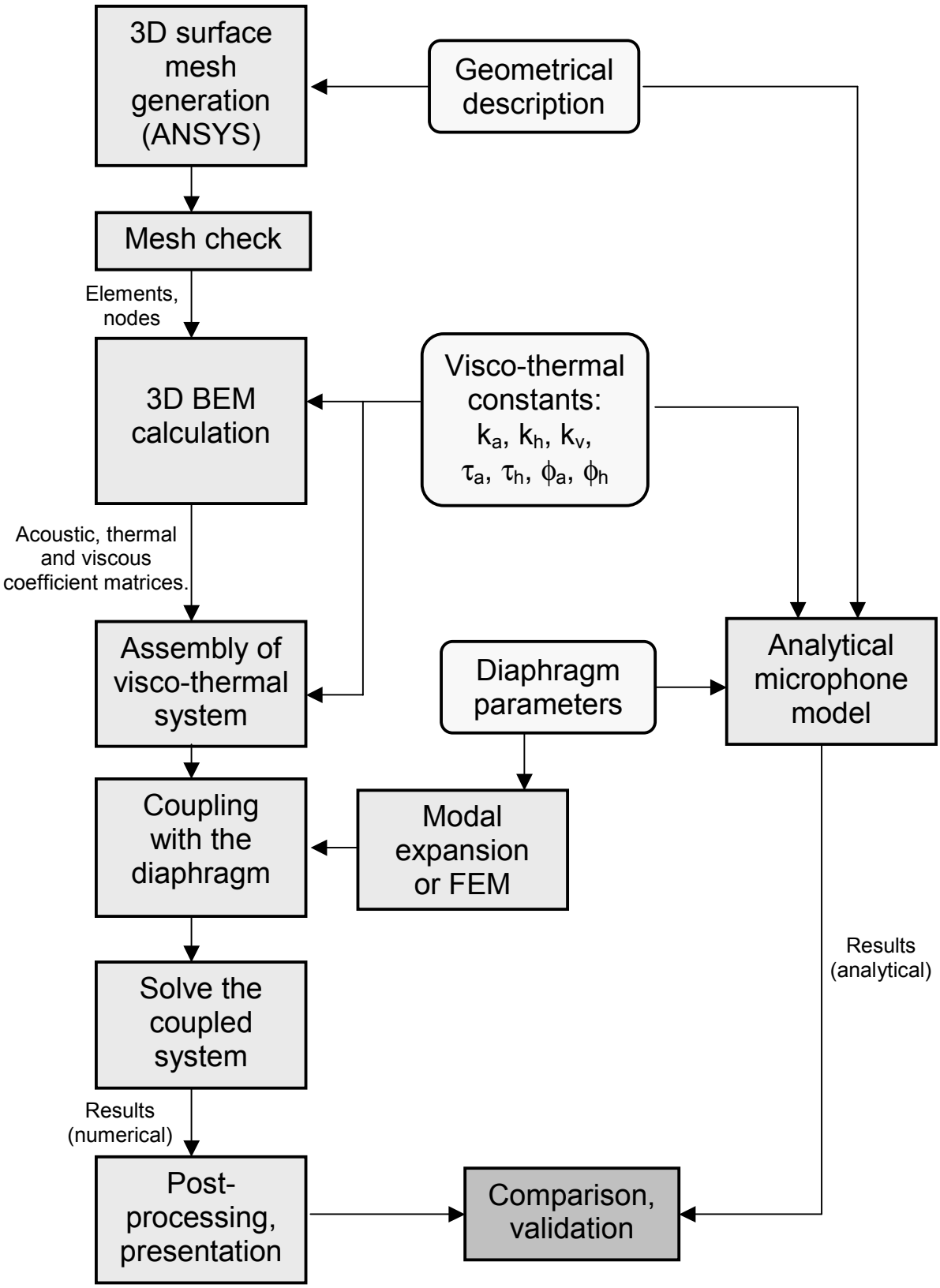

Figure C-1. Calculation flowchart.

The system of equations with viscous and thermal losses is assembled as described in 4.2. Three separated scripts in Matlab perform three different calculation phases, comprising most of the actions in Figure C-1:

- *Phase 1: Calculation of the BEM coefficient matrices for acoustic, thermal and viscous modes*. The 3D BEM code is run with the proper geometry, frequency and visco-thermal constants in order to obtain the coefficient matrices for the three modes (acoustic, viscous and thermal) at every frequency. The matrices are stored in data files after calculation. This is the most time-consuming phase. The matrices only depend on frequency and geometry; therefore they can be reused for different excitations and boundary conditions.

- *Phase 2: Solving of the system of equations*. The coefficient matrices are loaded from the data files and the combined matrix with visco-thermal losses assembled, as in equation (4.20). It is coupled to the membrane in a system of equations as in equation (4.42). The system is solved and the acoustic pressure p_a obtained. The remaining acoustic variables are calculated using the expressions (4.21), (4.22), (4.23) and (4.24). Only normal components of the velocities are calculated.

- *Phase 3: Post-processing*. The results are formatted for presentation in graphs. The analytical model is run and measurements loaded for comparison.

The scripts that perform the three phases are not shown in this appendix; they vary depending on the calculation's requirements. However, some custom-made functions used in the different phases are worth including here. These are:

- *VTconst*: It produces all physical constants needed in phases 1 and 2, including wavenumbers for acoustic, thermal and viscous modes, and visco-thermal constants.

- *Plantier*: Implements the analytical model in the paper by G. Plantier and M. Bruneau, used for validation in this thesis.[34] It is used in phase 3.

- *Laplacian*: Contains the code corresponding to the development in 4.3 for the implementation of the tangential laplacian. It is used in phase 2 to assemble the visco-thermal system of equations.

- *Bodyfind*: It checks the surface meshes from ANSYS in order to find holes, elements that do not match, correct the directions of normal vectors for every element to make them all point outwards, and number the different bodies if there is more than one. It must be run on the raw mesh prior to phase 1.

In the following we reproduce the Matlab functions just described.

Function "VTconst"

```
function [rho,c,kp,ka,kh,kv,tau_a,tau_h,phi_a,phi_h]=VTconst(f,varargin)

% [rho,c,kp,ka,kh,kv,tau_a,tau_h,phi_a,phi_h]=VTconst(f,S)
%
% ****************************
% *  VISCO-THERMAL CONSTANTS  *
% ****************************
%
% Calculates visco-termal constants as defined in the paper:
%
% Bruneau M., Herzog Ph., Kergomard J and Polack J.D.
% "General formulation of the dispersion equation in bounded visco-thermal
% fluid, and application to some simple geometries"
% Wave Motion 11 (1989), pp. 441-451
%
% Input:
%    -f: vector with frequencies to be used.
%    -S: sign convention: +1 corresponds to exp(-iwt), Karra's, and -1
%        corresponds to exp(iwt), Bruneau's.
%        If not supplied, -1 is used.
%        If abs(S) is not 1, it is a constant that divides the viscosity.
%        Suggested value S = -100, to get rid of most viscosity effects.
%
% Output: (all vectors of the same length as 'f')
%   -kp: perfect fluid wavenumber
%   -ka: acoustic wavenumber
%   -kh: thermal wavenumber
%   -kv: viscous wavenumber
%   -tau_a, tau_h, phi_a, phi_h: constants in Bruneau's model.

% Vicente Cutanda 11-2000

if nargin > 1
   S=sign(varargin{1});
   fact=abs(varargin{1});
else
   S=-1;
   fact=1;
end

% physical constants (MKS units) of air in normal conditions:
mu=184.6e-7/fact; %viscosity (N*s/m2)
nu=110e-7/fact;   %2nd viscosity (N*s/m2)
rho=1.1614;       %density (Kg/m3)
c=340;            %sound speed (m/s)
cpcv=1.403;       %ratio of specific heats (Cp/Cv)
landa=2.6e-2;     %thermal conductivity (J/(s*m*K))
Cp=1010;          %specific heat, constant pressure (J/kg*C)
Cv=720;           %specific heat, constant volume (J/kg*C)
beta=rho*(Cp-Cv); %thermal expansion coefficient(1/K)*ambient pressure(Pa)

% characteristic lengths:
lh=landa/(rho*Cp*c);
lv=(nu+4*mu/3)/(rho*c);
lvp=mu/(rho*c);
lvh=lv+(cpcv-1)*lh;
lvhp=(cpcv-1)*(lh-lv);

% wavenumbers:
kp=2*pi*f/c;                                  %perfect fluid
ka2=kp.^2./(1-S*i*kp*lvh-kp.^2*lh*lvhp);      %acoustic^2
                                              %Simplified: ka2=kp.^2.*(1+S*i*kp*lvh);
kh2=S*i*kp./(lh*(1+S*i*kp*lvhp));             %entropic^2
                                              %Simplified: kh2=S*i*kp.*(1-S*i*kp*lvhp)/lh;
kv2=S*i*kp/lvp;                               %viscous^2
```

```
% The result of the square root is considered positive:
ka=sqrt(ka2);   %acoustic
kh=sqrt(kh2);   %entropic
kv=sqrt(kv2);   %viscous

% thermal boundary condition constants:
tau_a=(cpcv-1)./(beta*cpcv*(1+S*i*lh*ka2./kp));
tau_h=(cpcv-1)./(beta*cpcv*(1+S*i*lh*kh2./kp));

% velocity boundary condition constants:
phi_a=-S*i./(rho*2*pi*f.*(1+S*i*lv*ka2./kp));
phi_h=-S*i./(rho*2*pi*f.*(1+S*i*lv*kh2./kp));
```

Function "Plantier"

```
Function [pa,ph,var,vaz,vhr,vhz,vtr,vtz,er]=...
                              plantier(f,Rad,Hgh,r,z,n,pinc,Tm,mu_m,varargin);

% [pa,ph,var,vaz,vhr,vhz,vtr,vtz,er]=plantier(f,Rad,Hgh,r,z,n,pinc,Tm,mu_m,fact);
%
% Calculates the analytical solution for the sound field inside a thin
% cylindrical cavity with a coupled membrane and visco-thermal losses,
% as described in the reference.
%
% Input variables:
%   -f:      frequency, vector with frequencies to calculate.
%   -Rad:    radius of the cavity.
%   -Hgh:    height of the cavity.
%   -r:      values of the r-coordinate to calculate. Row vector.
%   -z:      values of the z-coordinate to calculate. Row vector.
%   -n:      number of terms in the expansions.
%   -pinc:   uniform incident pressure on the exterior of the membrane.
%   -Tm:     tension of the membrane.
%   -mu_m:   mass per unit area of the membrane.
%   -fact:   reduction factor of the viscosity (optional).
%            If fact > 1, the viscosity constants are reduced.
%            Suggested value fact = 100, to get rid of most viscosity effects.
%
% Output variables. Arranged in 3D matrices (except 'er'), the dimensions are
% respectively r-values, z-values and frequency values:
%   -pa:     acoustic pressure.
%   -ph:     thermal pressure.
%   -var:    radial component of the acoustic velocity.
%   -vaz:    normal component of the acoustic velocity.
%   -vhr:    radial component of the thermal velocity.
%   -vhz:    normal component of the thermal velocity.
%   -vtr:    radial component of the viscous velocity.
%   -vtz:    normal component of the viscous velocity.
%   -er:     normal displacement of the membrane, vector, one column per 'r',
%            one row per frequency.
%
% Reference:
%   G. Plantier and M. Bruneau, "Heat conduction effects on the acoustic response
%   of a membrane separated by a very thin air film from a backing electrode".
%   J. Acoustique 3 (1990), pp 243-250.

% Vicente Cutanda 5-2001

if nargin > 9
   fact=-abs(varargin{1});
else
   fact=-1;
end

% visco-thermal constants and convert to Plantier's notation.
[rho,c,kp,ka,kh,kv,tau_a,tau_h,phi_a,phi_h]=VTconst(f,fact);
Lambda_a=1./tau_a;Lambda_h=1./tau_h;
alfa_a=phi_a./tau_a;alfa_h=phi_h./tau_h;
w=2*pi*f;K2=mu_m*w.^2/Tm;

% calculate zeros of Bessel function order 0.
xx=2;
kn=fzero('besselj(0,x)',xx)/Rad;
kni=kn;
for nn=2:n
   while round(kni*1e3)==round(kn(end)*1e3)
      xx=xx+1;
      kni=fzero('besselj(0,x)',xx)/Rad;
   end
   kn=[kn;kni];
end
```

```
kazn=sqrt(repmat(ka.^2,n,1)-repmat(kn.^2,1,length(f)));
khzn=sqrt(repmat(kh.^2,n,1)-repmat(kn.^2,1,length(f)));
kvzn=sqrt(repmat(kv.^2,n,1)-repmat(kn.^2,1,length(f)));

% calculate constants for all n-terms and frequencies and make the summations
pa=zeros(length(r),length(z),length(f));
ph=pa;var=pa;vaz=pa;vhr=pa;vhz=pa;vtr=pa;vtz=pa;
er=pinc./(Tm*repmat(K2.',1,length(r))).*(1-besselj(0,sqrt(K2).'*r)./...
   besselj(0,repmat((sqrt(K2)*Rad).',1,length(r))));

zeros(length(f),length(r));
for ff=1:length(f)
   AB=zeros(6);RHS=zeros(6,1);
   for nn=1:n

      % build the system of equations and solve it to get a set of constants
      AB(1,[1 3])=1;
      AB(2,1:4)=[cos(kazn(nn,ff)*Hgh) sin(kazn(nn,ff)*Hgh) ...
                 cos(khzn(nn,ff)*Hgh) sin(khzn(nn,ff)*Hgh)];
      AB(3,[2 4 5])=[alfa_a(ff)*kazn(nn,ff) alfa_h(ff)*khzn(nn,ff) 1];
      AB(4,[1 3 6])=[alfa_a(ff)*kn(nn) alfa_h(ff)*kn(nn) kvzn(nn,ff)/kn(nn)];
      AB(5,:)=[-alfa_a(ff)*kn(nn)*cos(kazn(nn,ff)*Hgh) ...
               -alfa_a(ff)*kn(nn)*sin(kazn(nn,ff)*Hgh) ...
               -alfa_h(ff)*kn(nn)*cos(khzn(nn,ff)*Hgh) ...
               -alfa_h(ff)*kn(nn)*sin(khzn(nn,ff)*Hgh) ...
               kvzn(nn,ff)/kn(nn)*sin(kvzn(nn,ff)*Hgh) ...
               -kvzn(nn,ff)/kn(nn)*cos(kvzn(nn,ff)*Hgh)];
      AB(6,:)=[(i*w(ff)*Lambda_a(ff)*cos(kazn(nn,ff)*Hgh))./...
               (Tm*(kn(nn)^2-K2(ff)))+alfa_a(ff)*kazn(nn,ff)*sin(kazn(nn,ff)*Hgh) ...
               (i*w(ff)*Lambda_a(ff)*sin(kazn(nn,ff)*Hgh))./(Tm*(kn(nn)^2-K2(ff)))...
               -alfa_a(ff)*kazn(nn,ff)*cos(kazn(nn,ff)*Hgh) ...
               (i*w(ff)*Lambda_h(ff)*cos(khzn(nn,ff)*Hgh))./(Tm*(kn(nn)^2-K2(ff)))...
               +alfa_h(ff)*khzn(nn,ff)*sin(khzn(nn,ff)*Hgh) ...
               (i*w(ff)*Lambda_h(ff)*sin(khzn(nn,ff)*Hgh))./(Tm*(kn(nn)^2-K2(ff)))...
               -alfa_h(ff)*khzn(nn,ff)*cos(khzn(nn,ff)*Hgh) ...
               -cos(kvzn(nn,ff)*Hgh) -sin(kvzn(nn,ff)*Hgh)];
      RHS(6)=2*i*w(ff)*pinc/(Tm*(kn(nn)^2-K2(ff))*kn(nn)*Rad*besselj(1,kn(nn)*Rad));
      const=AB\RHS;
      Aan=const(1);Ban=const(2);Ahn=const(3);Bhn=const(4);Avn=const(5);Bvn=const(6);

      % calculate acoustic variables
      pa(:,:,ff)=pa(:,:,ff) + besselj(0,kn(nn)*r).'*...
         (Aan*cos(kazn(nn,ff)*z)+Ban*sin(kazn(nn,ff)*z))*Lambda_a(ff);
      ph(:,:,ff)=ph(:,:,ff) + besselj(0,kn(nn)*r).'*...
         (Ahn*cos(khzn(nn,ff)*z)+Bhn*sin(khzn(nn,ff)*z))*Lambda_h(ff);
      var(:,:,ff)=var(:,:,ff) + kn(nn)*besselj(1,kn(nn)*r).'*...
         (Aan*cos(kazn(nn,ff)*z)+Ban*sin(kazn(nn,ff)*z))*alfa_a(ff);
      vaz(:,:,ff)=vaz(:,:,ff) - besselj(0,kn(nn)*r).'*...
         (Aan*sin(kazn(nn,ff)*z)-Ban*cos(kazn(nn,ff)*z))*alfa_a(ff)*kazn(nn,ff);
      vhr(:,:,ff)=vhr(:,:,ff) + kn(nn)*besselj(1,kn(nn)*r).'*...
         (Ahn*cos(khzn(nn,ff)*z)+Bhn*sin(khzn(nn,ff)*z))*alfa_h(ff);
      vhz(:,:,ff)=vhz(:,:,ff) - besselj(0,kn(nn)*r).'*...
         (Ahn*sin(khzn(nn,ff)*z)-Bhn*cos(khzn(nn,ff)*z))*alfa_h(ff)*khzn(nn,ff);
      vtr(:,:,ff)=vtr(:,:,ff) + kvzn(nn,ff)/kn(nn)*besselj(1,kn(nn)*r).'*...
         (Avn*sin(kvzn(nn,ff)*z)-Bvn*cos(kvzn(nn,ff)*z));
      vtz(:,:,ff)=vtz(:,:,ff) + besselj(0,kn(nn)*r).'*...
         (Avn*cos(kvzn(nn,ff)*z)+Bvn*sin(kvzn(nn,ff)*z));
      er(ff,:)=er(ff,:) + 1/(Tm*(kn(nn)^2-K2(ff)))*besselj(0,kn(nn)*r)*...
         (Lambda_a(ff)*(Aan*cos(kazn(nn,ff)*Hgh)+Ban*sin(kazn(nn,ff)*Hgh))+...
        Lambda_h(ff)*(Ahn*cos(khzn(nn,ff)*Hgh)+Bhn*sin(khzn(nn,ff)*Hgh)));

   end
end
```

Function "Laplacian"

```
function D=laplacian(xyzb,topology)

% D=laplacian(nodes,topology)
%
% Calculate the matrix used to obtain the tangential laplacian from
% the nodal values. Second derivatives of the shape functions are used.
% The elements must be quadratic quadrilateral (8 nodes).
%
%    Tangential laplacian = D * p
%
% Input variables:
%    -xyzb:      node x, y and z coordinates. One node per row.
%    -topology:  numbers of the nodes in each element, ordered.
%                One element per row.
%
% Output variable:
%    -D:         Tangential laplacian
%
% References: -Peter M. Juhl: "The Boundary Element Method for Sound
%             Field Calculations", Report No. 55, DTU 1993. Section 4.7.
%             -O. C. Zienkiewicz, R. L. Taylor: "The Finite Element Method"
%             4th Ed., Volume 1, Section 8.5.

% Vicente Cutanda 4-2001

% Local coordinates of the nodes.
IP=[-1 -1;1 -1;1 1;-1 1;0 -1;1 0;0 1;-1 0];

nipts=size(IP,1);   % number of input points, 8 in this implementation.
M=size(xyzb,1);     % number of nodes.
N=size(topology,1); % number of elements.

% Quadratic Shape functions derivatives.
dNde1=[0.25*(1-IP(:,2)).*(2*IP(:,1)+IP(:,2)) ...
       0.25*(1-IP(:,2)).*(2*IP(:,1)-IP(:,2)) ...
       0.25*(1+IP(:,2)).*(2*IP(:,1)+IP(:,2)) ...
       0.25*(1+IP(:,2)).*(2*IP(:,1)-IP(:,2)) ...
      -IP(:,1).*(1-IP(:,2)) ...
       0.5*(1-IP(:,2).^2) ...
      -IP(:,1).*(1+IP(:,2)) ...
      -0.5*(1-IP(:,2).^2)];

dNde2=[0.25*(1-IP(:,1)).*(2*IP(:,2)+IP(:,1)) ...
       0.25*(1+IP(:,1)).*(2*IP(:,2)-IP(:,1)) ...
       0.25*(1+IP(:,1)).*(2*IP(:,2)+IP(:,1)) ...
       0.25*(1-IP(:,1)).*(2*IP(:,2)-IP(:,1)) ...
      -0.5*(1-IP(:,1).^2) ...
      -IP(:,2).*(1+IP(:,1)) ...
       0.5*(1-IP(:,1).^2) ...
      -IP(:,2).*(1-IP(:,1))];

% Quadratic Shape functions second derivatives.
d2Nde12=[0.25*(1-IP(:,2))*2 ...
         0.25*(1-IP(:,2))*2 ...
         0.25*(1+IP(:,2))*2 ...
         0.25*(1+IP(:,2))*2 ...
        -(1-IP(:,2)) ...
         zeros(nipts,1) ...
        -(1+IP(:,2)) ...
         zeros(nipts,1)];

d2Nde22=[0.25*(1-IP(:,1))*2 ...
         0.25*(1+IP(:,1))*2 ...
         0.25*(1+IP(:,1))*2 ...
         0.25*(1-IP(:,1))*2 ...
         zeros(nipts,1) ...
        -(1+IP(:,1)) ...
         zeros(nipts,1) ...
        -(1-IP(:,1))];
```

```
% Fill the global laplacian matrix with the contributions from all elements.
D=zeros(M,M);
topology=topology(:,1:8);
for ii=1:M
   [rr,cc]=find(topology==ii);
   for jj=1:length(rr)
       elknxyzb=xyzb(topology(rr(jj),:),:);

       % Elements of the Jacobian matrix for all input points:
       % dr/de1 and dr/de2, r=(x,y,z).
       dxde1=dNde1*elknxyzb(:,1);
       dyde1=dNde1*elknxyzb(:,2);
       dzde1=dNde1*elknxyzb(:,3);

       dxde2=dNde2*elknxyzb(:,1);
       dyde2=dNde2*elknxyzb(:,2);
       dzde2=dNde2*elknxyzb(:,3);

       % Normal vector at input points: scalar product (dr/de1 x dr/de2).
       nx=(dyde1.*dzde2-dzde1.*dyde2);
       ny=(dzde1.*dxde2-dxde1.*dzde2);
       nz=(dxde1.*dyde2-dyde1.*dxde2);
       jacobi=sqrt(nx.^2+ny.^2+nz.^2);

       Di=(d2Nde12(cc(jj),:) + d2Nde22(cc(jj),:))./jacobi(cc(jj));

       D(ii,topology(rr(jj),:)) = D(ii,topology(rr(jj),:)) + Di/length(rr);
   end
end
```

Function "Bodyfind"

```
function [nodesb,topologyb,toposhrinkb,segmopen]=bodyfind(nodes,topology)

% [nodesb,topologyb,toposhrinkb,segmopen]=bodyfind(nodes,topology)
%
% Finds body numbers and checks normal vectors.
% All normal vectors are set to point outwards.
%
% Input variables:
%    -nodes:     node x, y and z coordinates. One node per row.
%                Do not include body numbers.
%    -topology:  numbers of the nodes in each element, ordered.
%                One element per row. Do not include body numbers.
%
% Output variables:
%    -nodesb:    node x, y and z coordinates and body number.
%                One node per row.
%    -topologyb: numbers of the nodes in each element, ordered,
%                plus body number. One element per row.
%    -toposhrinkb:numbers of the nodes in each element, ordered,
%                plus body number. Only the elements that had a
%                duplicated node are included, with that node
%                supressed. One element per row.
%    -segmopen:  list of segments that are open edges. First column
%                is the element it belongs to, second column is
%                the first node of the segment within the element,
%                and third column is the body number.
%
% Each body is plotted in a separate figure, a different shade
% of green indicating which elements had an opposite direction.
% The element chosen to decide the overall direction is painted
% in darker green: it is the farthest from the center of mass.
% The open edges, if any, are indicated in blue.
%
% The user must change manually the signs for every body number
% in the node list (nodesb) and in the element list (topologyb) to
% indicate the BEM which domain to consider. The convention is:
%                    +: exterior domain
%                    -: interior domain

% Vicente Cutanda 08.2000

if size(nodes,2)>3
   error('Error: do not include body numbers in the input arrays - Checking aborted');
end

[N,nknel]=size(topology);
if nknel==8
   nknel=4;
   quad=1;
else
   quad=0;
end

topology=[topology zeros(N,1)];

segmopen=[];
elemcorr=[];
body=0;
while ~isempty(find(topology(:,end)==0)) % body loop
   body=body+1;
   elez=find(topology(:,end)==0);
   eln=1;
   segms=[elez(ceil(eln/4)) mod((eln-1),nknel)+1]; %start a stack list of segments to test
   flag=1; % first segment is different

   while ~isempty(segms) % segment loop
      randseg=1; %ceil(rand*size(segms,1));   %it can be random
      segmin=segms(randseg,:); % choose one segment in the list
      segms(randseg,:)=[]; % remove it from the list
```

```
      [segmout,topology]=elstep(topology,segmin,body,nknel,N,quad);

      if segmout(1)==0 % the segment is open, just add it to a list
         if flag==1 % just in case the first segment is open, get another instead
            eln=eln+1;
            segms=[elez(ceil(eln/4)) mod((eln-1),nknel)+1];
         else
            disp(['There is an open edge! - Element nr.: ' ...
                  num2str(segmin(1)) ' Segment pos.: ' num2str(segmin(2))]);
            segmopen=[segmopen ; segmin body];
         end
      elseif segmout(2)==0 % a node number is duplcated within an element, do nothing
         if flag==1 % just in case the first segment is duplicated, get another instead
            eln=eln+1;
            segms=[elez(ceil(eln/4)) mod((eln-1),nknel)+1];
         end
      else
         if segmout(1)<0
            segmout=abs(segmout);
            elemcorr=[elemcorr ; segmout(1) body];
         end

         if topology(segmout(1),end)==0 % unchecked element found
            segms=[segms ; [ones(nknel+flag-1,1)*segmout(1) ...
                     (mod((segmout(2)-flag):(nknel+segmout(2)-2),nknel)+1)']];
            topology(segmout(1),end)=body;
            nodes(topology(segmout(1),1:nknel*(1+quad)),4)=body;
         elseif topology(segmout(1),end)==body % checked element found
            pos=find(sum((abs(segms-ones(size(segms,1),1)*segmout))')==0);
            if length(pos)==1 %the adjoining segment should be in the stack list: remove it
               segms(pos,:)=[];
            else
               error('Program error: segment count failure - Checking aborted');
            end
         else % the new element belongs to another body!
            error('Error: two bodies are connected - Checking aborted');
         end
         flag=0;
      end
   end
end


for bb=1:body
   tx=find(topology(:,end)==bb);
   Nb=length(tx);
   nx=find(nodes(:,end)==bb);
   topologytmp=topology(tx,1:nknel*(quad+1));
   nodestmp=nodes(nx,1:3);

   Cdata=[ones(Nb,1)]*[0.7 .92 0.75]; % color data, B&K green

   if ~isempty(elemcorr) %darken the elements that were corrected before
      corrbod=elemcorr(find(elemcorr(:,end)==bb),1);
      for ee=1:length(corrbod)
         Cdata(find(tx==corrbod(ee)),:)=Cdata(find(tx==corrbod(ee)),:)*0.9;
      end
   end

   for qq=1:length(nx)
      [ii,jj]=find(topology(tx,1:nknel)==nx(qq));
      for iii=1:length(ii)
         topologytmp(ii(iii),jj(iii))=qq;
      end
   end

   IP=[0 0 0 1]; % Select point in center
   rc=[];
   for ff=1:Nb  % Find the position and the normal vector at the center of body's elements
      elknxyzb=nodestmp(topologytmp(ff,:),:);
      [psi, xq, yq, zq, nx, ny, nz]=elemshape([elknxyzb ones(nknel*(quad+1),1)],IP);
```

```
      rc=[rc ; xq yq zq nx ny nz]; % Save centers of elements and normals for later use
   end

   centr=mean(nodestmp); % mass center of the body
   % find the farthest element
   [dummy,elmax]=max(sum((rc(:,1:3)-ones(Nb,1)*centr).^2,2));
   rcm=rc(elmax(1),:);
   Cdata(elmax,:)=Cdata(elmax,:)*0.6;%[Cdata(elmax,2) Cdata(elmax,1) Cdata(elmax,3)];
        %indicate the chosen element by a color change
   ferel=topologytmp(elmax(1),:);

   % Are the radiusvector and the farthest element's normal vector in the same hemi-space
   direction=sign((rcm(1)-centr(1))*rcm(4)+...
                  (rcm(2)-centr(2))*rcm(5)+...
                  (rcm(3)-centr(3))*rcm(6));

   % change all normal vectors in the body if they point inwards
   if direction < 0
      topology(tx,1:nknel)=fliplr(topology(tx,1:nknel));
   end

   figure; % one figure for each body, in case they hide one another
   view(-135,45);
%   axis equal;
   rotate3d on;
   hold on;
   title(['Body nr. ' num2str(bb)]);
   xlabel('x');ylabel('y');zlabel('z');
   patch('faces',topologytmp(:,1:nknel),'vertices',nodestmp,'FaceVertexCData',...
         Cdata,'FaceColor','flat');
   hold on;
   if quad==1
      temp=topologytmp(:,5:8);
      plot3(nodestmp(temp(1:end),1),nodestmp(temp(1:end),2),nodestmp(temp(1:end),3),'k.');
   end

   % draw normal vector on the farthest element (debugging)
%   h=line([rcm(1);rcm(4)+rcm(1)],[rcm(2);rcm(5)+rcm(2)],[rcm(3);rcm(6)+rcm(3)]);
%   set(h,'LineWidth',1,'Color',[0 0 1]);
   if ~isempty(segmopen) % draw lines where the body is open
      openbod=segmopen(find(segmopen(:,end)==bb),1:2);
      for ee=1:length(openbod)
         segtmp=topologytmp(find(tx==openbod(ee,1)),...
                mod((openbod(ee,2)-1):(openbod(ee,2)),nknel)+1);
         h=line(nodestmp(segtmp,1),nodestmp(segtmp,2),nodestmp(segtmp,3));
         set(h,'LineWidth',1.5,'Color',[1 0 0]);
      end
   end
end

topologyb=topology;
nodesb=nodes;

toposhrinkb=[];
for rr=1:N
   for cc=1:nknel
      col=mod((cc-1):cc,nknel)+1;
      if topologyb(rr,col(1))==topologyb(rr,col(2))
         topotmp=topologyb(rr,:);
         topotmp(cc)=[];
         toposhrinkb=[toposhrinkb ; topotmp];
      end
   end
end


function [segmout,topology]=elstep(topology,segmin,body,nknel,N,quad)
% find element number and position of the segment that matches a given segment
%    -topology: numbers of the nodes in each element, ordered.
%               One element per row. This function re-orders them if necessary
%    -segmin:   row vector with input segment description:
%               element number and position within the element.
```

```
%    -body:     current body number.
%    -nknel:    number of nodes per element.
%    -N:        number of elements.
%
%    -segmout:  row vector with output segment description:
%               element number and position within the element.
%               It is [0 1] if an open edge is found, [1 0] if the
%               input segment is duplicated and negative if the
%               new element direction has been corrected.

segbad=[];
segood=[];

% find all attached segments, matching or not the original segment's direction
for kk=1:nknel
   if quad==1
      col=mod((kk-1):(nknel+kk-2),nknel)+1;

      tmp1=ones(N,1)*topology(segmin(1),...
           [mod((segmin(2)-1),nknel) mod((segmin(2)-1),nknel)+4 mod(segmin(2),nknel)]+1);
      tmp1(segmin(1),:)=[0 0 0];
      tmp_g=find(sum((abs(topology(:,[col(2) col(1)+4 col(1)])-tmp1))')==0);
      tmp_b=find(sum((abs(topology(:,[col(1) col(1)+4 col(2)])-tmp1))')==0);

      segood=[segood ; tmp_g'  kk*ones(length(tmp_g),1)];
      segbad=[segbad ; tmp_b'  kk*ones(length(tmp_b),1)];
   else
      col=mod((kk-1):(nknel+kk-2),nknel)+1;

      tmp1=ones(N,1)*topology(segmin(1),mod((segmin(2)-1):segmin(2),nknel)+1);
      tmp1(segmin(1),:)=[0 0];
      tmp_g=find(sum((abs(topology(:,col(2:-1:1))-tmp1))')==0);
      tmp_b=find(sum((abs(topology(:,col(1:2))-tmp1))')==0);

      segood=[segood ; tmp_g'  kk*ones(length(tmp_g),1)];
      segbad=[segbad ; tmp_b'  kk*ones(length(tmp_b),1)];
   end
end

% consider all options and correct direction if necessary
szgood=size(segood,1);
szbad=size(segbad,1);
if (szgood+szbad)>1
   if topology(segmin(1),mod((segmin(2)-1),nknel)+1)==...
               topology(segmin(1),mod(segmin(2),nknel)+1)
      segmout=[1 0];
   else
      error('Error: more than two adjoining elements - Checking aborted');
   end
elseif (szgood+szbad)==0
   if topology(segmin(1),mod((segmin(2)-1),nknel)+1)==...
               topology(segmin(1),mod(segmin(2),nknel)+1)
      segmout=[1 0];
   else
      segmout=[0 1];
   end
elseif szgood==1
   segmout=segood;
elseif szbad==1
   dummy=topology(segbad(1),:);
   col=mod((segbad(2)-1):(nknel+segbad(2)-2),nknel)+1;
   topology(segbad(1),col(1))=dummy(col(2));
   topology(segbad(1),col(2))=dummy(col(1));
   topology(segbad(1),col(3))=dummy(col(4));
   topology(segbad(1),col(4))=dummy(col(3));
   if quad==1
       topology(segbad(1),col(2)+4)=dummy(col(4)+4);
       topology(segbad(1),col(4)+4)=dummy(col(2)+4);
   end
   segmout=-segbad;
end
```

APPENDIX D - JOURNAL PAPER "ON THE MODELING OF NARROW GAPS USING THE STANDARD BOUNDARY ELEMENT METHOD"

On the modeling of narrow gaps using the standard boundary element method

Vicente Cutanda[a)]
Brüel & Kjær Sound & Vibration, Skodsborgvej 307, DK-2850 Nærum, Denmark

Peter Møller Juhl[b)]
ITF Institute of Applied Physics, Odense University/The Engineering College of Odense, Niels Bohrs Allé 1, DK-5230 Odense M, Denmark

Finn Jacobsen[c)]
Department of Acoustic Technology, Technical University of Denmark, Ørsteds Plads, Building 352, DK-2800 Kgs. Lyngby, Denmark

(Received 6 October 1999; revised 9 September 2000; accepted 21 December 2000)

Numerical methods based on the Helmholtz integral equation are well suited for solving acoustic scattering and diffraction problems at relatively low frequencies. However, it is well known that the standard method becomes degenerate if the objects that disturb the sound field are very thin. This paper makes use of a standard axisymmetric Helmholtz integral equation formulation and its boundary element method (BEM) implementation to study the behavior of the method on two test cases: a thin rigid disk of variable thickness and two rigid cylinders separated by a gap of variable width. Both problems give rise to the same kind of degeneracy in the method, and modified formulations have been proposed to overcome this difficulty. However, such techniques are better suited for the so-called thin-body problem than for the reciprocal narrow-gap problem, and only the first is usually dealt with in the literature. A simple integration technique that can extend the range of thicknesses/widths tractable by the otherwise unmodified standard formulation is presented and tested. This technique is valid for both cases. The modeling of acoustic transducers like sound intensity probes and condenser microphones has motivated this work, although the proposed technique has a wider range of applications.
[DOI: 10.1121/1.1350399]

PACS numbers: 43.20.Fn [ANN]

I. INTRODUCTION

Phenomena where the physical setup contains very close domain boundaries are not uncommon in practice. Typical cases are fins or appendages from bulky structures, thin plates, and shells. All of them have parts that are very thin compared to the overall dimensions. It is well known that the conventional boundary element method has difficulties in dealing with such tasks. Considerable effort has been put into this so-called thin-body problem in recent years in order to make it tractable with BEM, and different formulations have been proposed that can alleviate or remove such difficulties.[1–4]

There is a second family of cases that shares many features with thin bodies. This may be named the narrow-gap problem. Examples are coatings, lubricant layers, cracks, and some acoustic transducers. The domain of interest in these cases is situated *between* the close boundaries, and very often a two-dimensional simplification cannot be used if the transversal variations are of physical relevance.

BEM formulations that can deal effectively with thin bodies become of no use in narrow gaps, and only a few techniques remain that can provide results in practical engineering work. One of these techniques is described in this paper, which has been motivated by numerical modeling of sound intensity probes and condenser microphones.[5] The behavior of sound fields inside narrow gaps plays a central role in these devices. Therefore, the performance of BEM formulations in such situations must be understood in order to obtain meaningful results.

The conventional BEM has two difficulties whenever two parts of the surface are very close.[4] First, the coefficient matrix becomes ill-conditioned as the distance gets smaller, and second, the integrals are near singular and difficult to solve numerically. The methods proposed to get around these difficulties in the thin-body variant fall into two groups: multidomain methods and normal-derivative equation methods. In multidomain methods an imaginary surface is constructed so as to replace the original problem of a thin body in a single domain with bulky bodies in two domains or more, coupled at an imaginary surface.[2] Such methods are advantageous for certain problems such as muffler analysis, but for other cases the imaginary surface may be quite large and will therefore give rise to considerable computational work. The alternative methods involve the normal derivative of the Helmholtz integral equation (HIE). A popular implementation is a combination of the HIE with its normal derivative, since this combination also can be shown to overcome the nonuniqueness problem of the standard HIE.[6] A strategy often chosen is to apply the combined equation on the midsurface of the thin body.[1,3] Another procedure, which does not

[a)]Electronic mail: vcutanda@bksv.com
[b)]Electronic mail: pmjuhl@itf.sdu.dk
[c)]Electronic mail: fjac@oersted.dtu.dk

assume the approximation of an infinitely thin body, applies the HIE on one side of the thin body and its normal derivative on the other.[4]

For a plane narrow gap a multidomain strategy could be used in which the gap could be modeled as a two-dimensional problem coupled to an exterior three-dimensional problem. However, this approach is only approximate for any finite gap width, and not suitable for problems where the sound field details inside the gap are important. As to the combined formulation in Ref. 4, the regularizing effect seems to rely on a medium being present outside, as in the case of inclusions.

Since complete removal of the ill-conditioning in the gap case is problematic, it is interesting to examine whether the conventional formulation can still provide correct results for practical cases under such circumstances. As pointed out in Ref. 4, adequate treatment of the near-singular integrals can prevent a breakdown due to poor integration, but it leaves the ill-conditioning. We will show in this paper how a simple numerical integration strategy can extend the range of aspect ratios (smaller dimension/overall dimension) by several orders of magnitude despite ill-conditioning, thus placing most practical gap problems within reach of the standard BEM. Besides, the proposed numerical integration only requires a very small increase of computing resources.

The nature of the problem of close boundaries is reviewed in the next section, with emphasis on the features of the gap case. An explanation of the numerical integration technique developed follows. The remainder of the paper is dedicated to thin-body and narrow-gap test cases. An axisymmetrical formulation is used, which is outlined along with details of the study methodology. The behavior of the method's convergence towards the solution is analyzed on the test cases, as well as the ill-conditioning of the coefficient matrix. The influence of frequency, mesh density, and aspect ratio is investigated.

II. THE PROBLEM OF CLOSE DOMAIN BOUNDARIES

A. The standard Helmholtz integral equation (HIE)

The BEM approach to acoustic radiation and scattering problems is based on the Helmholtz integral equation that relates the pressure $p(Q)$ and normal velocity $\nu(Q)$ on the surface of a body of any shape (see Fig. 1) with the pressure at any point $p(P)$ and the pressure of an incoming wave $p^I(P)$.[7] The harmonic time dependence $e^{i\omega t}$ is omitted, giving

$$C(P)p(P)=\int_S\left(\frac{\partial G}{\partial n}p(Q)+ikz_0\nu(Q)G\right)dS+4\pi p^I(P), \tag{1}$$

where S is the surface of the body, Q a point on that surface, and P any exterior or interior point. The normal vector n is directed into the computational domain. The Green's function for 3D free space is

$$G(R)=\frac{e^{-ikR}}{R},\quad R=|P-Q|. \tag{2}$$

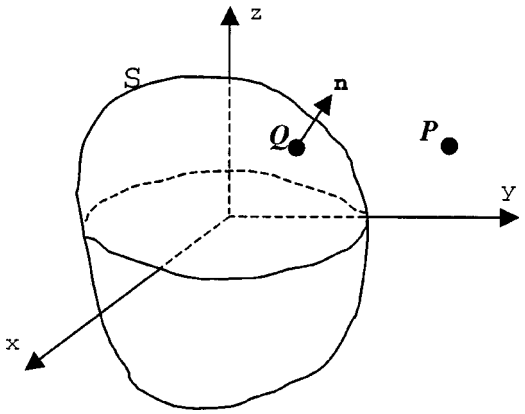

FIG. 1. Generic integration domain and boundary surface.

The factor $C(P)$ is the geometrical constant and represents the exterior solid angle at P. It is calculated by

$$C(P)=4\pi+\int_S\frac{\partial}{\partial n}\left(\frac{1}{R}\right)dS. \tag{3}$$

The expression (3) is valid for exterior problems; for interior problems 4π should be subtracted. In the present study only scattering by rigid bodies is considered; thus, $p^I(P)$ is the excitation and $\nu(Q)=0$, making Eq. (1) simpler. However, the coefficient matrix obtained from the BEM numerical implementation of (1) will be the same as for radiation problems, and therefore the conclusions discussed below will still be general. The standard collocation formulation will be used.

B. The thin-body problem

The case of a thin planar body has been discussed extensively in the literature, and hence the results are merely listed. For a thin disk using constant elements and unmodified numerical integration, the coefficient matrix of the BEM becomes

$$2\pi\begin{pmatrix}\mathbf{I} & \sim\mathbf{0}\\ \sim\mathbf{0} & \mathbf{I}\end{pmatrix}, \tag{4}$$

where $\mathbf{I}$ is the identity matrix and $\sim\mathbf{0}$ is approximately a matrix of zeros. This matrix is perfectly conditioned, but does not lead to the correct solution of the problem.[8] The problem is grounded in the nonhandling of the near singularity of the integral as the integration point Q to the surface S_+ passes the collocation point P on the near surface S (see Fig. 2). With proper treatment of the near singularity, one finds a correct matrix representation for the problem[4,8]

$$2\pi\begin{pmatrix}\mathbf{I} & \sim\mathbf{I}\\ \sim\mathbf{I} & \mathbf{I}\end{pmatrix}. \tag{5}$$

Here, the near degeneracy is reflected in an ill-conditioned matrix, which potentially may lead to incorrect solutions. As mentioned in the Introduction, two solutions have been proposed to deal with thin bodies, the multidomain method and the use of the normal derivative. Both of them reformulate the problem in a way that makes the ill-conditioning disappear, although in the case of some combined formulations

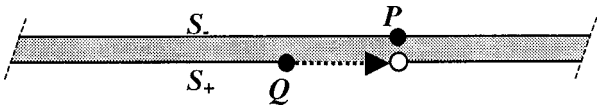

FIG. 2. Thin-body setup.

using the normal derivative, near-singular integrals are still present and must be taken care of.[4,9]

C. The narrow-gap problem

Consider a rigid bulky object with a narrow gap, as represented in Fig. 3. The surface on the exterior of the object is denoted by S, and the surfaces in the gap by S_- and S_+, respectively. Since there is no pressure jump across the gap in the limit of a gap of zero thickness, the normal derivative methods do not pose any new information for this kind of problems. The standard HIE for a scattering problem with such an object is

$$C(P)p(P)=\int_S p(Q)\frac{\partial G}{\partial n}dS+\int_{S_-} p_-(Q)\frac{\partial G}{\partial n}dS + \int_{S_+} p_+(Q)\frac{\partial G}{\partial n}dS+4\pi p^I(P). \tag{6}$$

Let P be on S. In the limit of an infinitely narrow gap, continuity of the pressure requires that $p_-=p_+$ so the two integrals for the two gap surfaces cancel out. Hence, in the limit of narrow gaps the sound field outside the gap is not influenced by the sound field inside the gap. This is in agreement with what one would expect physically. Therefore, the solution strategy for a problem involving a very narrow planar gap with rigid surfaces could be to solve an exterior problem neglecting the gap, and then to solve the gap problem as a two-dimensional interior problem with the pressures obtained for the exterior problem as the boundary conditions. However, if the gap width cannot be neglected, if parts of the gap surface are of finite impedance, and/or if viscosity is to be taken into account, the need for a simultaneous analysis of the gap and the exterior field is envisaged. If the near singularity is properly taken into account, the block of identity matrices of Eq. (5) is found in the matrix equivalent of Eq. (6)

$$\begin{pmatrix} \mathbf{A} & \mathbf{D} & -\mathbf{D} \\ \mathbf{C} & 2\pi\mathbf{I} & \sim 2\pi\mathbf{I} \\ \sim\mathbf{C} & \sim 2\pi\mathbf{I} & 2\pi\mathbf{I} \end{pmatrix}\begin{pmatrix} p \\ p_- \\ p_+ \end{pmatrix}=4\pi p^I. \tag{7}$$

The first block of rows in Eq. (7) refers to collocation points on the exterior surface S, and the second and third block of rows refer to collocation points on S_- and S_+, respectively. Again, the near degeneracy due to the two close surfaces is reflected in ill-conditioning of the coefficient matrix. If the near singularity is not dealt with properly, the lower right corner of the coefficient matrix is to be replaced with Eq. (4)

$$\begin{pmatrix} \mathbf{A} & \mathbf{D} & -\mathbf{D} \\ \mathbf{C} & 2\pi\mathbf{I} & \sim\mathbf{0} \\ \sim\mathbf{C} & \sim\mathbf{0} & 2\pi\mathbf{I} \end{pmatrix}\begin{pmatrix} p \\ p_- \\ p_+ \end{pmatrix}=4\pi p^I, \tag{8}$$

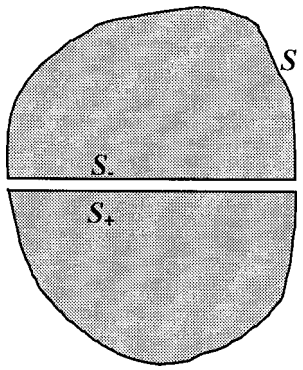

FIG. 3. Narrow-gap setup.

and the resulting (false) system of equations will be well-conditioned. In the latter case, which represents a standard numerical implementation, it is easy to show that the solution will tend towards zero inside the gap as the gap width tends towards zero. The solution outside the gap will still tend towards the solution of the equivalent exterior problem with the gap removed.

III. IMPROVEMENT OF THE NUMERICAL INTEGRATION

To achieve the goal of obtaining valid solutions for narrow-gap problems, the strategy chosen is the improvement of the numerical integration technique. A system of equations of the form in (7) should be guaranteed for a range of aspect ratios of practical importance. As mentioned in the last section, there is still ill conditioning, and therefore the accuracy of the elements in the coefficient matrix, which are obtained by numerical integration, imposes a limit to the aspect ratio that can be calculated. Nevertheless, if this limit is high enough, the cases left out will be too narrow to have practical use or even physical meaning.

Several authors propose ways to handle near-singular integrals. For example, in Refs. 4 and 9 an analytical removal of the near singularity that splits the integral is performed. The resulting terms are treated with variable changes and the Stokes theorem in order to reduce or eliminate their difficulty. However, the approach taken in this paper will be numerical, not analytical.

The behavior of a near-singular integrand differs in many ways from a genuine singularity. If a collocation point is in the neighborhood of an element to be integrated, it produces a perturbation on the integrand around its projection on the element, more localized and more acute the shorter the distance. This effect can be observed in Fig. 4, which is a near-singular integrand along a one-dimensional element. It has been obtained from the disk test case to be presented in the following section. Note that integrand values are represented in a logarithmic scale and that only a part of the element is shown. It becomes clear from Fig. 4 why standard numerical integration methods, like Gauss–Legendre, miss this troublesome area for a given relative distance and lead to results as shown in Eqs. (4) and (8). This situation has often been described as the ''breakdown'' of the BEM standard formulation.

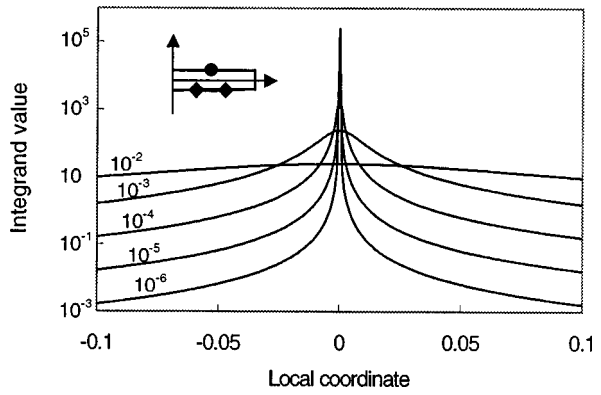

FIG. 4. Near-singular behavior of an integrand in the thin disk calculation. Abscissas are local coordinates along the element $[-1,1]$; ordinates are values of the integrand on a logarithmic scale. The curves are integrands with a collocation point at 10^{-2}, 10^{-3}, 10^{-4}, 10^{-5}, and 10^{-6} units' distance from the local coordinate 0. The disk radius is 1 unit. Five elements per disk side are used.

Only very limited improvement is obtained by merely increasing the order of the numerical integration formula. The integration does not concentrate the effort around the near singularity, where the integrand has a peak. The use of numerical formulas designed for singular integrals has also been considered, but they do not perform well due to the different nature of the near-singular integrand.

Another possible choice is an adaptive numerical integration routine. Such routines have been used for many years on all kinds of problems and are implemented in most mathematical software packages. Basically, the algorithm tries to decrease the integration error down to a given value. To do this, the error is estimated during every iterative step, and more integration points are used on the difficult areas. When applied to near-singular integrals in BEM, there is a clear improvement. However, these methods often fail in the limit of very close collocation points. The floating-point precision of the machine is reached during the internal calculation of integration error estimates, with unpredictable results. This lack of reliability and control on the routine behavior seems to rule them out.

An optimal numerical integration scheme for this particular problem should be simple enough to minimize errors but, on the other hand, it should concentrate the effort around the difficult area. If the information about the near singularity and its strength can be used in order to perform each integration in the most appropriate way, the computer load can also be reduced.

In view of this, the approach finally adopted employs an exponential interval division according to the expected near-singular behavior, as shown in Fig. 5. In this study, one-dimensional quadratic elements are used, but the technique can be translated to other implementations. The distance from each subinterval boundary to the collocation point projection is expressed by $c \cdot b^n \cdot d$, where b and c are constants, d is the distance from collocation point to the element, relative to the element size, and n is the subinterval number. In practical calculations, it was adjusted to $b=2$ and $c=2^{-5}$. Each subinterval can be numerically integrated using low-order standard techniques. In this way the information available about the integrand is used to perform the numerical integration, and no complex adaptive integration strategy is needed.

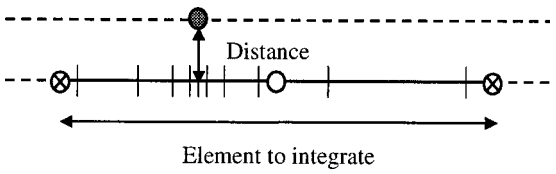

FIG. 5. Exponential interval division on a one-dimensional quadratic element. Relative distance and local coordinate of the collocation point are used to calculate the number and sizes of the subintervals.

TABLE I. Processing time results on a DEC Alpha 433 MHz for the two-cylinder test case (see Sec. IV B) with 60 elements. Gauss–Legendre numerical integration of order 20 and the interval division technique are compared.

Gap width	Integration	Time (s)	Result
10^{-2}	Gauss	82.7	Good
	Division	91.4	Good
10^{-3}	Gauss	83.0	Fail
	Division	93.2	Good
10^{-4}	Gauss	83.2	Fail
	Division	93.9	Good
10^{-5}	Gauss	82.7	Fail
	Division	94.4	Good
10^{-6}	Gauss	82.6	Fail
	Division	96.7	Fail

The improved integration does not involve a significant increase in computer load. Computational effort is only applied where it is necessary; that is, only in those cases where the collocation point is very close to the element and, within that element, around the near singularity and proportional to its strength. Table I presents some run times for the narrow-gap test case and a 60-element fixed mesh. The interval division technique adds around 10%–20% to the normal processing time, with a slight increase for narrower gaps. This is logical if we consider that the technique is only used to calculate an order of N elements in an $N \times N$ matrix.

IV. TEST CASES

A. BEM axisymmetrical formulation

If an axisymmetric body or bodies on the same axis are considered, it is possible to simplify the standard BEM from a surface integral to an integral along the generator and another over the angle of revolution, in a cylindrical coordinate system. The use of a cosine expansion of $p(Q)$ and $\nu(Q)$ in orthogonal terms allows the isolation of the singularities contained in the revolution integrals so that only the generator has to be discretized, saving computing time and storage capacity. Although the excitations described in this paper are also axisymmetrical, the cosine expansions permit nonaxisymmetrical boundary conditions. This implementation retains most features of the full 3D version, which means that the problem of close boundaries can be studied more easily and over a larger number of test cases.[10]

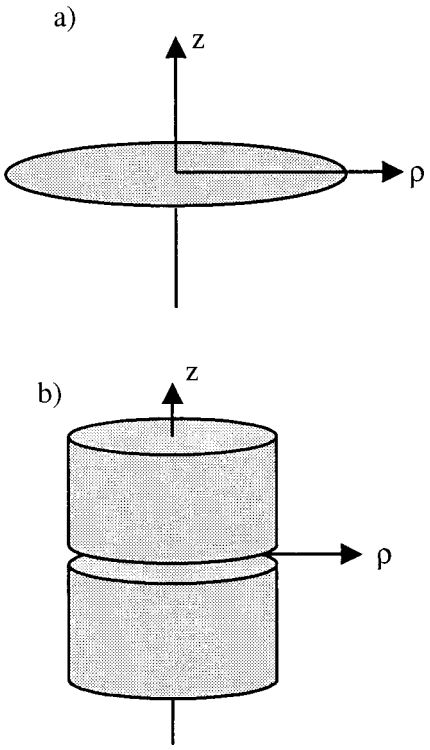

FIG. 6. Test cases. (a) thin disc; (b) narrow gap.

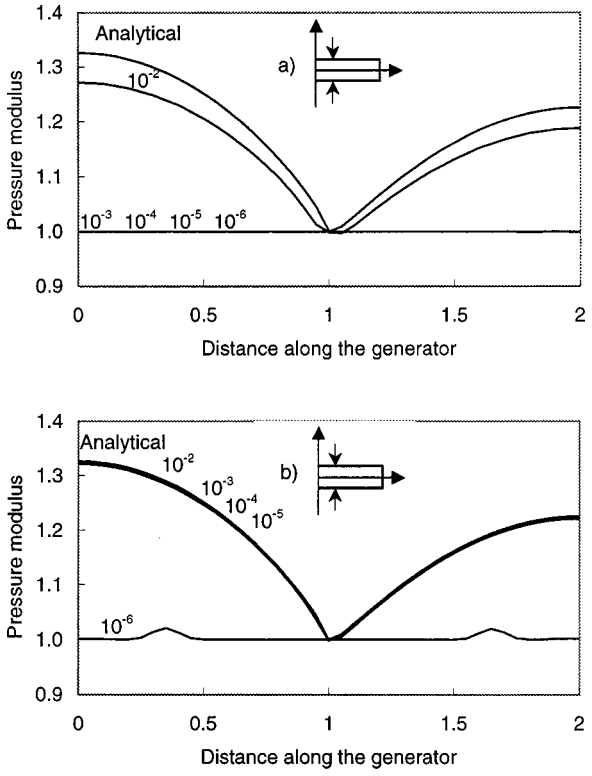

FIG. 7. Calculated sound-pressure modulus on the generator of a disk [see Fig. 6(a)] of variable thickness using a mesh of 10 elements per unit, 20 elements in total. The thicknesses are 10^{-2}, 10^{-3}, 10^{-4}, 10^{-5}, and 10^{-6}. The analytical solution for a infinitely thin disk is also plotted. An axial plane wave of $ka=1$ and unit amplitude is scattered by the disk. Calculations using (a) Gauss–Legendre numerical integration of order 20; (b) with interval division as explained in Sec. III.

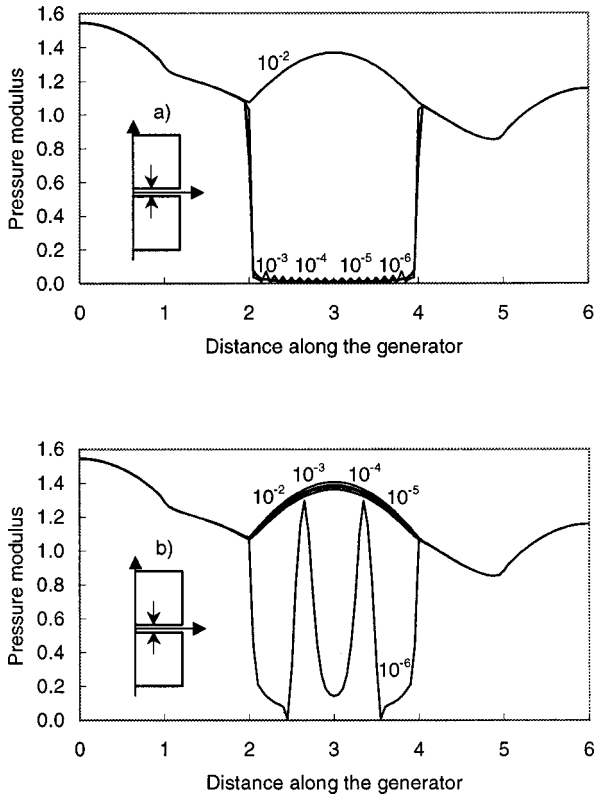

FIG. 8. Calculated sound-pressure modulus on the generator of two coaxial rigid cylinders [see Fig. 6(b)] separated by a variable narrow gap calculated using a mesh of 10 elements per unit, 60 elements in total. The gap widths are 10^{-2}, 10^{-3}, 10^{-4}, 10^{-5}, and 10^{-6}. An axial plane wave of $ka=1$ and unit amplitude is scattered by the setup. Calculations using (a) Gauss–Legendre numerical integration of order 20; (b) with interval division as explained in Sec. III.

B. Test cases

Two test cases have been chosen to represent the thin-body problem and the narrow-gap problem. These are, respectively, a disk of variable thickness and two cylinders with a common axis that form a narrow gap. They are represented in Fig. 6.

These cases have rotational symmetry along the cylindrical coordinate θ and therefore the axisymmetrical BEM formulation can be applied. The bodies are supposed to be rigid (infinite impedance) and excited by a plane wave coming from the z^+-axis direction. Several values of ka (wave number times radius) have been used in the calculations, but only the results for $ka=1$ are presented, since no relevant variation with the frequency has been observed. The radius a of disk and cylinders is normalized to 1, as well as cylinder lengths.

The numerical implementation is made by dividing the generators into line elements. Both pressure and geometry are modeled using quadratic shape functions.

C. Sound-pressure results

The sound-pressure modulus along the generator of the objects in Fig. 6 is shown in Figs. 7 (disk) and 8 (gap) for a variety of thicknesses/widths. Standard Gauss–Legendre integration [Figs. 7(a)/8(a)] succeeds only if the disks or gaps are thicker than 10^{-2} units, while the proposed interval di-

vision can give good results down to 10^{-5} units [Figs. 7(b)/8(b)]. The two breakdowns are different. An integration failure causes the pressure to drop to zero on the close surfaces, while the improved integration avoids this down to a point where ill-conditioning is too serious for the limited precision of the computer to cope with, and unpredictable results appear. Other calculations not shown here have demonstrated that neither mesh density nor frequency has any influence on the ill-conditioning breakdown. It is only dependent on the aspect ratio.

Figure 7 also includes the corresponding analytical solution for a disk of zero thickness, which can be obtained as a series of oblate spheroidal functions. This solution has been calculated in order to validate the results and study the convergence. A brief summary is given in the Appendix of this paper.

The pressure increase in the gap observed in Fig. 8 can be explained in the limiting case of a vanishing gap. Ideally, the external sound field would not be influenced by the presence of a very narrow gap. Therefore, considering the gap as two-dimensional, the sound pressure along the radius (generator) inside the gap has the form of a Bessel function.[11] Its boundary condition is the sound pressure on the external surface connected to the gap (abscissas 2 and 4 in Fig. 8). For $ka=1$, there are no zeros of the Bessel function within the gap; therefore, only a pressure increase is observed.

D. Convergence of the improved solution

Using the calculated complex sound pressure on the generator nodes and the corresponding analytical values for an infinitely thin disk, it is possible to study the convergence of the thin-disk calculation as a function of mesh density and disk thickness.

The thicknesses examined are small enough to make them physically very similar to a disk with no thickness. The error is calculated as the length of the residual vector relative to the analytical solution

$$\text{Relative error}=\frac{\sqrt{\Sigma_{j=1}^{M}[(\mathrm{Re}(P_{j\ \text{analytical}})-\mathrm{Re}(P_{j\ \text{calculated}}))^2+(\mathrm{Im}(P_{j\ \text{analytical}})-\mathrm{Im}(P_{j\ \text{calculated}}))^2]}}{\sqrt{\Sigma_{j=1}^{M}[\mathrm{Re}(P_{j\ \text{analytical}})^2+\mathrm{Im}(P_{j\ \text{analytical}})^2]}}, \tag{9}$$

where $P_{j\ \text{analytical}}$ is the analytical solution at node j and $P_{j\ \text{calculated}}$ is the calculated complex pressure at the same node. M is the total number of nodes of every solution. See Fig. 9.

Unfortunately, the narrow-gap case does not have a suitable analytical solution. The two-dimensional analogy mentioned in the last section is not precise enough to study convergence, since it is dependent on the boundary conditions at the rim that are themselves subject to calculation errors, which are aggravated because of the sharp edge singularity.[12] The convergence can nevertheless be studied by using a solution with a very fine mesh as a reference. This is what Fig. 10 represents.

The convergence is clear in the disk case, and independent of the thickness. Only the 10^{-6} case cannot converge due to the ill-conditioning of the coefficient matrix, but thicker disks do not show any strange behavior. The gap case is physically more complicated because what happens inside the gap is strongly influenced by the phenomena on the gap rim; therefore, the convergence pattern differs. Nevertheless, the solutions clearly converge again except for the 10^{-6} case. The use of a calculated solution as a reference produces also a shift in the error scale.

E. Ill-conditioning

The condition number of the coefficient matrix has been calculated for a number of mesh densities and disk/gap thicknesses. It was shown in Sec. III that a good numerical integration in a problem of close surfaces produces an ill-

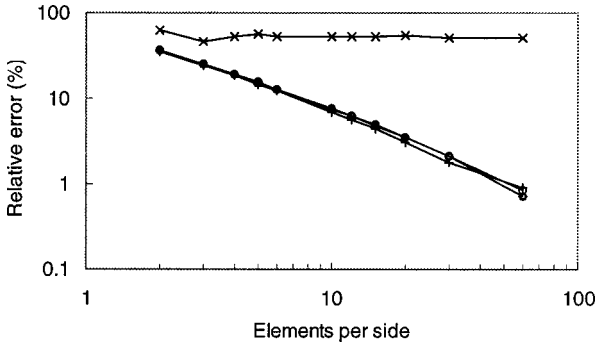

FIG. 9. Convergence towards the analytical solution of a thin disk [see Fig. 6(a)] of variable thickness, using the proposed numerical integration. The thicknesses are 10^{-2} (+), 10^{-3} ($\diamond$), 10^{-4} ($\square$), 10^{-5} ($\bigcirc$), and 10^{-6} ($\times$). The relative error is represented as a function of the mesh density. An axial plane wave of $ka=1$ and unit amplitude is scattered by the disk.

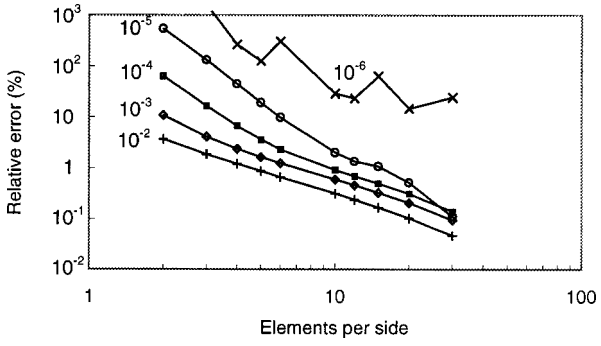

FIG. 10. Convergence towards the ''true'' solution of a narrow gap [see Fig. 6(b)] of variable width, using the proposed numerical integration. The widths are 10^{-2} (+), 10^{-3} ($\diamond$), 10^{-4} ($\square$), 10^{-5} ($\bigcirc$), and 10^{-6} ($\times$). The relative error in the gap nodes is represented as a function of the mesh density. An axial plane wave of $ka=1$ and unit amplitude is scattered by the cylinders.

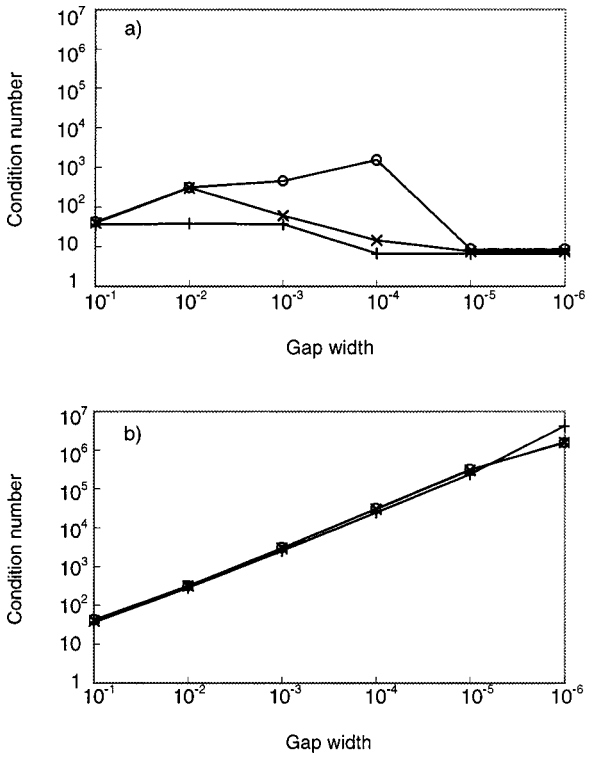

FIG. 11. Condition number of the coefficient matrix for the narrow-gap test case, as a function of gap width. Three mesh densities are plotted: 2 (+), 10 (×), and 60 (○) elements per unit. Calculations using (a) Gauss–Legendre numerical integration of order 20; (b) with interval division as explained in Sec. III. Calculation made with $ka=1$.

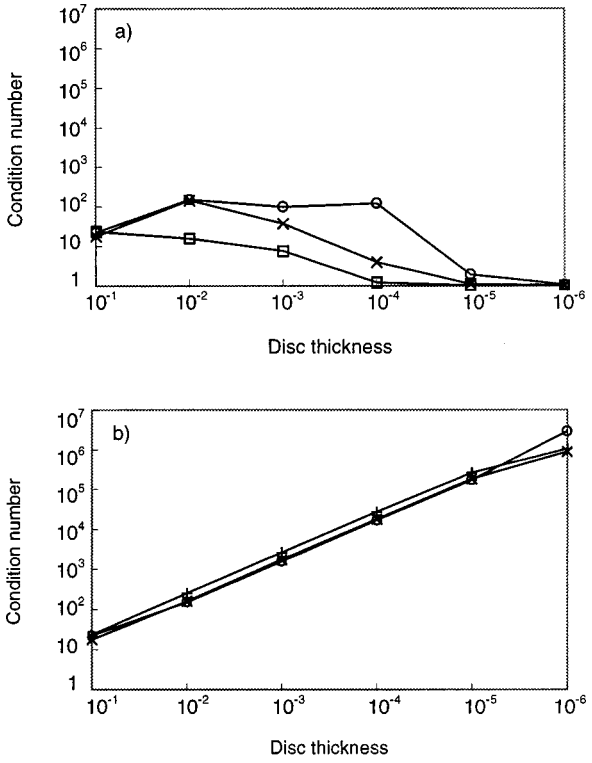

FIG. 12. Condition number of the coefficient matrix for the thin-disk test case, as a function of thickness. Three mesh densities are plotted: 2 (+), 10 (×), and 60 (○) elements per side. Calculations using (a) Gauss–Legendre numerical integration of order 20; (b) with interval division as explained in Sec. III. Calculation made with $ka=1$.

conditioned system of equations, and therefore a high condition number of the coefficient matrix. Conversely, a failure of the integration generates low condition numbers, but with erroneous solutions.

Figures 11 and 12 show that the ill-conditioning behaves similarly in the two test cases. If the near-singular integrals are not dealt with, the condition number does not grow very much, but the calculation gives erroneous results. When the interval division technique is used the condition number grows exponentially as the surfaces get closer, no matter which mesh density is used. The frequency also has very little influence, as other calculations not presented here have shown. Hence, the aspect ratio indeed seems to determine the condition number, independently of whether we deal with narrow gaps or thin bodies.

V. CONCLUSIONS

It has been shown that a case of practical importance in engineering like the narrow gap can be modeled using conventional BEM despite the ill-conditioning of the coefficient matrix and with no need of denser meshes. A convergence study has also revealed that the solution improves normally for gradually denser meshes. A simple strategy of interval division with low computational cost is enough to extend the range of tractable aspect ratios by three orders of magnitude, from 10^{-2} to 10^{-5}. This makes it possible to deal with problems like condenser microphones and sound intensity probes, which have motivated this study. For example, the air layer behind the diaphragm of a 1/2-in. condenser microphone is about 20 μm, giving an aspect ratio of about 10^{-3}.

APPENDIX: ANALYTICAL SOLUTION FOR SCATTERING BY A FLAT DISK

The infinitely thin disk is the limiting case of the oblate spheroid, which is better described in the oblate spheroidal coordinate system (ξ, η, ϕ). Its relation with rectangular Cartesian coordinates is

$$x=\tfrac{1}{2}d\sqrt{(\xi^2+1)(1-\eta^2)}\cos\phi,$$
$$y=\tfrac{1}{2}d\sqrt{(\xi^2+1)(1-\eta^2)}\sin\phi, \quad z=\tfrac{1}{2}d\xi\mu. \tag{A1}$$

The wave equation is separable in this coordinate system into spheroidal wave functions, thus providing analytical solutions for a range of cases. The particular solution used in this paper corresponds to an infinitely thin hard disk ($\xi=0$ and $d=$diameter) excited by a plane wave coming from the positive z axis. The sound pressure (incident and scattered) on its surface can be expressed by the series[13]

$$P^i+P^s=\frac{2}{ka}\sum_{n=0}^{\infty}\frac{i^n}{N_{0n}(-ika)}\frac{S_{0n}(-ika,-1)S_{0n}(-ika,\eta)}{R_{0n}^{(3)\prime}(-ika,i0)}, \tag{A2}$$

where S_{mn} are the oblate spheroidal angular functions, $R_{mn}^{(3)}$ are the derivatives of the oblate spheroidal radial functions of the third kind, and N_{nm} are the normalization factors.[14] These functions are also expressed as infinite series, and computer algorithms have been used to calculate them with sufficient accuracy.[15]

[1] R. Martinez, ''The thin-shape breakdown (TSB) of the Helmholtz integral equation,'' J. Acoust. Soc. Am. **90**, 2728–2738 (1991).
[2] C. Y. R. Cheng, A. F. Seybert, and T. W. Wu, ''A multidomain boundary element solution for silencer and muffler performance prediction,'' J. Sound Vib. **151**, 119–129 (1991).
[3] T. W. Wu and G. C. Wan, ''Numerical modeling of acoustic radiation and scattering from thin bodies using a Cauchy principal integral equation,'' J. Acoust. Soc. Am. **92**, 2900–2906 (1992).
[4] G. Krishnasamy, F. J. Rizzo, and Y. Liu, ''Boundary integral equations for thin bodies,'' Int. J. Numer. Methods Eng. **37**, 107–121 (1994).
[5] F. Jacobsen, V. Cutanda, and P. M. Juhl, ''A numerical and experimental investigation of the performance of sound intensity probes at high frequencies,'' J. Acoust. Soc. Am. **103**, 953–961 (1998).
[6] A. J. Burton and G. F. Miller, ''The application of integral equation methods to the numerical solutions of some exterior boundary value problems,'' Proc. R. Soc. London, Ser. A **323**, 201–210 (1971).
[7] A. F. Seybert, B. Soenarko, F. J. Rizzo, and D. J. Shippy, ''An advanced computational method for radiation and scattering of acoustic waves in three dimensions,'' J. Acoust. Soc. Am. **77**, 362–368 (1985).
[8] T. W. Wu, ''A direct boundary element method for acoustic radiation and scattering from mixed regular and thin bodies,'' J. Acoust. Soc. Am. **97**, 84–91 (1995).
[9] Y. Liu and F. J. Rizzo, ''Scattering of elastic waves from thin shapes in three dimensions using the composite boundary integral equation formulation,'' J. Acoust. Soc. Am. **102**, 926–932 (1997).
[10] P. M. Juhl, ''An axisymmetric integral equation formulation for free space nonaxisymmetric radiation and scattering of a known incident wave,'' J. Sound Vib. **163**, 397–406 (1993).
[11] P. M. Morse, *Vibration and Sound*, 2nd ed. (The Acoustical Society of America, New York, 1983).
[12] P. M. Juhl, ''A note on the convergence of the direct collocation boundary element method,'' J. Sound Vib. **212**, 703–719 (1998).
[13] J. J. Bowman, T. B. A. Senior, and P. L. E. Uslenghi, *Electromagnetic and Acoustic Scattering by Simple Shapes* (North-Holland, Amsterdam, 1969).
[14] C. Flammer, *Spheroidal Wave Functions* (Stanford University Press, Stanford, 1957).
[15] S. Zhang and J. Jin, *Computation of Special Functions* (Wiley, New York, 1996).